Aalto University
School of Chemical
Engineering

Phuong Nguyen Thi Thanh

PURIFICATION OF AQUEOUS, PROTIC IONIC LIQUID BY DISTILLATION

Master´s Programme in Chemical, Biochemical and Materials Engineering

Major in Chemical Engineering

Master's thesis for the degree of Master of Science in Technology submitted for inspection,

Espoo, 31st July 2020

Supervisor Professor Pekka Oinas
Instructor D.Sc Petri Uusi-Kyyny

Author Phuong NguyenThi Thanh

Title of thesis Purification of aqueous, protic ionic liquid by distillation

Degree Programme Chemical, Biochemical and Materials Engineering

Major Chemical Engineering

Thesis supervisor Professor Pekka Oinas

Thesis advisor(s) / Thesis examiner(s) D.Sc Petri Uusi-Kyyny

Date 31.07.2020 **Number of pages** 82 + Appendices **Language** English

Abstract

Protic ionic liquid (PIL) is an equimolar mixture of a superbase and a carboxylic acid. Acetate-based PILs have been developed to dissolve cellulose for fiber production. However, the high price of PILs currently is one of the barriers to the industrial application of PILs on a large scale. The recovery and recycling processes are essential to increasing the application of PILs. Purification is the last step of the recovery process of the fiber manufacturing process. Short path distillation is a potential purification method for thermo-sensitive materials like PILs.

In this study, short path distillation experiments were conducted to study whether it is possible to distill pure PIL. The operating pressure and the evaporator jacket temperature were varied to test the separation efficiency of PIL. The recovery yield of the base was 97 wt.% at 1.3 mbar and 160°C. The maximum base yield in the distillate was 94 wt.%. The minimum base yield in the residue was 1 wt.%. By-product was lower in the distillate than in the residue. The discoloration of PIL in the distillate product indicated the removal of chromophores as impurities from the initial material. The residual water was found in the cold trap. The base was possible to trap partly in the cold trap.

There is still insufficient data on the thermodynamic properties of PILs. Batch distillation experiments were implemented to study the evaporation behavior of pure acetate- based PIL. The purity of the base was 99 wt.% in the first fraction with mass fraction less than 20 wt.% of the initial material. By-product was found only in the residue.

Keywords Protic ionic liquid, purification, distillation, short path distillation, vacuum, vapor pressure, hydrolysis product

ACKNOWLEDGEMENTS

This master's degree thesis has been accomplished in recognition of lifelong learning and my dedication to chemical engineering research.

Firstly, I express my deepest gratitude to my Prof. Pekka Oinas who has trusted my competence and given me a chance to work on an interesting research project. I am deeply grateful Prof. Herbert Sixta who has encouraged me during the research process and funded my thesis. Also, I sincerely thank Prof. Ville Alopaeus who has instructed me to work with simulation models.

Secondly, I would like to express my appreciation and thanks to Dr. Petri Uusi-Kyyny who has assisted me for the last six months with thorough instructions on laboratory tests, consultation for solving problems, checking of test results as well as previewing this thesis.

This thesis would also not be accomplished without supporting from group of experts. I truly appreciate technical support from Timo Ylönen, Terho Konttinen, Hans Orassaari, Tuyen Nguyen, Timo Kotilahti; those who have promptly and professionally repaired problems of the short path distillation device. In addition, I sincerely thank to Juha-Pekka Pokki for his instructions to work on batch distillation column. I truly appreciate for instructions and invaluable experience from: Inge Schlapp-Hackl; Jari Koivisto; Joanna Witos; Krishna Ojha; and Sherif Elsayed, to work on analytical instruments. I sincerely thank other colleagues from groups of Human Resources, Plant design, Biorefinery, Chemical engineering of Aalto University; those who have helped me with administration procedure or spent time after work.

I am in sincere gratitude for valuable discussions with my mentor – Jyrki Kettunen, helpful proof-reading from Hendrik Hielkema, Victoria von Vagabonde, Taimi Pimentola-Heikkinen, John Powell and John Weston, as well as best encouragements from my beloved friends in Vietnam, Finland, and Portugal.

Finally, I greatly appreciate my husband - Thao Pham and my son - Dang Pham, who are inseparable parts of my life, have given me strength to fulfill the research work and keep balanced between work and life. I am thankful that my mother, sister and relatives in Vietnam who are in good self-care so that I am able to concentrate on the thesis.

TABLES OF CONTENTS

LIST OF ABBREVIATIONS

ILs	Ionic liquids
PILs	Protic ionic liquids
DILs	Distillable ionic liquids
SILs	Switchable ionic liquids
SPD	Short path distillation
NMR	Nuclear magnetic resonance spectroscopy
CE	Capillary electrophoresis
K-F	Karl- Fischer titration
UV-Vis	Ultraviolet-Visible spectrophotometer

LIST OF TABLES

LIST OF FIGURES

1. INTRODUCTION

1.1. Background

The demand for textile fibers has been predicted to increase rapidly in line with global population growth (Parviainen et al., 2015). Cellulose-based fibers, with their outstanding properties, have been developed to produce fibers for the world fibers market (Parviainen et al., 2015). The viscose and Lyocell processes are dominant in commercial man-made cellulose fiber production processes (Michud, 2016). However, the viscose process uses highly toxic chemicals and gases causing safety issues and environmental pollution, and the Lyocell process can experience dangerous thermal runaway reactions and side products formation (Michud, 2016).

Ionic liquids (ILs) have been developed for cellulose dissolution to produce man-made cellulose fibers (Parviainen et al., 2015). Ioncell-F technology has been developed to produce cellulosic fibers with a novel ionic liquid synthesized by Helsinki University and a dry-jet wet spinning process operated by Aalto University. The Ioncell-F process is similar to Lyocell spinning technology as shown in Figure 1 (Michud, 2016). The cellulose pulp can be mixed with the ionic liquid to form a dope. Solid impurities and undissolved cellulose can be filtered out before extruding the dope into the spinning bath containing water and diluted ionic liquid. The dope can be extruded through multi-hole spinnerets, then drawn via an air gap (or dry-jet wet spinning process) into a coagulation bath. The filament tow can be washed by hot water before cutting to staple fibers. The staple fibers continue to the second washing or post treatment, including finishing, drying and baling. The vacuum thin film evaporation can be used to remove water from the ionic liquid containing coagulation bath solution, and the evaporated water can be recycled to the spinning bath and fiber washing stages. The purification (as a red box in Figure 1) is the final step to remove impurities from the IL and recycle it back to the premixing process.

Unfortunately, ILs are currently more expensive than traditional organic solvents (Parviainen et al., 2015). An ionic liquids recycling process is essential for the commercialization of Ioncell-F process (Parviainen et al., 2014). However, the inertness and low volatility of ionic liquids can cause difficulties in the recovery process (Sklavounos et al., 2016) (Sklavounos E., Helminen J. K. J. , Kyllönen L., Kilpeläinen I. & King A. W. T., 2016). Moreover, the physical chemical properties of ILs are as yet still unknown or unpublished (Siriwardana, 2015). It is necessary to study ILs properties, especially vapor pressure of ILs.

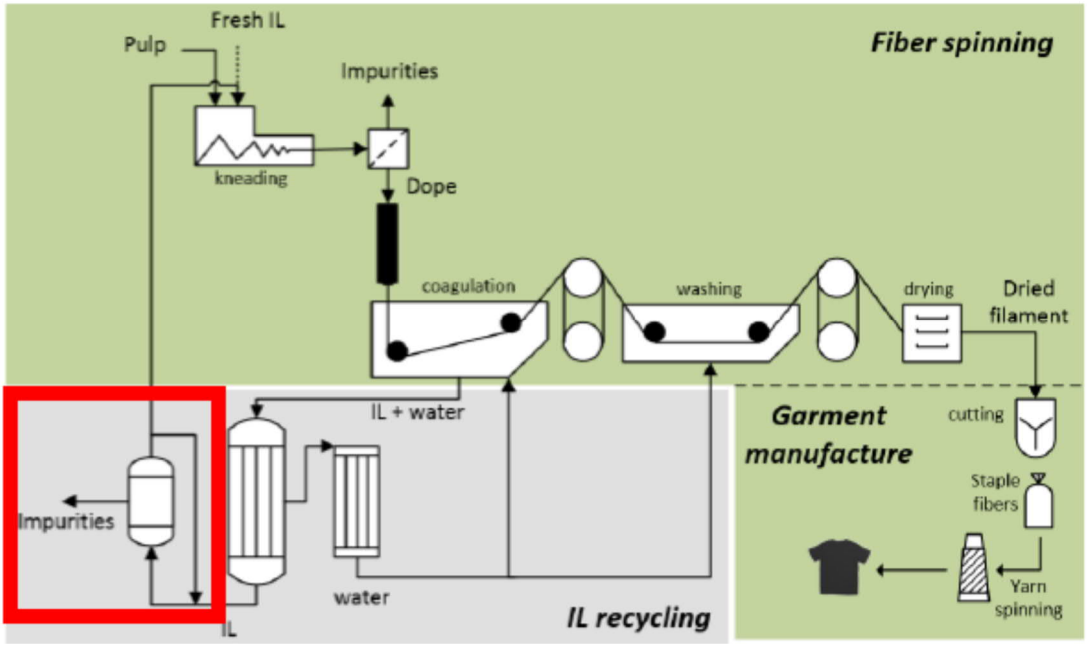

Figure 1. Ioncell-F process to produce manmade cellulose fibers (Michud, 2016)

Some impurities can be accumulated in ILs during the process and after being reused many times (Kuzima, 2016). There are several recycling methods for ILs, including phase separation, extraction, distillation, adsorption, membranes, and crystallization (Sklavounos et al., 2016). However, the optimal method has not yet been found or fully studied (Kuzima, 2016). Purification of ILs is a big challenge for both users and producers of ILs (Siriwardana, 2015). The purification process needs

to avoid the decomposition of ILs (Kuzima, 2016). Distillation under vacuum can be a possible method to distil ILs or protic ionic liquids (PILs) into neutral molecules (Siriwardana, 2015). Short path distillation (SPD) is a potential purification method for thermo-sensitive substances. Short path distillation is a non-equilibrium process with a short residence time, low operating temperature and high vacuum (Zhu et al., 2016). In addition, the ILs recycling processes have been published at the lab or bench scale, and a few at pilot scale, but there is no industrial technology (Siriwardana, 2015). There is a need to study SPD performance for PILs purification.

1.2. Objectives of the study

The aim of the thesis is to determine whether it is possible to purify PIL, such as PIL solvent 2 (S2), via distillation. The scope of the study covers an experimental implementation using a Vigreux batch distillation column and a short path distillation (SPD) device for S2. The analytical methods employed including nuclear magnetic resonance (NMR), capillary electrophoresis (CE), Karl-Fischer titration (K-F), and ultraviolet-visible spectroscopy (UV-Vis), have been developed by a group of the Biorefinery department in Aalto university. The author, after training, will undertake the analysis of samples of the initial material and products. The experimental results of batch distillation and short path distillation will be evaluated using a process simulator (Aspen), with a phase equilibrium model developed by the research group of chemical engineering.

The study will address the following objectives:

1. The vapor pressure of S2 will be studied through batch distillation experiments
2. The SPD performance will be checked with PIL solvent 1 (S1)
3. The evaporative behavior of S2 will be conducted via the SPD

1.3. Structure of the thesis

The thesis structure contains two major sections including a literature review and an applied part described experimental investigation. The literature is reviewed from Chapters 2 to 5. Chapter 2 provides an overview of protic ionic liquids (PILS) with their classification, synthesis mechanisms and properties. Chapter 3 introduces the separation methods for the purification of PILs, including batch distillation and molecular distillation as short path distillation. Chapter 4 presents process simulation approaches for chemical processes with ionic liquids. The applied part consists of Chapters 5 to 8. Chapter 5 presents the methodology applied to the study, especially the setting up of batch distillation and short path distillation experiments, and the analytical methods. Chapter 6 reports the batch distillation experimental results for S2. Chapters 7 and 8 report the short path distillation experimental results for S2 and S1, respectively. Chapter 9 summarizes the main achievements of the study and makes recommendations for future studies.

LITERATURE REVIEW

2. PROTIC IONIC LIQUIDS OVERVIEW AND APPLICATIONS

Ionic liquids have been developed as green solvents to substitute volatile organic solvents. Ionic liquid is a molten salt in a liquid state with a low melting temperature (e.g. below 100°C). Ionic liquids have a low melting point temperature. Each ionic liquid owns a unique set of properties for special applications. Generally, common ionic liquid properties are low vapor pressure, non-flammability, high ionic conductivity, high thermal, mechanical and electrochemical stability (Sklavounos et al., 2016).

2.1. Ionic liquid classification

There are several classification definitions of ionic liquids. Ionic liquids can be classified based on their synthesis mechanism and chemical behavior, including protic and aprotic ionic liquids (Sklavounos et al., 2016). Protic ionic liquids (PILs) are polar solvents with the capability of forming hydrogen bonds (Clare et al., 2009). PILs contain bonds between atoms with different electronegativities, such as O–H bond in hydroxyl groups and N–H bond in amine groups (Clare et al., 2009). PILs can be synthesized through a neutralization reaction of a Brønsted acid with a Brønsted base in an equimolar mixture (Clare et al., 2009).

Ionic liquid recycling is crucial for economically viable scalable industrial applications. There are several technologies applied to the purification of organic solvents, including adsorption, crystallization, extraction, phase-separation, and so on. Distillation is one of the potential purification methods for ionic liquids via distilling ionic liquids and leaving impurities behind (Sklavounos et al., 2016). Therefore, ionic liquids can be classified as distillable ionic liquids (DILs) or switchable

ionic liquids (SILs). DILs exist in two different states in the equilibrium phase, including intact ionic pairs charged form (i.e. non-volatile species) and volatile neutral species (Sklavounos et al., 2016). DILs can be distilled via proton transfer between cations and anions; consequently, the neutral cation molecules can be condensed and recombined with the anions to reform ionic liquids (Fig. 2) (Sklavounos et al., 2016). On the other hand, SILs are derived from organo-superbases and acidic industrial flue gases. SILs are extreme basicity and contain neutral nitrogen species such as acyclic and cyclic guanidine or amidine derivatives (Nowicki et al., 2016). In addition, SILs are considered as CO_2-reactive species. SILs can switch between ionic and non-ionic compounds by adding or removing one compound as a trigger, such as CO_2 (Anugwom et al., 2014).

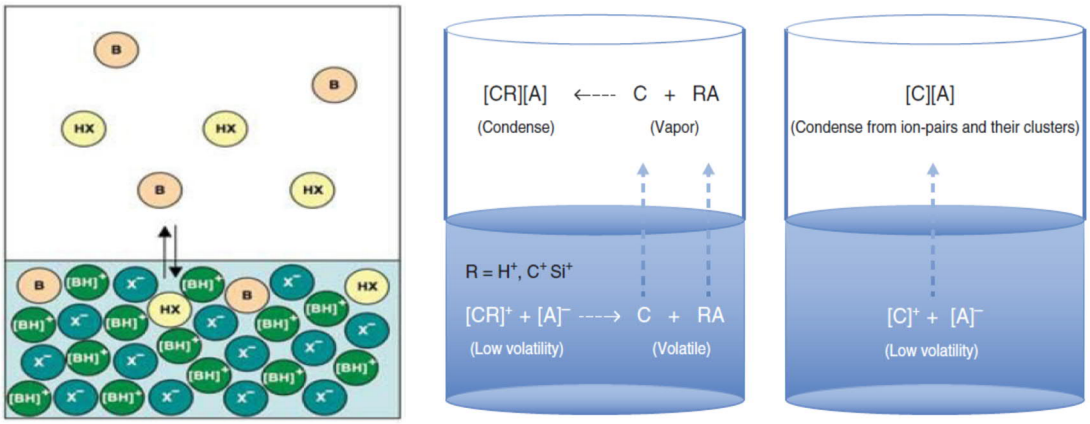

Figure 2. The schematic diagrams of evaporation and distillation mechanism of PILs (Earle et al., 2006) (Sklavounos et al., 2016)

Based on the chemical structures, ionic liquids generally contain the alkylate heterocyclic cations and the counter-anions (Sklavounos et al., 2016). The choice of cation defines stability properties, whereas the choice of anion defines chemistry and functionality properties of ionic liquids (Sigma-Aldrich, 2019). Ionic liquids' cations

are generally asymmetric organic compounds (Clare et al., 2009). ILs can be divided into five groups (Table 1) based on the cations' types (Clare et al., 2009). On the other hand, the anions of ILs are usually weak basic inorganic or organic compounds. ILs can be classified into six groups (Table 2) based on the anions' types (Clare et al., 2009).

Table 1. ILs groups based on the cations of ILs (Clare et al., 2009)

No.	ILs groups	Chemical structures
1	Five membered heterocyclic cations	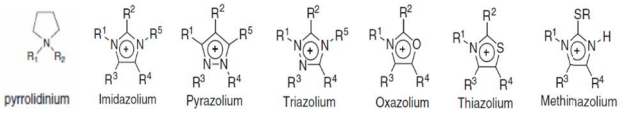 pyrrolidinium, Imidazolium, Pyrazolium, Triazolium, Oxazolium, Thiazolium, Methimazolium
2	Six membered and benzo-fused heterocyclic cations	 Pyridinium, Benzotriazolium, Isoquinolinium, Viologen-type
3	Ammonium, phosphonium and sulfonium-based cations	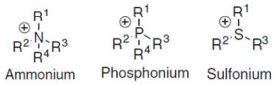 Ammonium, Phosphonium, Sulfonium
4	Functionalized imidazolium cations	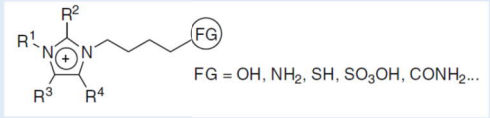 FG = OH, NH_2, SH, SO_3OH, $CONH_2$...
5	Chiral cations	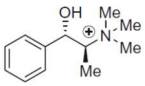 (1*S*, 2*R*)-(+)-*N*,*N*-dimethylephedrinium ion

ILs can be synthesized through two steps, including the formation of the desired cations, and the direct combinations of the functionally- designed anions or the anion exchange reactions. There are novel ILs groups recently synthesized; therefore, the cations of ILs can be extended to new groups. Dicationic ionic liquids are a new ionic liquid family. Dicationic ionic liquids include homoanionic dicationic ionic liquids and heteroanionic dicationic ionic liquids. (Masri et al., 2016)

Table 2. ILs groups based on the anions of ILs (Clare et al., 2009)

No.	ILs groups	Chemical structures
1	$AlCl_3$ and organic salts	
2	Anions like PF_6^-, BF_4^-, SbF_6^-	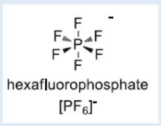
3	Amide and methanide anions	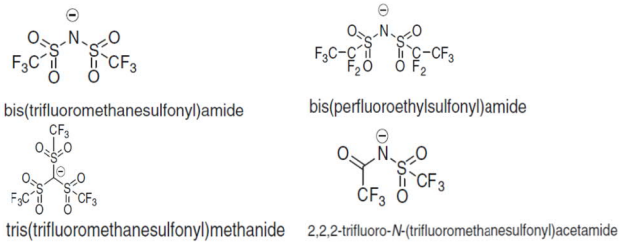
4	Anions like alkylsulphates, alkylsulphonates, alkylphosphates, alkylphosphinates, and alkylphosphonates	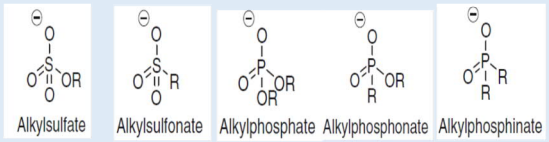
5	Anions like mesylate, aceate, tosylate ($CH_3PhSO_3^-$), trifluoroacetate ($CF_3CO_2^-$), acetate, SCN^-, triflate ($CF_3SO_3^-$), and dicyanamide [$(N(CN)_2^-$]	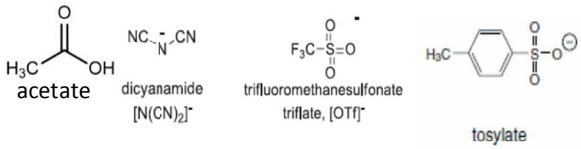
6	Anions like borates and carboranes	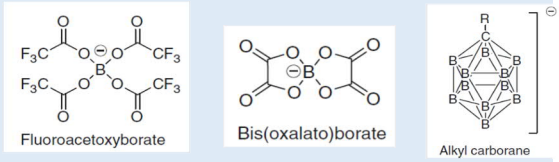

2.2. Ionic liquids in biomass processing

ILs have been used to dissolve lignocellulosic biomass through the hydrogen bonds disruption of hydroxyl groups (Tan & MacFarlane, 2009). Aprotic ionic liquids have been dominating in the literature, which is related to biomass processing but PILs have received more attention because of their easy preparation process (Osch et al., 2017). Figure 3 shows several common cations and anions of PILs. Acetate-based PILs have been found to be effective in cellulose dissolution (Osch et al., 2017).

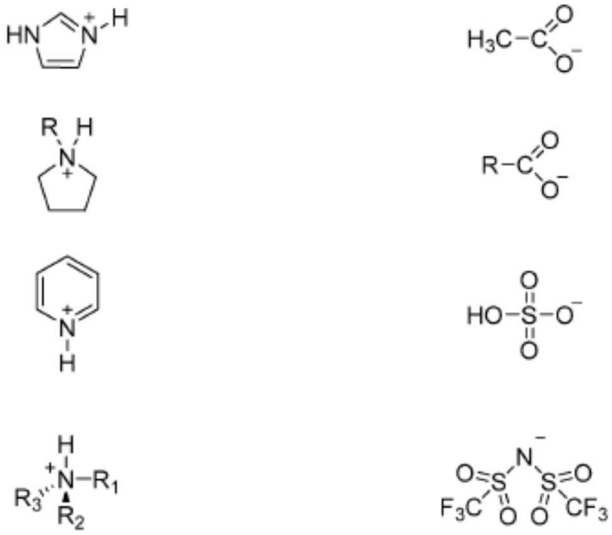

Figure 3. Common cations and anions of PILs (Osch et al., 2017)

2.3. Ionic liquid synthesis

Ionic liquids can be synthesized through two main mechanisms – quaternization or metathesis reaction and acid base neutralization reaction (Losetty et al., 2016). PILs can be easily prepared by proton transfer from Brønsted acids to Brønsted bases through neutralization reaction (Fig. 4). The method to obtain pure PILs without by-products is simple (Ferraz et al., 2015).

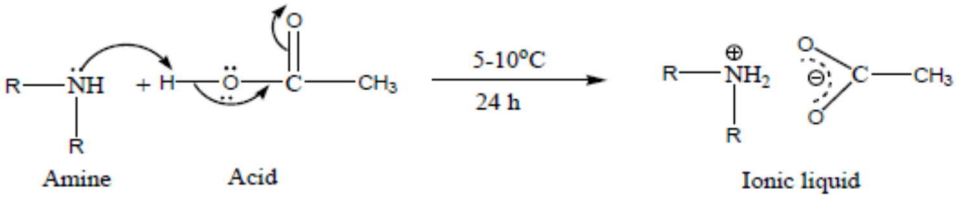

Figure 4. The synthesis schematic of acetate- based PILs (Losetty et al., 2016)

The dimer or oligomeric acids can appear in the case of highest degree of ionicity by adding higher stoichiometric amount of acid dropwise to a base (Clare et al., 2009). The possible formation of the acid acetic dimer and oligomeric mixtures is shown in Figure 5.

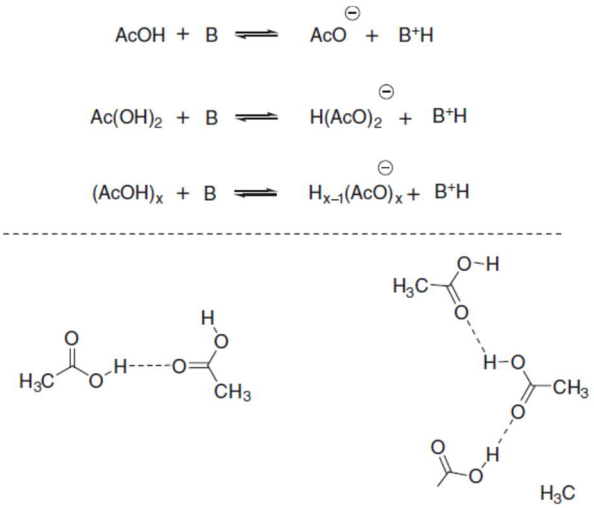

Figure 5. The synthesis schematic of dimeric or oligomeric of acid acetic in a mixture of PIL (Clare et al., 2009)

2.4. Ionic liquid properties

The lack of knowledge regarding the physical and chemical properties of PILs currently limit their applications (Losetty et al., 2016). There are several published databases of ionic liquids' physicochemical properties, including IL Thermo, DDBST,

Merck, DelphIL, and Institute of Process Engineering (IPE) (Zhou et al., 2011). The physicochemical properties generally include thermal phase behavior, density, viscosity, specific heat capacity, and surface tension.

a. Thermal phase behavior

Thermal phase behavior can be defined by the liquidus range, which is the temperature range to keep ILs in liquid forms (Rooney et al., 2009). The liquidus range is the difference between the lower temperature as the melting point or the glass transition temperature and the upper temperature as the thermal decomposition temperature (Osch et al., 2017). The melting point and the glass transition temperature are lower in the presence of impurities like water (Rooney et al., 2009). In addition, the melting point is lower with the larger asymmetrical cation than the symmetrical cation. The branched alkyl chain cation displays a higher melting point than the straight chain cation (Rooney et al., 2009). The increasing molecular weight and the accumulation of charge increase the melting point (Zhou et al., 2011). On the other hand, the thermal stability of ILs depends on the strength of heteroatom carbon or hydrogen bonds of both cations and anions (Losetty et al., 2016). The decomposition temperature of ILs varies between 100 and 430 °C (Ghandi, 2014). The thermal decomposition condition can create undesired products such as water, carbon dioxide, hydrocarbons, or reverting original components (Rooney et al., 2009). ILs are known for their negligible vapor pressure, but some PILs have been found to distill under vacuum condition without decomposition (Greaves & Drummond, 2015). Moreover, ILs with large pK_a differences have both molecular and ionic aggregates coexisting that lead to ILs' evaporation as ion pairs (Greaves & Drummond, 2015). Consequently, the vapor phase consists of acid and base molecules (Greaves & Drummond, 2015).

b. Density

Density is an important property for process designs, hydrodynamic calculations, and simulation of heat and mass transfer (Zhou et al., 2011). The typical density range of ILs is 1.05-1.64 g/mL at ambient pressure and 293 K (Rooney et al., 2009). Density decreases with the increase of alkyl chain length of both cations and anions (Zhou et al., 2011). The density of a water-saturated ionic liquid sample is lower than the dried one under atmospheric pressure (Rooney et al., 2009).

c. Viscosity

Viscosity should be considered for scaling up ionic liquids' applications, especially with distillation columns, liquid-liquid extractors, heat transfer units, process piping and pumping, and reactors (Rooney et al., 2009). The viscosity range is from 10 to 726 mPa·s (Rooney et al., 2009). Viscosity depends on the types of cations and anions (Rooney et al., 2009). The increasing alkyl chain length of cations increase viscosity, but the increasing asymmetric of anions decrease viscosity (Rooney et al., 2009). Viscosity is controlled by hydrogen bonding, Van der Waal force, molecular weight, and molecular mobility (Rooney et al., 2009). Moreover, viscosity decreases with the increase of temperature or in the presence of impurity traces like water (Zhou et al., 2011).

d. Ionic conductivity

Ionic conductivity of ILs depends on ion mobility, available charge carriers, molecular weight, and sizes of ions. Ionic conductivity decreases with the increase of the size of cations with longer alkyl chain length. Less symmetric cations and smaller molecular weight increase the ionic conductivity. (Ghandi, 2014)

Thermal conductivity of ionic liquids is approximately from 0.1 to 0.2 W/(m.K). The presence of impurities, or the types of cations and anions does not have significant effect on thermal conductivity. (Rooney et al., 2009).

e. Specific heat capacities

Specific heat capacities of ionic liquids are higher than for the conventional solvents in molar basis. Heat capacity is lower in the presence of impurities such as water or chloride. Heat capacity increases with the increasing sizes of cations and anions. (Rooney et al., 2009)

f. Surface tension

Surface tension influences vapor transfer rate at the vapor-liquid interface (Zhou et al., 2011). Surface tension decreases with increasing alkyl chain length of cations and increasing temperature (Rooney et al., 2009). The surface tension range is 1.55-65 mN/m (Zhou et al., 2011).

2.5. Ionic liquid applications

Ionic liquids have been applied in a large number of applications for both academic and industrial usages recently. Ionic liquids can substitute conventional liquids or organic solvents; therefore, the range of applications of ionic liquids will be wide in the future (Plechkova & Seddon, 2007). Appendix 1 shows a summary of potential applications of ionic liquids in various fields at different applied scales, as R&D, Pilot (P), or Commercialized (C). PILs are known as low cost preparation and simple synthesis with high purity (Losetty et al., 2016). PILs have been applied widely in biological systems, chromatography, gas separations, extractive distillation, biomass processing, biocatalysts, heat transfer fluids, and as working fluids for fuel cells, solar cells, capacitors (Losetty et al., 2016). In addition, PILs have been used as

acid-base catalysts for organic reactions, especially Knoevenagel and Aldol condensation, Diels-Alder reaction, Fischer esterification, and Pinacol rearrangement (Ghandi, 2014).

Particularly, acetate based PILs are commonly used in biological and chemical fields with specific properties of PILs. For instance, PILs can be used in fuel cells with the reactivity of mobile protons. PILs can be applied as protein solvents for preventing protein aggregation, or as a solvent for zein polymer. In addition, PILs can be made lubricant additives, or catalysts or reaction media for several reactions like Heck reaction, Michael reaction (Losetty et al., 2016). Acetate-based PILs are studied in post-combustion carbon dioxide capture systems with specific features such as higher absorption capacity, lower energy requirement, but higher capital cost than conventional solvents (Losetty et al., 2016). Moreover, acetate-based PILs have been employed as solvents in bio-refineries. Lignocellulosic biomass dissolution traditionally occurs through Kraft or Sulphite or Organosolv pulping process, or man-made cellulosic fiber production mainly from Viscose or Lyocell process (Osch et al., 2017). Ioncell process is the innovative Lyocell-based process to produce man-made cellulose fibers with a novel acetate-based PIL (Michud, 2016).

The availability of commercialized ionic liquids and the higher price than conventional solvents are barriers to PILs' applications in larger scales (Plechkova & Seddon, 2007). The recycled ionic liquids with over 50 cycles can make the price of ionic liquids significantly cheaper (Plechkova & Seddon, 2007). The level of purity can influence the cost and applications of ionic liquids (Kuzmina & Hallett, 2016). Impurities cause significant impacts on PILs' properties (Kuzmina & Hallett, 2016). Therefore, purification can be performed on PILs' products during synthesis stages and on recycled PILs (Kuzmina & Hallett, 2016). Table 3 introduces several purification methods of ionic liquids.

Table 3. ILs' suppliers and their purification methods

Company names	Purification methods	Reference
BASF	Short path distillation	(BASF, 2010)
Sigma-Aldrich/Merck	Rotary evaporation	(Sigma-Aldrich, 2019)
IoLiTec	Carbonate based ionic liquid synthesis (CBILS) Ultrapure ILs >99%, water and halide content<10-50 ppm	(Beyersdorff et al., 2017)
Solvent Innovation GmbH	Phase separation, Distillation	(Runge, 2014)
Proionic	Carbonate based ionic liquid synthesis	(Proionic, 2019)
TCI Chemicals	Extraction with organic solvents	(TCI, 2019)
Liuotin Group Oy	Vacuum distillation Activated charcoal	(Vallinkoski, 2019)

3. SEPARATION AND PURIFICATION PROCESS REVIEW

There are several barriers for ionic liquid commercialization, including scaling up, price, chemical and thermal stability, purity, recovery and recycling, disposal, and toxicity. Currently, ILs are more expensive than conventional organic solvents produced at large application scale. Recovery and recycling ILs are critical to lower the material cost and reduce waste generation. However, purification of ILs is a big challenge for both manufacturers and ILs users. (Siriwardana, 2015)

3.1. Common impurities from ILs

Common impurities from ILs can be water, organic materials, particles or halides. The impurities can influence to the physicochemical properties and applications, likewise the cost of ionic liquids. (Siriwardana, 2015)

Water is the most abundant impurity found in ILs. Vacuum drying for several hours can be applied to remove water from ILs, but it can cause loss of conjugate acid or conjugate base from PILs. Anions as acetate ions can form conjugate acids with water and then evaporate to leave hydroxide impurities. The additives as chemical

drying agents can be used to remove residual water, but they can be remained in ILs as another impurities. The clean synthesis such as the synthesis in dry conditions and with dry reagents is recommended to avoid water accumulated in ILs. (Clare et al., 2009)

Unreacted organic starting materials and residual organic reaction solvents can be removed by vacuum evaporation. The vacuum extraction with a low boiling and immiscible organic solvent like diethyl ether can be used likewise to remove these impurities. (Clare et al., 2009)

Suspended particles come from by-products of synthetic reactions or from additives. Filtration can be applied to remove particulates, for instance, by simply using a 200 nm PTFE syringe filter. (Clare et al., 2009)

Halide and alkali metal salts come from by-products of metathesis. Washing with water can be used to remove these impurities for hydrophobic ILs, whereas hydrophilic ILs can be washed using water immiscible solvents such as dichloromethane. (Clare et al., 2009)

Many impurities are not detectable by using similar analytical techniques for IL structure confirmation as ^{1}H NMR. The water content can be identified by using ^{1}H NMR or Infrared spectroscopy or Karl-Fischer titration. Unreacted starting materials can be detected by ^{1}H NMR or atomic absorption spectroscopy. Halide impurities can be analyzed by ion chromatography, ion selective electrodes, or induced coupled plasma-mass spectrometry. (Clare et al., 2009)

3.2. Separation and purification methods overview

Several separation and purification methods have been studied and published for various ILs. The interaction of ionic liquid and water is a key factor in the selection

of the appropriate recovery technique (Sklavounos et al., 2016). The separation process of hydrophobic ILs is easy, whereas the separation process of hydrophilic ILs is complex and energy intensive (Sklavounos et al., 2016). Different technologies used to separate and purify ionic liquids present in Appendix 2, including phase separation, crystallization, extraction, distillation, membranes, adsorption, and force field. The use of one single method may not be enough to obtain the required purity of ILs in practice (Zhou et al., 2018). Consequently, combined recovery processes have been applied for recovery of ILs (Zhou et al., 2018). For instance, the combination of filtration and extraction and evaporation can be effective for the removal of both non-volatile and volatile impurities (Zhou et al., 2018). Other unit operation combinations such as crystallization of spent electrolytes after electrodeposition process with extraction of residue after crystallization and two steps nanofiltration can be implemented, but it requires further validation (Zhou et al., 2018). Furthermore, distillation and extraction were combined by the Eastman Chemical company to recover ILs (Zhou et al., 2018).

The optimization of the recovery process requires further studying, such as separation mechanism, thermodynamic and kinetic analysis, energy consumption, or capital costs (Zhou et al., 2018). It is possible to synthesize ILs as cleanly as possible to minimize impurities as by-products from side reactions or from the starting materials (Clare et al., 2009).

3.3. Batch distillation

Distillation is a method for separation of liquid mixtures based on gradient of boiling and condensation points (Zhou et al., 2018). The color of pure ILs can be clear or colorless. Chromophores impurities can cause the changing of color to yellow or orange ILs (Taylor et al., 2010). Distillation is a potential method to obtain clear and colorless ILs.

ILs can be distilled via three various distillation mechanisms. Firstly, distillation of volatile species can be implemented by a rotary distillation, or a thin-film evaporator, or a molecular distillation (Zhou et al., 2018). Secondly, carbene bases can be distilled and decomposed into distillable neutral compounds by deprotonation of ILs cations (Zhou et al., 2018). Lastly, distillation of intact ion pairs can occur (Zhou et al., 2018). Increasing temperature can enhance the distillation rate but cause decomposition reactions (Taylor et al., 2010). Consequently, evaporation from a relatively thin film without bubbling in ultra-high vacuum to keep the boiling point as low as possible can achieve the maximum distillation rate at the lowest temperature (Taylor et al., 2010).

Batch distillation can recover volatile compounds from liquid mixtures (McCabe et al., 2005). The working principle is feeding liquid solution into a bottom still heated to boil the liquid and vaporize through a column to a condenser (McCabe et al., 2005). Reflux controller can be mounted on the top of the column to improve the separation process (McCabe et al., 2005). The distillation process can be implemented at the constant reflux ratio and stop whenever getting a certain value of products (McCabe et al., 2005). The distillation can be conducted at total reflux to reach equilibrium phase before distillate is collected, for instance, a Vigreux column requires a half an hour while a packed column requires more time (Zuiderweg, 1957). It is not unnecessary, but dangerous to distil to empty the bottom still because of the high risk of decomposition by overheating (Zuiderweg, 1957).

A packed bed column filled with packing materials such as Dixon rings and an unpacked column as a Vigreux column can be used for vacuum distillation (Fig. 6). The packed bed column has a higher separation power than the Vigreux column in the same size. However, there are several disadvantages of packed bed columns, especially larger holdup, higher pressure drops, lower capacity, and longer time for reaching a steady operation regime than Vigreux columns. On the other hand, the

Vigreux column is a cylindrical glass tube with fixed glass structures inside the column (Fig. 6). The separation power is proportional to the length of the column but is inversely proportional to the diameter of the column. For instance, a Vigreux column one meter in length with the internal diameter around 25 mm can have three or four theoretical plates under total reflux. (Zuiderweg, 1957)

Figure 6. The inside structure of a Vigreux column and Dixon ring 1/8" of a randomly packed column (Nichols, 2019) (Alford et al., 2011)

3.4. Short-path distillation

Short-path vacuum distillation (SPD) is a gentle distillation method for thermally sensitive liquids, high viscosity, low vapor pressure, and high molecular weight (Kuzmina & Hallett, 2016). SPD is a single stage distillation unit (Walas, 1990). SPD consists an evaporator with the distance between the hot and cooling surfaces less than the mean free path of molecules (Walas, 1990).

SPD has lower evaporation temperature and shorter residence time (Kukla, 1997). The operating principle of SPD is similar with the principle of thin film evaporator, but the operating pressure can be in the range of μbars, and with the internal condenser located in the center of the evaporator (Kukla, 1997). The material is fed continuously onto the inner surface of the vertical evaporator glass or metal

cylinder (Kukla, 1997). The material flows downwards by gravity and the roller wiper system ensures a uniform thin film of feed product on the evaporator surface (Kukla, 1997). Scratches and the fouling of the evaporator surface can be avoided, and the pressure drop can be minimized (Kukla, 1997). The evaporator surface area can vary at different scales in laboratory, pilot plants, or industrial production plants (Kukla, 1997). The evaporator jacket can be a double wall which is heated by a heat carrier liquid (Kukla, 1997). The vapor evaporates from the liquid film and hits the internal condenser to condense as the distillate, while the compound which does not vaporize is collected as the residue (Kukla, 1997). Figure 7 shows the schematic diagram of a short-path distillation and the transfer behaviours of light and heavy components. The compound A can be considered as a low boiling compound running down from the evaporator surface to generate vapour pressure proportional to the molar fraction (Meyer et al., 2011). The evaporation of compound A can happen when the vapour pressure above the residue film (at the evaporation temperature) is higher than the partial pressure of the compound A (Meyer et al., 2011). Similarly, the condensation of compound A can occur when the partial pressure of the compound A is higher than the vapour pressure above the condensate film (at the condensation temperature) (Meyer et al., 2011). The evaporation stops when the vapour pressure above the residue film equals the vapour pressure above the condensate film (Meyer et al., 2011). On the other hand, the distillation process occurs whenever there is a difference between the evaporator and the condenser temperature (Hicknam, 1943).

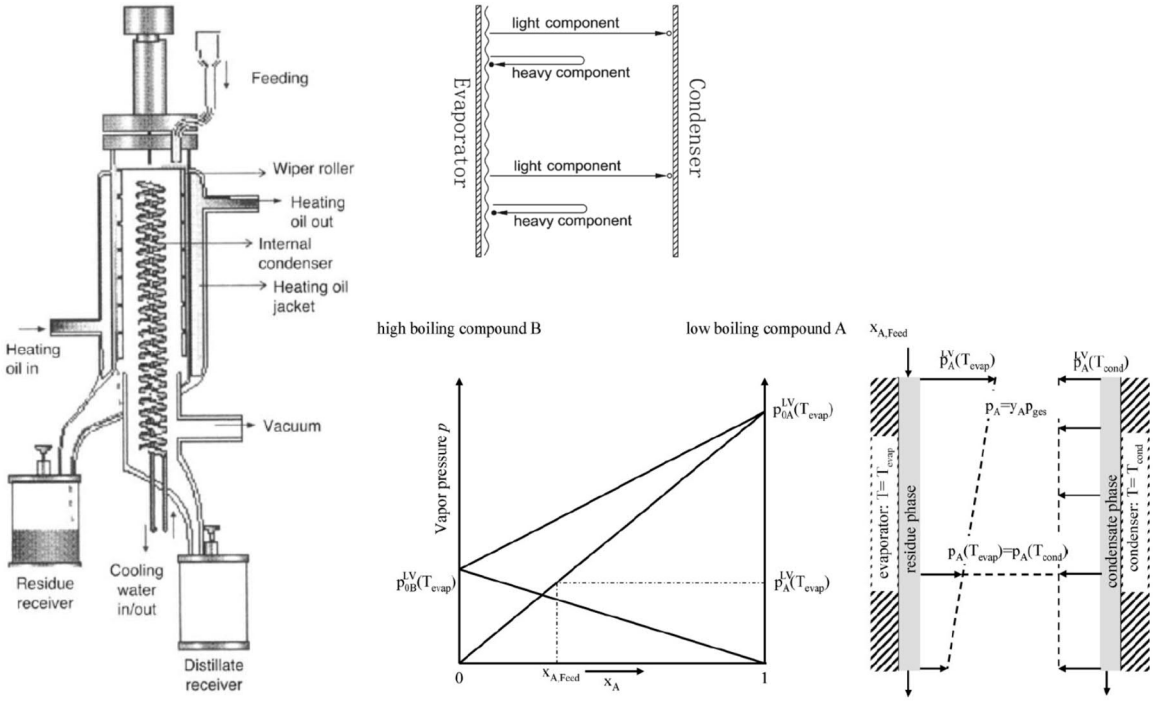

Figure 7. The schematic diagram and operating principles of a short path distillation (Xu, 2005) (Zhu et al., 2016) (Meyer et al., 2011)

There are several factors that affect the separation efficiency such as the feed rate, evaporator temperature, wiper speed, or feed temperature (Xu, 2005). Increasing feeding rate increases the process productivity but decreases the residence time (Xu, 2005). The separation efficiency can be reduced with too high evaporation temperature (Xu, 2005). Moreover, the speed of the wiper can be adjusted to control the thickness of the falling film, the flow mixing, and the splashing of residues to the distillate (Xu, 2005). Preheating and degassing feed can be implemented in large-scale evaporation operation (Xu, 2005). Splashing can ruin distillation and the reasons come from imperfect degassing of feed, fissures or cracks or dirt on the surface, or too rapid evaporation (Hicknam, 1943).

SPD has been developed for the separation and purification of intermediates and final products in the pharmaceutical, food and chemical industry (Kukla, 2000).

Appendix 3 shows various applications of SPD in laboratory and pilot scales. Appendix 4 presents the operating procedure and trouble shooting guideline for SPD.

4. THERMODYNAMIC MODELS AND OPERATION UNITS REVIEW

Phase behavior of binary of ionic liquid and water, or ionic liquid and organic solvent, are the important characteristics for designing separation process. The mutual solubility of ionic liquid and water depends on the type of anions and the alkyl chain length of cations. Increasing the alkyl chain length of cations decreases the mutual solubility. Figure 8 shows the upper critical solution temperature (UCST) behavior of imidazolium-based ionic liquid with water. The higher temperature increases the mutual solubility of the ILs and water, and limits to the UCST. The UCST can be found at very small fraction of the ILs. However, other binary system can have lower critical solution temperature (LCST) behavior. The structure of ionic liquid influences on the phase behavior (UCST or LCST). (Goodwin et al., 2010)

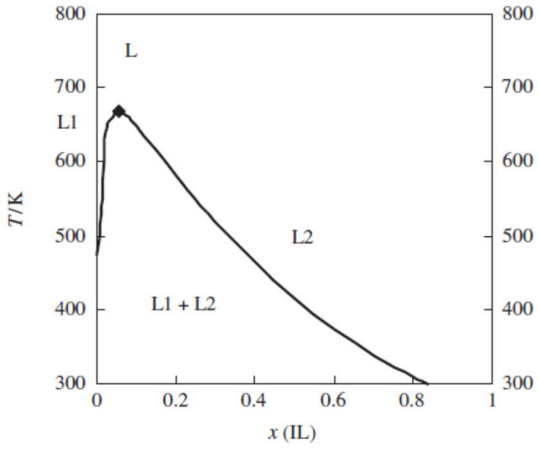

Figure 8. The UCST phase behavior of imidazolium - based ionic liquids (Goodwin et al., 2010)

There are several approaches to predict phase behavior of ionic liquid systems, including molecular simulation, excess Gibbs energy method, Equation of State modeling, and quantum chemical method. The molecular dynamic simulation can use to obtain thermodynamic properties and phase equilibrium data by using Monte Carlo simulation and to determine the solvation behavior of ionic liquid systems by means of solving Newtonian equations. The excess Gibbs energy method can be applied to correlate phase behavior of ionic liquid systems by measuring the pressure and temperature versus phase compositions and phase change. There are two popular excess Gibbs energy methods for nonelectrolytes mixtures, especially the nonrandom two liquid (NRTL) and the universal quasi-chemical equation (UNIQUAC). The NRTL model can be successfully used for correlating phase behavior of ionic liquid with water, or with organics. Nonelectrolytes models can be applied because ionic liquids exist as neutral ion pairs and an equimolar mixture of two dissociated cation and anion ions in the presence of water or alcohol. The statistical-mechanics based equations of state like truncated perturbed chain polar statistical associating fluid theory (tPC-PSAFT) is difficult to predict phase equilibria of ionic liquid system with strongly polar compounds like water or alcohols. The conductor screening model for real solvents (COSMO-RS) can be used for the prediction of the phase behavior of ionic liquid system containing water or alcohols. (Goodwin et al., 2010)

The accurate model of ionic liquids recycling process is quite important for the process design and optimization of a large industrial scale (Ilmanen, 2017). Currently, there are no models available for short-path distillation or molecular distillation in Aspen Plus ™ (Ilmanen, 2017). Other barriers are lack off thermodynamic data of ILs, also physical and chemical properties of ILs in data bank of the simulator software Aspen Plus ™ (Kazmi et al., 2019). ILs can be modeled as pseudo components so that physicochemical properties must be provided to Aspen Plus ™, such as molecular weights, normal boiling temperature, density, and vapor

pressure. The thermodynamic properties of ILs must include the enthalpy of vaporization, the standard state enthalpy of formation, heat capacity, and Gibbs free energy, also the equilibrium constant K_{eq}. The saturated vapor pressure data of ILs must be known and obtained from experimental data.

On the one hand, the use of UNIFAC, which is a predictive thermodynamic model required to decompose cations and anions of ILs into several electrically neutral groups (Kazmi et al., 2019). On the other hand, the NRTL model can be used for both vapor-liquid equilibrium (VLE) and liquid-liquid equilibrium (LLE) of multicomponent systems (Kazmi et al., 2019). The NRTL model is more accurate for liquid-liquid equilibria containing water and organic substances like ILs (Kubiczek & Kamiński, 2017). However, it is necessary to define the binary NRTL parameters based on experimental data (Kazmi et al., 2019). Table 4 indicates the binary NRTL parameters of the binary mixtures of water and pure base 1, and water with S1. Similarly, binary NRTL parameters of the binary mixtures were obtained from the experimental data for water and pure base 2, water and the complex of S2.

Table 4. Binary NRTL parameters for left side: water (1) and the base 1 (2), right side: water (1) and S1 (2) (Ostonen, 2017)

	NRTL[a]
a_{12} (K) or a_1	-111.3
a_{21} (K) or a_2	-11.87
b_{12} or a_3	4.88
b_{21} or a_4	-1.983
$\alpha_{12=21}$	0.48
P, AAD (%)	4.0
Number of points	63
T range (K)	312.7-352.1

	NRTL[a]
a_{12}	-0.78973
a_{21}	-6.28699
b_{12} (K)	1337.985
b_{21} (K)	550.334
$\alpha_{12=21}$	0.2
P, AAD %	3.74
Number of points	54
T range (K)	302.7 – 353.5

[a] NRTL parameters: $\tau_{ij} = a_{ij} + b_{ij}/T(\mathrm{K})$ and $G_{ij} = \exp(-\alpha_{ij}\tau_{ij})$

Note: ADD is the absolute average deviation

APPLIED PART

5. METHODOLOGY

5.1. Materials and chemicals

The experiments were implemented using two types of PILs named S1 and S2. The acetic acid was purchased from Sigma-Aldrich with the purity of 99.8 %. The thesis was studied mainly pure S2 contained the equimolar amount of base 2 and acetic acid. In addition, S1 was made from base 1 and acetic acid was used to study the short path distillation device. Moreover, one sample with added 3 wt.% of DI water and another one with added acetic acid (Sigma-Aldrich, 100 wt% purity) to S2, were prepared for the experiments.

5.2. Batch distillation experiments

The batch distillation experiments were conducted by using a randomly packed bed distillation and a Vigreux column (Fig. 9). The Vigreux distillation experiment setup consisted of a bottom round flask (1), a heating system (2), a Vigreux column (3), a condenser (4), a water bath (5), a fraction separator (6), round glass flasks of fraction collectors (7), a magnetic reflux control, a vacuum pump, a cold trap contained liquid nitrogen, two temperature sensors, a pressure meter. The randomly packed bed distillation column filled by 1/8 inches Dixon-ring was used to distillate pure S2. The isolation was applied for both columns to prevent heat loss during the experiments.

Figure 9. The randomly packed distillation column (left side) and Vigreux distillation column (right side)

The experiment was started by weighting an amount of S2 into a bottom flask. The flask was connected to a Vigreux column. A temperature probe (10) connected to a temperature reading panel (9) and was put in the temperature probe pocket located in the bottom flask. Another temperature probe (11) was put in the temperature probe pocket located in the top of the column. A fraction collector was connected to the condenser part. Three small round glass flasks were attached to the fraction collector. The column was sealed by using vacuum grease. Liquid nitrogen was filled to a cold trap. A vacuum pump was turned on and closed the vacuum relief

valve. A heating bath of the bottom flask was switched on level 2 indicated power of 106 W when the pressure was at the expected value. An agitator control was switched on to ensure the agitator working during the heating time. A water bath was used for cooling of the condenser and set up 50 °C. A magnetic reflux control was switched on to collect different fractions when the vapor rose to the top of the column. Temperature values were read manually for each fraction when it was collected and once the collection was ending. The heating bath was switched off when three fractions had been collected. The vacuum pump was turned off when temperature had been lower than 100 °C. The experiment was ended. All samples including the feed, fractions, residue, cold trap, were weighted, and the compositions were analyzed by NMR, CE, and K-F.

5.3. Short path distillation experiments

The short path distillation device is made by UIC GmbH and the model is UIC_KDL5. The maximum capacity is 1.5 kg/h. The SDP plant consists of a distillation part (1), a feed system (2), distillate (3) and residue system (4), heating units (5), internal condenser (6), and vacuum pump set (7) with a rotary vane and an oil diffusion pump with a vacuum measuring device (8) as shown in Figure 11. The feed system consists a 2 L vessel, a circulation thermostat and a circulation pump (230 V, 50 Hz, 2 kW), and a heating transfer oil container. The maximum temperature for the feed system is 150 °C. The feed rate can be adjusted between 0 - 1.8 L/h, and the maximum permanent rate is 1 L/h and the first feed rate can be at 0.2 L/h.

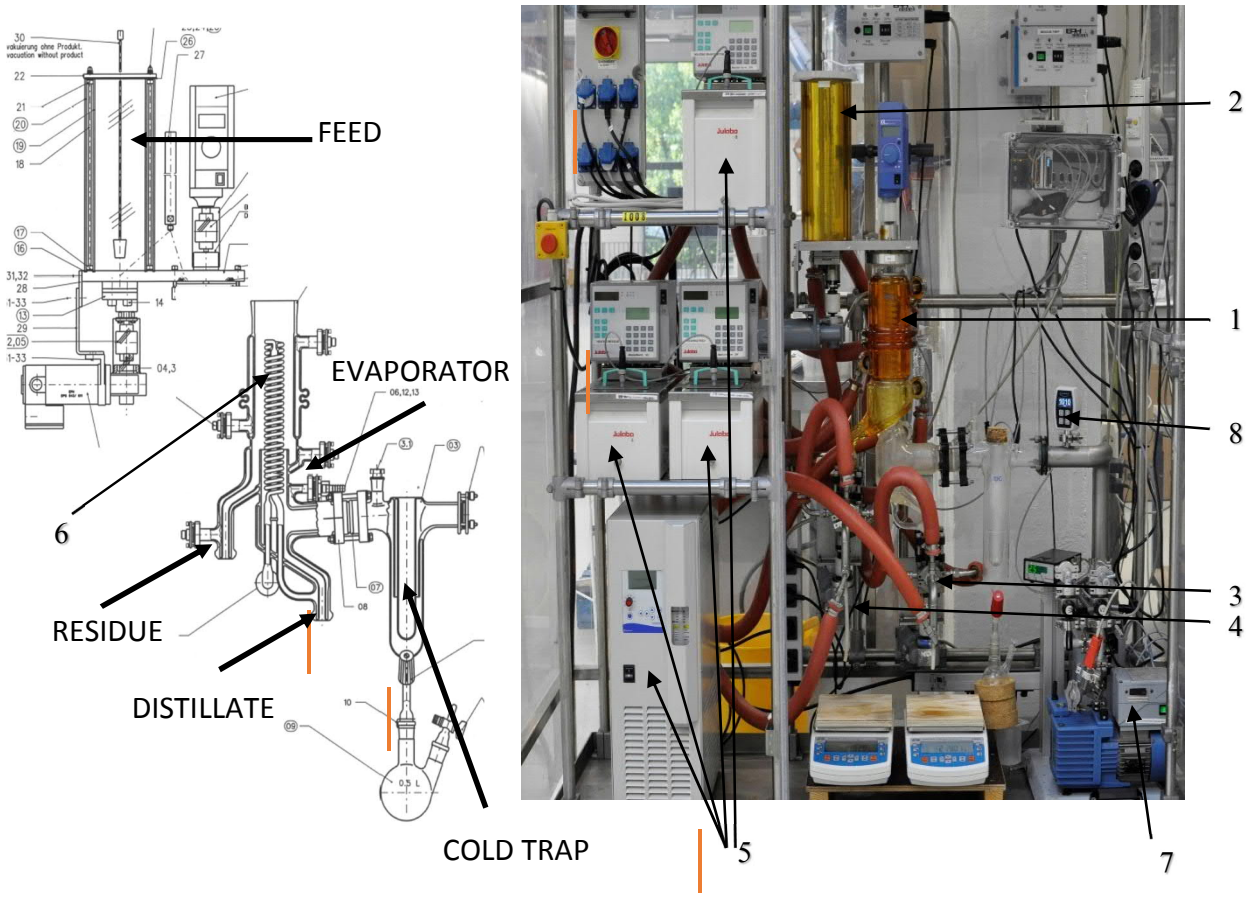

Figure 10. The short path distillation device

SDP is a glass apparatus with a double jacket for heating and cooling by a thermal fluid. The evaporator unit includes a circulation thermostat and a circulation pump (230 V, 50 Hz, 3 kW) with a heating oil bath for the jacket of the evaporator. The evaporator surface area is 0.048 m^2. The wall thickness of the evaporator is 3 mm. The evaporator temperature range is 25-250 °C. The internal condenser is connected to a heating transfer oil container included a circulation thermostat and a circulation pump (230 V, 50 Hz, 2 kW). The outlet nozzles for distillate and residue are heated or cooled by heat transfer fluid. The residue and distillate discharge systems include circulation thermostats and circulation pumps (230 V, 50 Hz, 2 kW) with heating transfer oil bath. The condenser surface is 6.5 dm^2. The thickness of the

condenser tube wall is 1 mm. The flanged cold trap connects a glass round bottom flask to collect condensate compounds. The roller wipe system (with motor 400 V, 50 Hz) can be manually adjusted to rate from 200 to 500 rpm, and the optimal speed is 300-400 rpm.

Experiments were made for S1 and S2 using SPD device. The distillation experiment with S1 was conducted at first at the lowest obtained pressure of SPD. As a cheaper PIL, S1 was used to check SPD performance including defining the operating procedure (Appendix 4.1) and finding problems of the SPD as mentioned in the troubleshooting guide (Appendix 4.2). The experimental steps were following to the operating procedure. In general, the experiment could be started after evacuation of the SPD at the expected vacuum level. The PIL was filled into the feed vessel. The feed pump was turned on when the temperature of the evaporator had reached the set point. The liquid was pumped to the evaporator and started to vaporize. The wiper was controlled to have a thin film layer on the evaporator surface. The vapor could reach to the internal condenser and condense as light components collected as the distillate. The heavy components could not vaporize, then were removed as the residue. All samples including the feed, distillate, residue, cold trap, were weighted and analyzed by NMR, CE, and K-F.

The recovery yield is calculated as the following equation (Babeanu et al., 2018):

$$Y = \frac{d \cdot C_D}{C_F} \cdot 100 \qquad (3.3.1)$$

where $d = \frac{D}{(D+R)}$ *: distillate weight fraction (D: distillate (g) and R: residue (g))*

C_D*: mass fraction of IL in distillate*

C_F*: mass fraction of IL in feed*

The yield of a compound in distillate phase and in residue phase can be calculated as the following equations (Meyer et al., 2011):

$$Y_{i,D} = \frac{C_{i,D} \cdot m_D}{C_{i,F} \cdot m_F} \quad (3.3.2)$$

$$Y_{i,R} = \frac{C_{i,R} \cdot m_R}{C_{i,F} \cdot m_F} \quad (3.3.3)$$

where $C_{i,D}$: concentration of compound i in distillate

$C_{i,R}$:concentration of compound i in residue

$C_{i,F}$: concentration of compound i in feed

m_D: mass of compound i in distillate

m_R: mass of compound i in residue

m_F: mass of compound i in feed

The Rayleigh equation is used to estimate the separation efficiency of continuous-film evaporators (Xu, 2005):

$$\alpha = 1 + \frac{\ln\left[\frac{X_R \cdot (1-X_F)}{X_F \cdot (1-X_R)}\right]}{\ln\left[\frac{R \cdot (1-X_R)}{F \cdot (1-X_F)}\right]} \quad (3.3.4)$$

where α: relative volatility

X_R: mole fractions of the residue and X_F: mole fractions of the feed

R: residual flow (mol/s) and F: feed flow (mol/s)

The evaporation rate (ER) can be calculated as the following equation (Krell, 1982):

$$ER = 0.0583 \cdot p \cdot \sqrt{\frac{M}{T}} \quad (3.3.5)$$

with ER: practically evaporation rate (g/cm^{2}s)

T: the temperature of the surface (K)

p: the vapor pressure of the substance (mmHg) at T

M: the molecular weight (g/mol)

The mean free path (MFP) can be computed by the following equation (Lutišan & Cvengroš, 1995):

$$MFP = \frac{R \cdot T}{\sqrt{2} \cdot \pi \cdot d^2 \cdot N_A \cdot p} \quad (3.3.6)$$

with R = 8.314 (m^3. Pa/ (K. mol)): gas constant

T: distillation temperature (K)

p: distillation pressure (Pa)

d: diameter of molecules (m)

N_A = 6.02214 ·10^{23}: Avogadro constant

5.4. Analytical methods

5.4.1. Nuclear Magnetic Resonance Spectroscopy (NMR) measurement

All samples were analyzed using an NMR Agilent AVIII400 instrument (Bruker). The analytical method was developed by the Biorefinery group of Aalto University. A small amount of the sample (e.g. 1 mL) was withdrawn and put into an NMR glass tube. The sample was diluted with dimethylsulfoxide D6 (99.8% D) (DMSO-d_6). The NMR tube contained the sample was mixed to ensure homogenous liquid. The

detailed operation procedure of the NMR instrument is explained in Appendix 5. The NMR results were evaluated with MestReNova program based on the analytical information of Helsinki University. The peaks of the base, acid and by-products were recognized. For S1, NMR results were computed for the group -CH_2 of the base and the group -CH_3 of the acid, therefore, the integral ratio of the base was at one, the integral ratio of the acid was multiple of 2/3. For S2, NMR results were computed for the methyl group of the base and the acid, therefore, the integral ratio was read directly from NMR spectrum. The mole fraction was computed based on the integral results. The acid to base ratio was calculated and presented in the experimental results chapter.

5.4.2. Capillary electrophoresis (CE) measurement

All samples were also analyzed by CE Agilent 7100 instrument. The sample preparation and measurement procedures are presented in Appendix 6. The integral results were recorded, and the mass fraction of the base and by-products were calculated based on the calibration curve. The mole fraction of the base and by-products were computed based on the mass fractions. The CE results were used as the reference data of distillation experiments.

5.4.3. Karl-Fischer titration (K-F)

The water content was measured by Karl-Fischer titration of Mettler Toledo DL53. The detailed operating procedure is explained in Appendix 7. The estimated water content in samples was 3 wt.%. However, it is necessary to handle careful S2 as it has high viscosity and crystallized easily at room temperature.

5.4.4. Ultraviolet-Visible spectrophotometer (UV-Vis)

The samples of SPD experiment with S2 were tested by UV-Vis of Shimadzu 2550 to compare change of color. Approximately one gram of the sample was

weighted and diluted with distilled water in 100 mL flask. The absorbance of the feed, distillate and reside were measured for each experiment. The absorbance was measured in the range of wavelengths from 200 to 600 nm.

6. RESULTS AND DISCUSSIONS FOR BATCH DISTILLATION EXPERIMENTS FOR PIL SOLVENT

Chapter 6 reports the batch distillation experimental results. Section 6.1 presents the experimental conditions used and material balance based on nuclear magnetic resonance (NMR) analysis; then it moves on to introduce the vapor pressure of pure base and its complex; and lastly by-product presents based on NMR results. Section 6.2 evaluates the Aspen simulation results with the experimental results. Section 6.3 summarizes discussions and conclusions of batch distillation for protic ionic liquids.

6.1. Distillation results

This section reports experimental results from a Vigreux distillation column to study the evaporation behavior of S2.

6.1.1. Batch distillation results of the Vigreux distillation column experiments

Fractional distillation process was carried out by evaporating a liquid mixture into number of distillate fraction products. The process occurs by applying heat to vaporize molecules of the liquid and condense the separated vapor into a liquid distillated by cooling. Table 5 summarizes the distillation results, especially the compositions of feed and products. The detailed information of each experiment is shown in Appendix 8.

Table 5. Distillation conditions and compositions of the feed, distillate, residue for Vigreux distillation experiments

Experiment Number	Pressure (mbar)	Average Bottom temperature (°C)	Average distillate temperature (°C)	Feed acid:base ratio	Distillate acid:base ratio	Residue acid:base ratio	Distillate from the top (wt.%)	Residue in the bottom (wt.%)	Cold trap (wt.%)	Loss ([c]) (wt.%)	Sample state of distillate (at room temperature and when fractions collected)
1	(1) 0.23	(1) 130	(1) 68	1.51: 1	(1) 0.13: 1	1.51:1	(1) 18	4	4	14	(1) clear liquid
	(2) 0.26	(2) 139	(2) 123		(2) 1.25: 1		(2) 31				(2) solid crystals
	(3) 0.21	(3) 143	(3) 123		(3) 1.5: 1		(3) 49				(3) clear liquid
	(4) 0.24	(4) 160	(4) 118		(4) 1.5: 1		(4) 60				(4) light yellow liquid
	(5) 0.31	(5) 181	(5) 113		(5) 1.5: 1		(5) 78				(5) yellow liquid
2	0.7	(1) 134	(1) 82	1.01:1	(1) 0.1: 1	1.52:1	(1) 19	42	2	0	(1) clear liquid
		(2) 143	(2) 102		(2) 1: 1		(2) 48				(2) solid crystals
		(3) 168	(3) 117		(3) 1.49: 1		(3) 56				(3) clear liquid
3	1.1	(1) 137	(1) 88	1:1	(1) 0.03: 1	1.55: 1	(1) 16	38	1	4	(1) yellow liquid
		(2) 143	(2) 110		(2) 1.04: 1		(2) 43				(2) whitish solid crystals
		(3) 153	(3) 123		(3) 1.5: 1		(3) 57				(3) yellow liquid
4	5	(1) 145	(1) 100	1:1	(1) 0.02: 1	1.57: 1	(1) 20	47	3	-2	(1) yellow liquid
		(2) 148	(2) 119		(2) 0.28: 1		(2) 26				(2) clear liquid
		(3) 148	(3) 139		(3) 1.46: 1		(3) 52				(3) clear liquid with whitish solid crystals
5 ([a])	0.7	(1) 137	(1) 108	1.45:1	(1) 0.64: 1	1.63:1	(1) 12	14	1	9	(1) yellow liquid with whitish solid crystals
		(2) 138	(2) 128		(2) 1.41: 1		(2) 19				(2) clear liquid with whitish solid crystals
		(3) 140	(3) 130		(3) 1.5: 1		(3) 39				(3) clear liquid
		(4) 137	(4) 111		(4) 1.5: 1		(4) 52				(4) clear liquid
		(5) 155	(5) 112		(5) 1.6: 1		(5) 67				(5) clear liquid
		(6) 195	(6) 106		(6) 1.6:1		(6) 76				(6) clear liquid
6 ([b])	0.7	(1) 139	(1) 119	1.66:1	(1) 1.64: 1	1.78:1	(1) 32	11	5	5	(1) light yellow liquid
		(2) 150	(2) 122		(2) 1.51: 1		(2) 60				(2) clear liquid
		(3) 170	(3) 119		(3) 1.48: 1		(3) 79				(3) clear liquid

Notes: ([a]) Pure PIL added acetic acid ([b]) Pure PIL added acetic acid and water ([c]) Loss included samples collected for analysis ((Number) – The number of the fraction

The feed compositions and the pressure were changed in each experiment. Four experiments used pure S2 as the initial material. For the fifth experiment, the feed was pure S2 with 10 wt.% of acetic acid added (Sigma-Aldrich, 99.8 wt.% purity). For the sixth experiment, the feed was pure S2 with adding 15 wt. % of acetic acid (Sigma-Aldrich, 99.8 wt.% purity) and 3 wt.% of distilled water.

Six batch distillation experiments were conducted in a vacuum. The experimental pressure ranged from 0.2 to 5 mbar. At first, the column was run at the lowest obtained pressure 0.2 mbar as in the first experiment. However, the pressure was unstable during distillation due to lack of experience in controlling a vacuum process. Therefore, the average pressure was presented for each fraction of the first experiment. In addition, an average pressure of 0.27 mbar could be represented for the first experiment. The pressures were measured using a Vacuuview® pressure gauge with an uncertainty of 15%.

Distillation pressure changes cause changes in boiling point and distillate temperatures. The average boiling point temperatures of the first fractions were 145, 137, 134, 130 ˚C, at the vacuum pressure of 5, 1.1, 0.7, and 0.27 mbar, respectively (Table 5). The distillate temperature was unstable during the time of collecting fractional samples (see Appendix 8/1-8/6). Consequently, for the first experiment, the distillate temperature of the first fraction could be chosen as the initial temperature. For the second and fourth experiment, the average temperatures from the initial to final temperatures were reported for the distillate temperatures. The distillate temperature of the third experiment was estimated by the average between the initial and the final distillate temperature. Consequently, the average distillate temperatures of the first fraction were 100, 88, 82, 68 ˚C, at the vacuum pressure of 5, 1.1, 0.7, and 0.27 mbar, respectively (Table 5). In comparison of the distillate temperatures of the first fractions from the second, fifth and sixth experiments, the pure PIL has lower the reboiler and distillate temperature than PIL with excess acid

or water. Lower distillation pressure decreases the boiling and distillate temperatures for the pure S2.

The experimental conditions can influence the composition of distillate fractions and residue. ^{1}H-NMR analysis results were used to calculate the acid to base ratios. Material balances are indicated in Appendices 8/1-8/6. Figure 11 shows that pure base could be collected in the first fraction until 20 wt.% of feed distilled. At the higher temperature, the later products can be collected as the complex of S2 with excess acetic acid. Due to the position limit of the temperature probe length in the bottom flask, the bottom temperatures were recorded improperly. Therefore, the feed can not be distilled until the flask was empty. Nevertheless, it was possible to distil over 60 wt.% of feed.

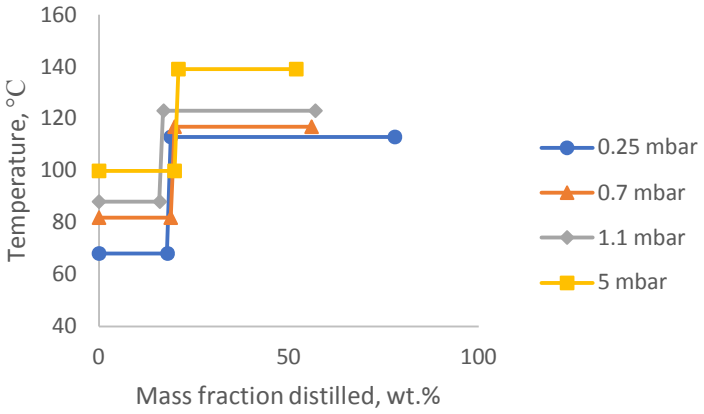

Figure 11. Distillate temperature profile of S2 (acid: base =1:1) as a function of mass fraction distilled at various pressures

For all material distilled, the acid to base ratios of the last fraction and the residue were the same as 1.5 (Fig. 12). This point can be considered as the azeotrope and no separation occurred. Therefore, the distillate temperature decreased in the last fractions while the bottom was still heating.

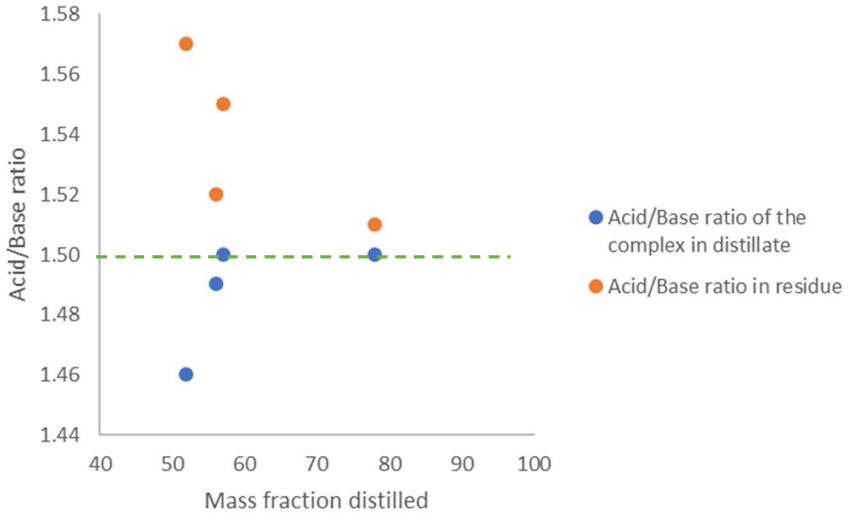

Figure 12. The acid to base ratios of the distillate and residue (bottom flask) from the 1st, 2nd, 3rd, 4th experiment with mass fraction distilled 78, 56, 57, 52 wt.%, respectively

Temperatures and compositions as a function of time for each experiment are presented in Figure 13. For pure PIL, the distillate temperature increased gradually when the pure base was distilled and reached the higher distillate temperature when the complex with 40 % mole of base was collected. This temperature was constant or reduced slightly to the end of distillation. However, the distillate temperature in experiments at 0.7 and 1.1 mbar was decreased in the beginning then increased back, because of the changing temperature of the bottom flask. PIL with excess acid kept the distillate temperature nearly constant and no pure base can be collected in the first fraction. In addition, the distillate temperature was dropping because of changing the fraction collectors as only three fractions were collected at the same time. Adding water affected to the separation of S2, and the complex was distilled.

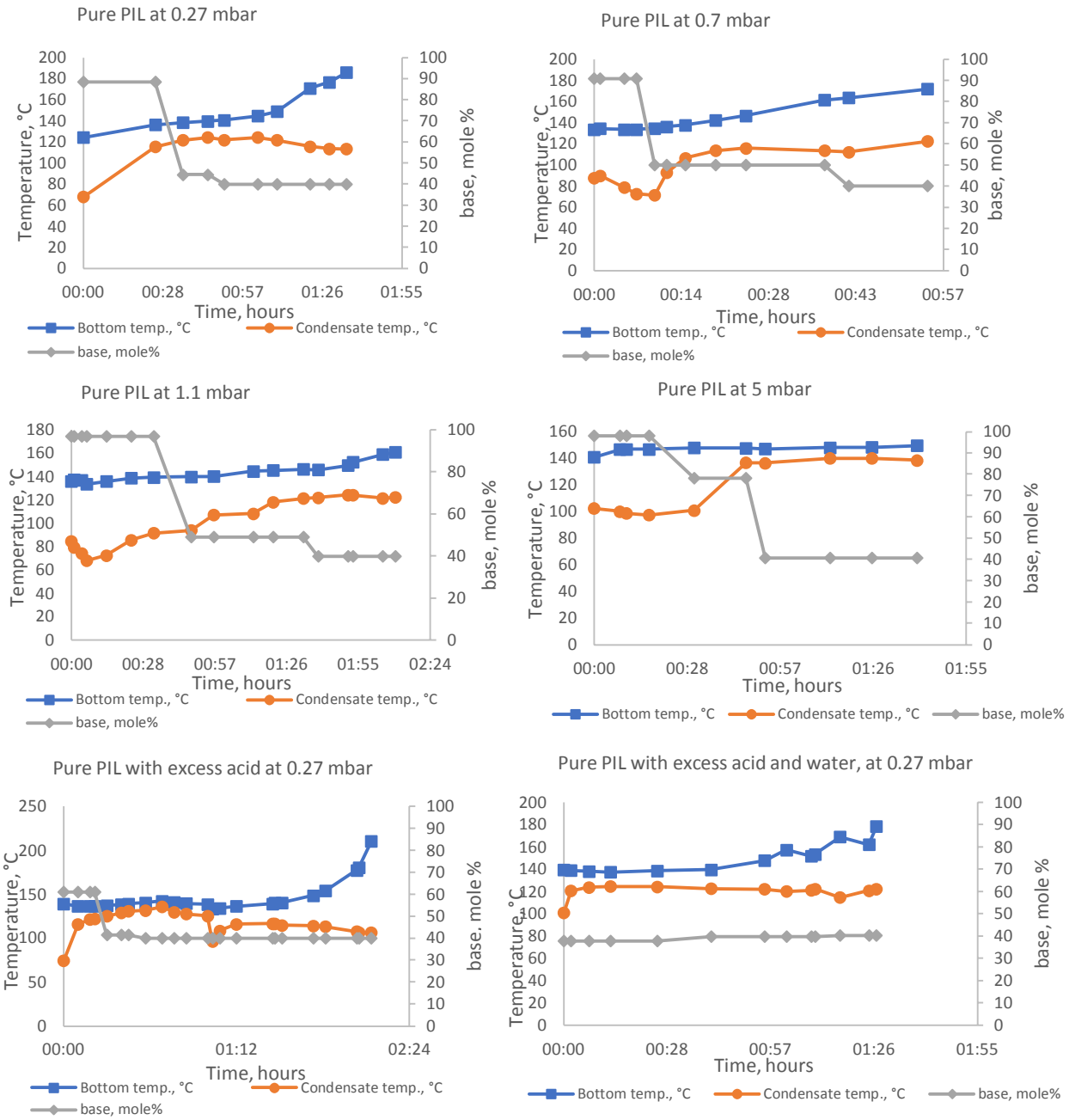

Figure 13. Distillation profile of batch distillation experiments using the Vigreux column

Molecular mass balance of each experiment indicated in Figure 14 based on measured mass of the initial feed, distillate fractions, residues, and cold trap, and NMR results. The loss can be from the column hold-up and in remnants in sample

containers due to the viscosity of the material. The loss of base was from 2 to 10 wt.% of feed. Hydrolysis product was found only in residue.

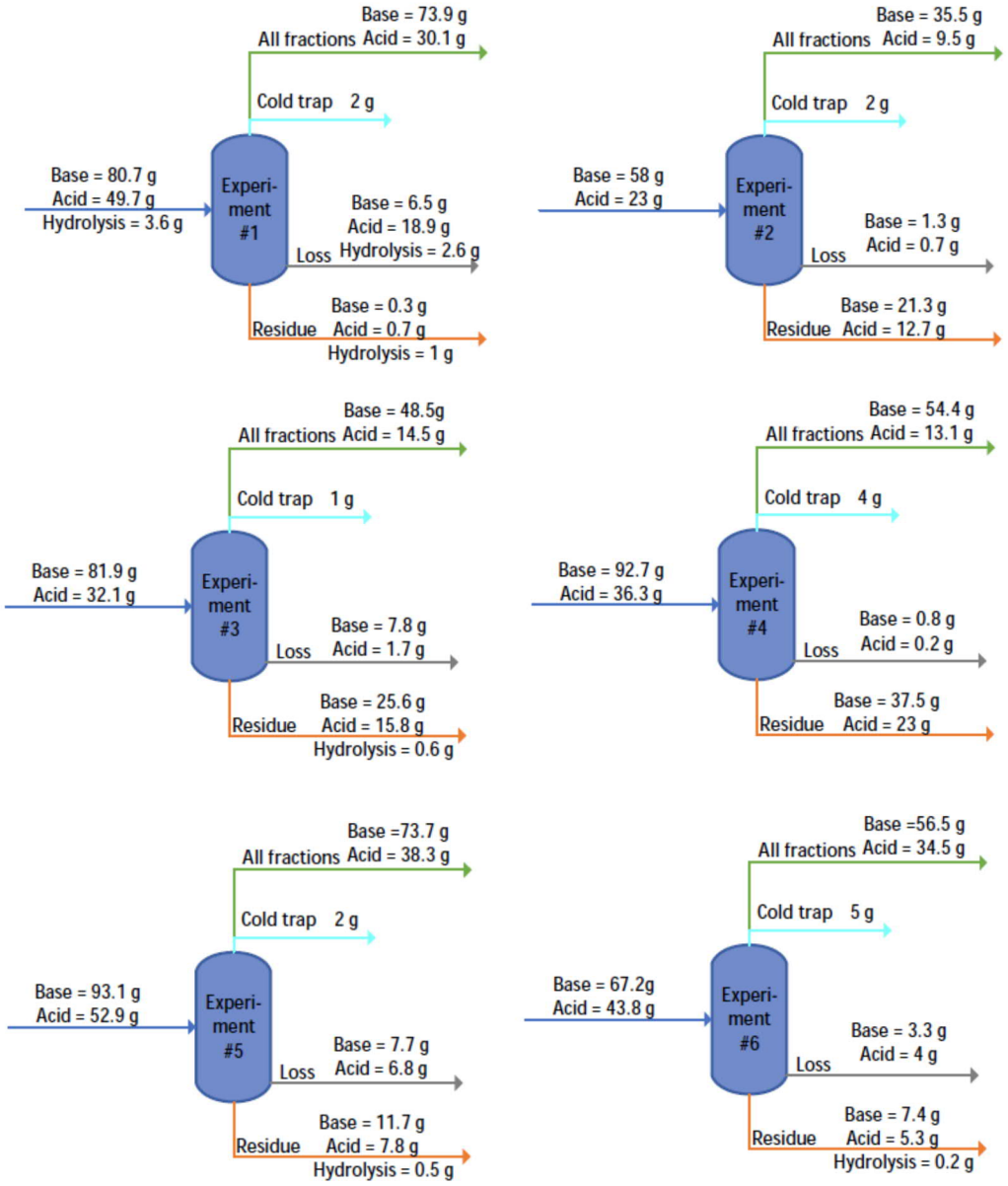

Figure 14. The molecular mass balance of the Vigreux distillation experiments

Batch distillation allowed to collect pure base and the complex with the appropriate conditions for pressure and temperature. The recovery was over 90 wt.% of the feed. The purity of the base 2 was obtained 99 wt.% in the first fraction. Hydrolysis product was not present in distillate but found in residue.

6.1.2. Evaporation behavior and vapor pressure of S2

The vapor pressure-temperature curve is necessary for a good understanding of the distillation process. The vapor pressure curve of pure base and the complex (acid: base =1.5:1) were compiled from the experimental results (Fig. 15). The distillate temperature of the pure base and the complex are shown for the experiments at 0.7, 1.1, and 5 mbar. The uncertainty of the pressure value is 15%, according to the manual of Vacuubrand®. The vapor pressure of pure base from the previous research was included in the vapor pressure curve (Baird et al., 2019). Consequently, the distillation process can be designed, for instance, the pressure of the column can be at 1 mbar equal to the vapor pressure of pure base with the distillate temperature at 80 °C, and at 120 °C for the complex.

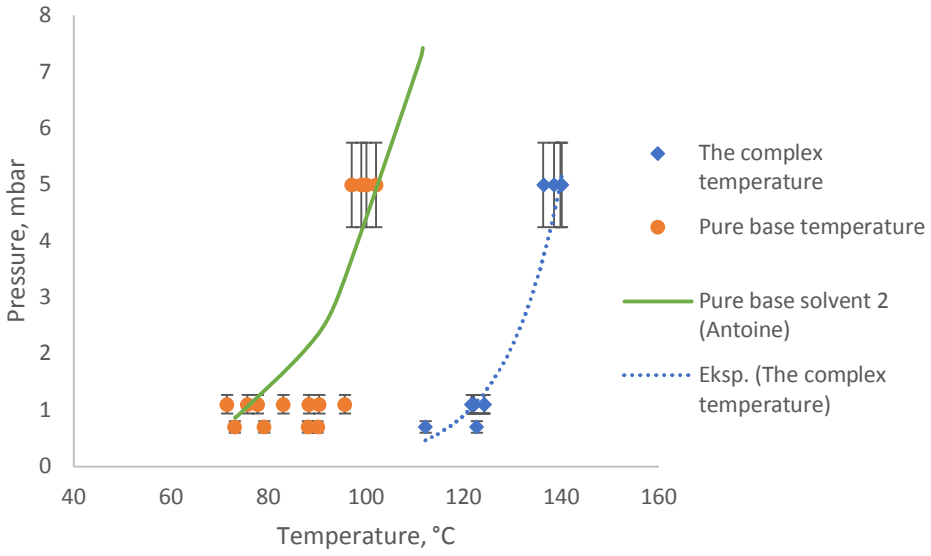

Figure 15. Vapor pressure curve of pure base 2 and its complex

6.1.3. By-product

By-product can be produced in the presence of water. There are two types of hydrolysis products as by-product, illustrated as seen in Figure 16. The first hydrolysis product was observed more than the second hydrolysis product in the residue. The second hydrolysis product was found in the first, fifth and sixth experiment. Distillation of pure PIL was observed without the second hydrolysis product, except the first experiment. In addition, in case of the feed contained hydrolysis product and distillation until no liquid left in the bottom flask, both hydrolysis products were significantly presented in the residue as in the first experiment.

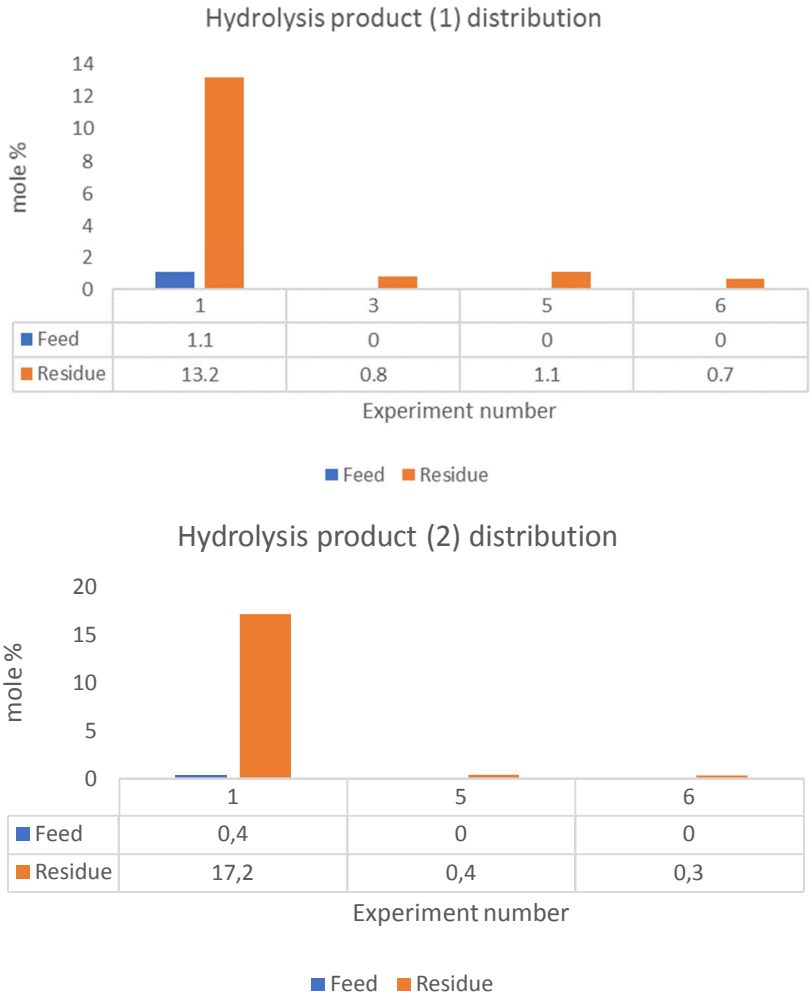

Figure 16. Hydrolysis products distribution in Vigreux distillation experiments

6.1.4. Randomly packed batch distillation column experimental results

Randomly packed batch distillation column was run for pure PIL in a range of 2.4 - 3 mbar (Table 6). Distillation was stopped after 22 wt.% of feed distilled. Only pure base was collected as a clear or yellow liquid. The condensate temperature and the bottom temperature were constant and increased slightly when the complex was distilled (Fig. 17). The molecular mass balance is introduced in Figure 18a and Appendix 8/7. The loss is higher than in the Vigreux column experiments due to larger hold-up. Hydrolysis products were found mostly in the residue.

Table 6. Distillation conditions of randomly - packed distillation experiments

Experi-ment #	Pressure (mbar)	The average bottom temperature (°C)	The average condensate temperature (°C)	Feed acid:base ratio	Distillate acid:base ratio	Residue acid:base ratio	Distillate from the top (wt.%)	Residue at the bottom (wt.%)	Cold trap (wt.%)	Loss (c) (wt.%)	Sample state of distillate
7	(1) 2.4	(1) 176	(1) 96	0.98: 1	(1) 0: 1	1.46:1	(1) 10	47	NA	31	(1) clear liquid
	(2) 2.8	(2) 178	(2) 98		(2) 0: 1		(2) 19				(2) yellow liquid
	(3) 3	(3) 179	(3) 105		(3) 0.58: 1		(3) 22				(3) yellow liquid with whitish crystals

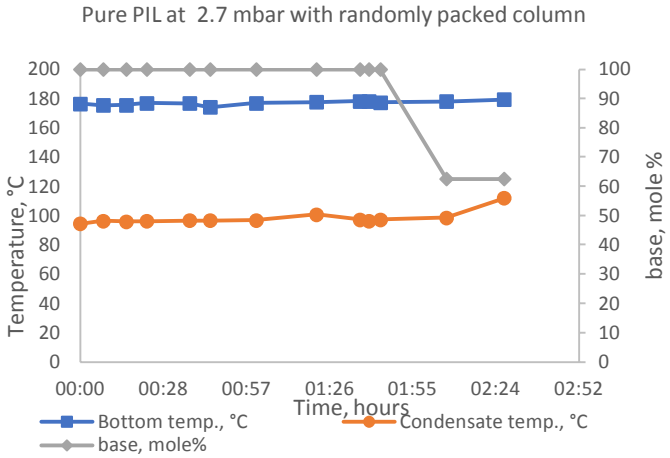

Figure 17. Distillation profile of randomly packed column

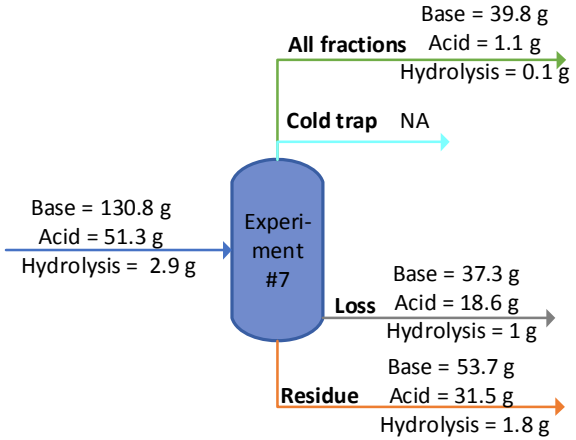

Figure 18. Molecular mass balance of randomly packed column

6.2. Distillation results in comparison with Aspen model

The equilibrium multistage model with better the evaporation efficiency is more accurate than the single stage simulation model (Ilmanen, 2017). In addition, the RadFrac unit with Newton's algorithm can be used to build batch distillation model for ILs (Kazmi et al., 2018). Therefore, an Aspen model comprised of 10 RadFrac units were made to simulate for the Vigreux distillation column experiments (Fig. 19).

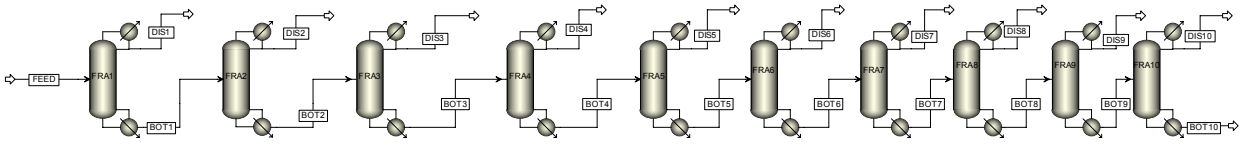

Figure 19. The flowsheet of Aspen model for batch distillation experiments

The properties of the Vigreux column was used to construct the simulation model as seen in Table 7.

Table 7. The Vigreux column properties

Inner diameter	15-25 mm
Column length	~ 1 m
The number of theoretical plates under total reflux (Zuiderweg, 1957)	3-4 stages
The experimental minimum equilibrium stages (see Appendix 9)	9-10 stages
The number of stages in the Aspen model	3 stages
Reflux ratio	1

The simulation was made for the Vigreux distillation column experiments at 0.23, 0.7, 1.1, and 5 mbar. The distillate to feed ratio was evaluated to get the mass fractions of the distillate and residue equal to the experimental results. The simulation results are shown in Appendix 10. A comparison was made between the simulation results and the experimental results for the first three fractions, including the mole fractions of compositions in distillate, acid/base ratio, and distillate temperature at each mass fraction distilled.

Figure 20 presents three fractions at one single pressure (i.e. grey points) with both the mole fraction of base from the Aspen simulation results (i.e. blue points) and the experimental results based on NMR results (i.e. orange points). The Aspen results can't get the pure base in the first fraction, while the experimental results were indicated nearly 100 % of base. Nevertheless, the Aspen results matched the experimental results for the later fractions where higher than 30 wt-% of mass fraction was distilled.

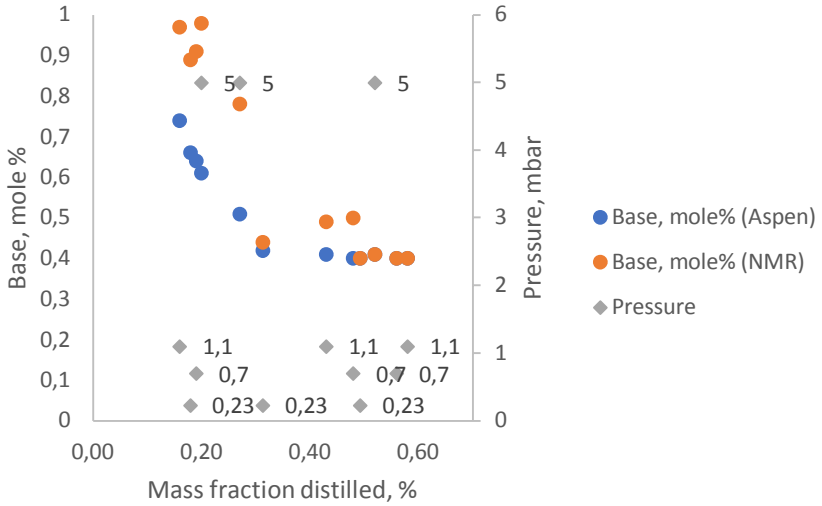

Figure 20. The mole fraction of the base as a function of mass fraction distilled from the simulation and experimental results

The acid to base ratios of the simulation were higher than the experimental results based on NMR analysis (Table 8). However, the acid to base ratios of the first fractions based on CE analysis were in good accord with the experimental results.

Table 8. The acid to base ratios of the simulation and experimental results

Pressure, mbar	Mass fraction	Acid/Base (from Aspen results)	Acid/Base (from NMR results)	Acid/Base (from CE results)
0.27	0.18	0.52	0.12	0.54
0.27	0.31	1.37	1.27	1.13
0.27	0.49	1.5	1.5	1.17
0.7	0.19	0.56	0.1	0.64
0.7	0.48	1.49	1	1.27
0.7	0.56	1.5	1.5	1.38
1.1	0.16	0.35	0.03	0.59
1.1	0.43	1.45	1.04	0.79
1.1	0.58	1.5	1.5	1.38
5	0.20	0.63	0.02	0.75
5	0.27	0.95	0.28	0.54
5	0.52	1.45	1.44	1.13

In addition, the distillate temperature of Aspen simulation results was higher than the experimental results with the difference between 4 and 22°C, except at 0.23 mbar due to instability of the experimental conditions (Fig. 21).

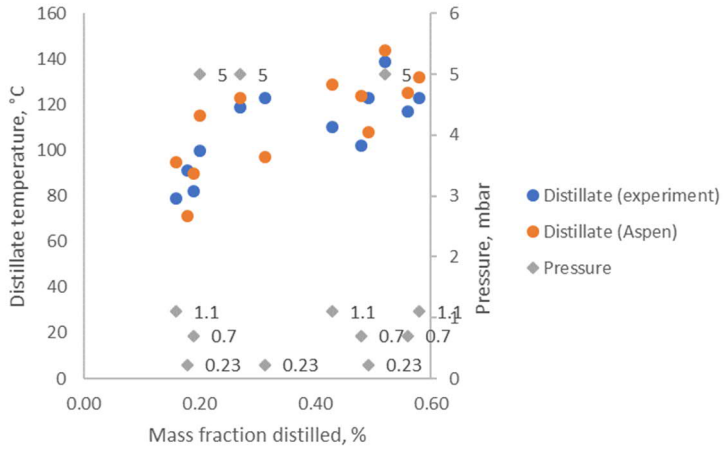

Figure 21. Distillate temperature of the simulation and experimental results

6.3. Discussions and conclusions

Distillation is a commonly used method for purification of organic and inorganic chemicals. Distillation of PILs have been known as distillation of volatile neutral components (Sklavounos et al., 2016). Neutral species vaporize dominantly because of weaker interactions than the ions (Ribeiro et al., 2018). The deprotonation of the strong base forms the volatile base vaporized in the gas phase, then it condenses and recombines with the acid to reform PIL (Sklavounos et al., 2016). PILs formed by equimolar amounts of organic superbases and carboxylic acids. The 1:1 stoichiometry equation of PIL synthesis is written through the proton-exchange process between the Brønsted acid and the Brønsted base (Lopes & Rebelo, 2010):

HA (Brønsted acid) + B (Brønsted base) $\rightleftharpoons$ [BH]A (PIL) $\rightleftharpoons$ $[BH]^+$ (PIL cation) + $[A]^-$ (PIL anion)

^{1}H-NMR analysis indicated the initial PIL had the acid to base ratio of 1, except the first experiment of 1.5. While the CE result showed the acid to base ratio of 1.2 for the initial PIL of the first experiment. In addition, PIL can be considered as a multi-component mixture of ions (i.e. the right size of the above equation) and neutral species (i.e. the left size of the above equation) (Lopes & Rebelo, 2010). Moreover, PILs often have an azeotrope formed from initial PILs (Ribeiro et al., 2018). Furthermore, the azeotrope can be considered as a mixture of ion pairs and neutral species with the composition of the vapor phase identical to the composition of the liquid phase (Lopes & Rebelo, 2010). The acid to base ratio of the azeotrope does not change with further vaporization of PIL (Ribeiro et al., 2018).

The distillation experimental results exhibited an azeotropic mixture with an acid to base molar ratio 3:2. The azeotrope can contain more of the acidic component in the mixture. The acidity of the carboxylic group is not strong enough to convert all the neutral acid into ions. Therefore, the remained liquid mixture can have a significant amount of the neutral base and neutral acid. In addition, the carboxylic

acid forms strong hydrogen bonds (Ribeiro et al., 2018). Consequently, the first distillate fractions contained pure base. Later distillate fractions had the same acid to base ratio 1.5, and nearly to 1.51 of the acid to base ratio in the residue as in the first experiment. PIL can be defined as a mixture of an acid-rich complex and free unreacted neutral base (Ribeiro et al., 2018). The azeotrope compositions remained in liquid phase at room temperature, whereas pure PIL (acid to base ratio of 1) was in solid state.

A PIL mixture can be distilled at a given temperature when the vapor pressure of the liquid equals to the applied pressure. The boiling point temperature near the azeotropic composition is higher in the presence of small proportion of neutral species attached to its hydrogen bonds network (Lopes & Rebelo, 2010). The vapor pressure of pure base (lower boiling compound) is higher than the vapor pressure of the complex as azeotrope (higher boiling compound) at the fixed experimental temperature. Distillation pressure and temperature influences the compositions of the obtained products. The pure base product can be distilled at the appropriate distillation conditions.

Furthermore, ^{1}H-NMR results showed the impurities like decomposition products or hydrolysis products in the distillate were negligible. Hydrolysis products were found in the residue. A base purity of 99 wt.-% can be obtained in the first distillate fraction. The heated PIL mixture can either evaporate or undergo decomposition reactions (Taylor et al.,2010). Distillation can occur when the evaporation activation energy is less than the reaction activation energy as following Arrhenius equation (Taylor et al.,2010). Therefore, the distillation temperature process can be kept as low as possible to minimize decomposition reactions (Taylor et al.,2010). The experiments were conducted at medium vacuum range (e.g. 1-5 mbar) or at the lowest pressure (e.g. 0.2 mbar). The pure PIL can be mostly clear and colourless (Taylor et al.,2010). Chromophores impurities can develop through PIL

synthesis causing a yellow or orange discoloration. From the experiment results, discoloration in the process was observed in both pure base and the complex (see Appendices 8/1-8/4). The first fractions (< 20 wt.% of the feed) of four first experiments contained only pure base and it was of clear or light-yellow liquid state at room temperature. The later fractions (< 50 wt.% of the feed) were collected with the acid to base ratio of 1, 1.3 and 1.4 in a whitish crystalized solid state. Distillations were continued through the last fractions with the acid to base ratio of 1.5 in yellow liquid state at room temperature. However, the color of these fractions changed from white in fraction collectors to yellow in samples containers after melting at 80-90 °C for samples storage. This color change can be due to contact with oxygen or moisture.

Both ^{1}H-NMR and CE method were carried out to analyze samples. Two analytical methods gave different results, especially for the base molar fraction in the first fractions. However, ^{1}H-NMR results of the first fraction were higher than CE results. The composition from simulation results were close to the CE results. In addition, the uncertainty of the NMR peaks integration and NMR measurement were considered less than of CE method. For instance, NMR measurement were implemented within 24 hours after the experiment, while CE measurement were conducted more than 24 hours. The sample storage condition can affect to the components of distillate products. NMR method can be analyzed fast after stopping the experiments.

Finally, according to chemical suppliers, the purity of the base is 98 wt.% and the purity of the acid is 99.8 wt.%. Total impurities of the initial PIL can be estimated as 2.2 wt.%. As can be seen from the residue of the first experiment (Appendix 8/1), it was a dark brown sticky paste of 4 wt.% of the initial material. In addition, 4 to 5 wt.-% of the feed was found in the cold trap. Consequently, it is possible that 91 or 92 wt.% the initial PIL can been recovered, if the material loss was assumed of zero. Distillation is a possible method to purify PILs like S2.

7. RESULTS AND DISCUSSIONS FOR SHORT PATH DISTILLATION EXPERIMENTS FOR S2

Chapter 7 presents the experimental results for S2 distillation carried out by short path distillation (SPD). Chapter 7.1 introduces the distillation conditions with the component material balances. In addition, this section calculates the separation efficiency of SPD. By-product discusses in this section based on NMR analytical results. Chapter 7.2 compares the results of an Aspen simulation with the experimental results. Lastly, chapter 7.3 summarizes discussions and conclusions for the short path distillation experiments.

7.1. Distillation results

This section reports the SPD parameters effect on the separation efficiency of S2, including the distillation pressure, distillation temperature, and feed flow rate. Based on the experimental results, the recovery of the base, the yield of base in distillate and residue, the separation efficiency, the evaporation rate, the relative volatility and the mean free path, were calculated.

7.1.1. Distillation conditions and material balance

The purpose of the experiments is to determine the optimal operating conditions for obtaining the maximum recovery yield of the base and study whether it is possible to remove traces of impurities from the initial material. Table 9 presents the distillation conditions and the distillation results accomplished from eight experiments (experiments from 8 to 15). Four types of starting materials were used: 1) pure S2, 2) S2 with added water, 3) S2 with added acetic acid, and 4) Recycled S2.

Table 9. Distillation conditions for short path distillation experiments with S2

Experi-ment #	Type of feed	Pressure (mbar)	Evapora-tor jacket temp. (ºC)	Feed flow rate (L/h)	Feed jacket temp. (ºC)	Wiper speed (rpm)	Condensate jacket temp. (ºC)	Distillate rate (L/h)	Residue jacket temp. (ºC)	Residue rate (L/h)	Distillate (wt.%)	Residue (wt.%)	Cold trap (wt.%)	Feed acid:base	Distillate acid:base	Residue acid:base	Cold trap
8	Pure S2	1.4	120	0.37	80	300	80	0.37	80	0.37	24	40	NA	1.05: 1	0.9: 1	1.29: 1	NA
9	Pure S2	1.4	160	0.37	80	300	80	0.37	80	0.37	87	1.2	0.8	1.13: 1	1.1: 1	1.25: 1	only base
10	Pure S2	1.3	160	0.37	80	300	80	0.37	80	0.37	94	3	8	1.02: 1	1.06: 1	NA	0.31: 1
11	Pure S2 added water	1.3	150	0.37	80	300	80	0.37	80	0.37	63	3	3	1.05: 1	1.18: 1	1.29: 1	only base
12	Pure S2 added water	1.3	160	0.37	80	300	80	0.94	100	0.94	52	2	2	1.16: 1	1.22: 1	1.49: 1	only base
13	Recycled S2	1.3	160	0.37	80	300	80	0.94	100	0.94	81	3	3	1.05: 1	1.16: 1	1.46: 1	only base
14	Pure S2 added acid	1.8	160	0.37	80	300	80	0.37	80	0.37	68	6	NA	2.32: 1	2.1: 1	1.94: 1	NA
15	Pure S2 added acid	1.8	160	0.94	80	300	80	0.94	80	0.94	58	37	12	2.32: 1	2.13:1	1.61:1	only acid

According to the vapor pressure curve of pure base from batch distillation experiment results, the distillation pressure was planned at one mbar. However, the distillation pressures or the operating pressures were performed at 1.3, 1.4, 1.8 mbar, based on the actual condition of SPD on the experimental days. The melting point of S2 is approximately 80 °C. Therefore, on the one hand, the internal condensate jacket temperature was set 80 °C to prevent solidification of the material inside SPD, especially the condensing surface, piping, and dosing pumps. On the other hand, the distillation temperature was assumed as the evaporator jacket temperature. The evaporator jacket temperatures were implemented at 120, 150, and 160 °C. The feed flowrate set-point was fixed at 0.37 L/h on the control panel of the feed dosing pump, except for the experiment 19 at 0.94 L/h. The feed jacket temperature was fixed at 80 °C. The wiper speed was maintained at 300 rpm. The residue jacket temperature was set at 80 °C and increased to 100 °C when the residue pump stuck and failed to run properly as in experiments 12 and 13. The distillate and residue flowrate set-points were controlled at 0.37 L/h. They were increased to 0.94 L/h when the residue pump was stuck by material solidification and the feed flowrate set-point was raised up to 0.94 L/h as in experiment 14.

The operating time ranged from six to sixteen minutes recorded from the starting and stopping of the feed dosing pump. The distillate fraction was from 24 to 94 wt.% of the feed (Table 9). The residue fraction was from 1.2 to 40 wt.% of the feed (Table 9). The cold trap samples were collected after the experiment had finished. The cold trap captured from 0.8 to 12 wt.% of feed (Table 9). On the one hand, the cold trap can trap the water which did not condense on the condenser due to water vapor pressure behavior. Therefore, removing moisture from the device was essential prior to start experiments. On the other hand, the cold trap was emptied at the end of two experiments conducted on the same experimental day, for instance, one cold trap collected for experiments 8 and 9, or similarly for experiments 14 and

15. It was necessary to control the cold trap to define low molar mass components properly (Appendix 11).

^{1}H-NMR analysis was applied to analyze samples and calculate the acid to base ratios. Figure 22 indicates the components mass balance. The acid to base ratio in the distillate was lower than in the residue, except for experiments with the feed as S2 excess acid in experiments 14 and 15. Almost all of the base was distilled and obtained in distillate, except for experiments 8 and 15. Nevertheless, a small amount of the base was collected in the residue, except for experiments 8 and 15. The composition of the residue of experiment 10 was not defined due to unknown peaks found in NMR analytical spectra (see Appendix 11.3). In addition, hydrolysis compounds can be formed from the base in the presence of water. Hydrolysis compounds were presented in all the feeds with exception of the feed for experiment 9. However, hydrolysis products were found in all distillate, also for experiment 9. Moreover, ^{1}H-NMR results showed that only base was captured in the cold trap in experiments 9, 11, 12, and 13. Furthermore, the minimum base loss of 2 wt.% was observed in experiment 10. A part of S2 was lost due to the SPD device hold-up. The hold-up was due to the internal volume of the device. The problems of the distillate and residue dosing pumps caused more loss as in experiments 12 and 13.

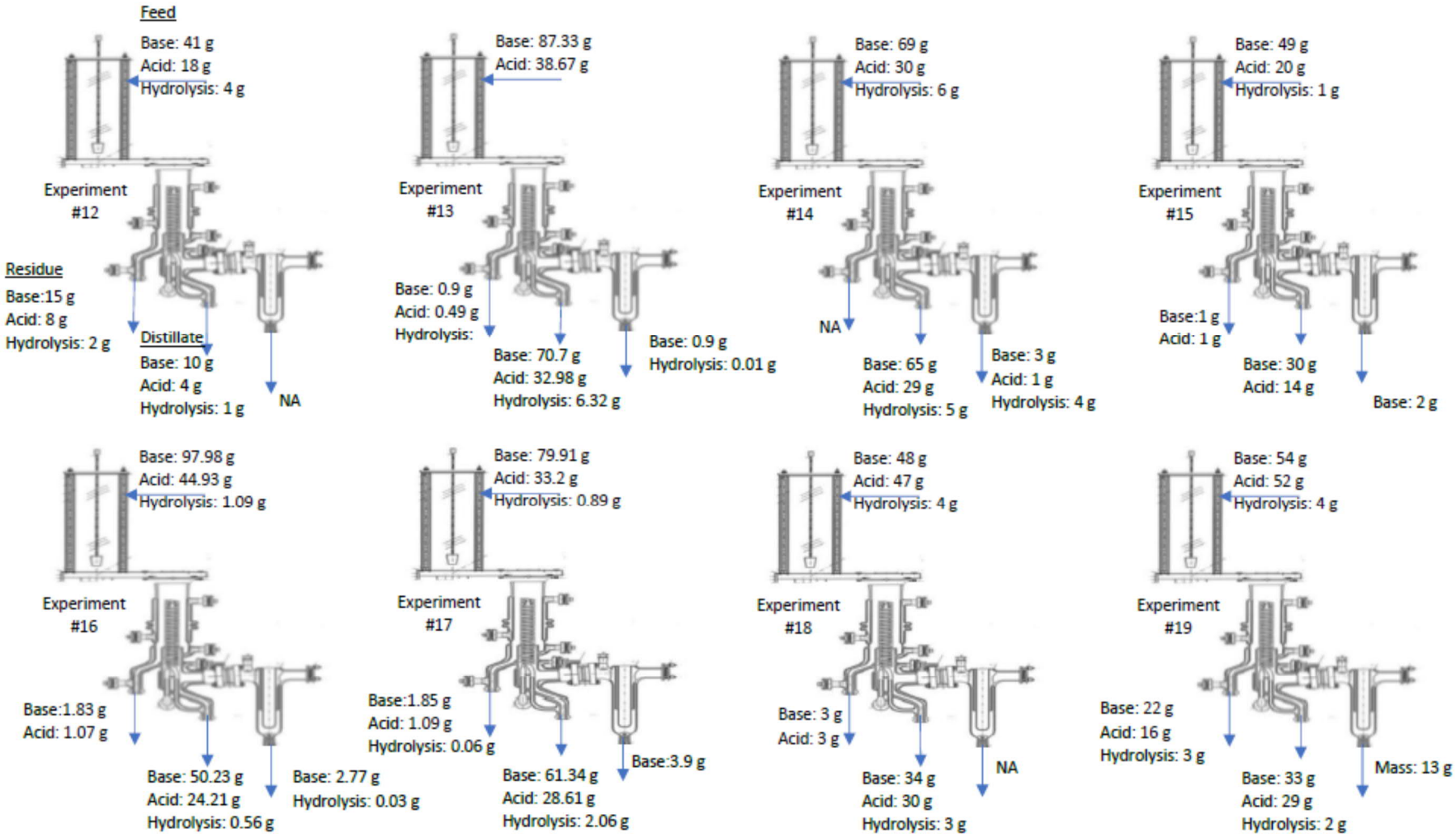

Figure 22. Components mass balance of SPD experiments with S2

7.1.2. The recovery and the yield of components

The distillation performance was evaluated through the recovery and the yield of the base in the distillate and in the residue as equations (3-1, 3-2, 3-3). Three factors of SPD: operating pressure, evaporator jacket temperature and feed flow rate, were studied for their effects on the separation and recovery efficiency of S2 (Table 10). The operating pressure was decreased from 1.8 to 1.3 mbar whereas the recovery yield increased to 97 wt.% as in experiment 10, although the base yield in the residue of this experiment can not be calculated since ^{1}H-NMR analysis was not recognized the base peak. The base yield in the residue was 1 wt.% as in experiment 9. In addition, the recovery yield was 91 wt.% and the base yield in distillate was 81 wt.% at 160 ˚C of the evaporator jacket temperature. The base yield in the residue decreased from 36 to 1 wt.%, corresponding to an increase of evaporator jacket temperature from 120 to 160 ˚C. Moreover, the slower feed flow rate of 0.37 L/h produced the higher recovery of 96 wt.%, as in experiment 14, in comparison with experiment 15. Furthermore, the recycled S2(i.e. 92 wt.%), or S2 with added acetic acid (i.e. 96 wt.%), or S2 with added water (i.e. 95 wt.%), gained lower recovery yields than pure S2 (i.e. 97 wt.%).

Table 10. The distillate to residue ratio, the recovery, and the components yield in the distillate and residue of SPD experiments with S2

Experiment #	Distillate/Residue, g/g	Recovery, %	Base yield in distillate, %	Base yield in residue, %
8	0.6	40	25	36
9	73.3	91	81	1
10	35.2	97	94	NA
11	22	92	61	3
12	25.9	95	51	2
13	30.7	92	77	2
14	11.2	96	71	6
15	1.6	65	62	42

7.1.3. The separation efficiency

The separation efficiency is expressed by the relative volatility α which was calculated by the Rayleigh equation for distillation on continuous-film evaporators (equation 3.3.4). Table 11 shows the relative volatility α calculated according to equation 3-4 for SPD experiments of S2. The values of α are constant and slightly higher than one in experiment from 8 to 13. However, the relative volatility decreased with increasing evaporator jacket temperature from 120 to 160 ˚C, as in experiment 8 and 9. Excess acetic acid in the feed as in experiment 10 and 11 showed relative volatility less than one.

Table 11. The relation volatility of SPD experiments with S2

Experiment #	X_r	X_f	$1-X_r$	$1-X_f$	R	F	α
8	0.39	0.45	0.61	0.55	0.0025	0.01	1.34
9	0.40	0.47	0.60	0.53	0.0001	0.01	1.06
11	0.43	0.48	0.57	0.52	0.0002	0.01	1.06
12	0.40	0.46	0.60	0.54	0.0003	0.01	1.06
13	0.40	0.48	0.60	0.52	0.0003	0.01	1.10
14	0.31	0.28	0.69	0.72	0.0007	0.01	0.95
15	0.34	0.28	0.66	0.72	0.0042	0.01	0.76

7.1.4. The evaporation rates

The rate of evaporation depends on the vapor pressure of the distilled substance (e.g. base 2) at the evaporating surface temperature. Based on the result of experiment 10, 1.3 mbar pressure can be considered as the base vapor pressure and used to study the evaporation rate. The theoretical evaporation rate of the base was computed using Langmuir equation (3.3.5).

If the temperature of the evaporator surface assumed same as the evaporator jacket temperature of 433 K, the evaporation rate of the base in vacuum was 0.34 g/cm^{2}s.

From the vapor pressure curve of the base, the evaporator temperature of the base at 1.3 mbar can be 350 K, according to batch distillation experimental results. If the temperature of the surface was assumed the same as the evaporator temperature of the base at 1.3 mbar, the evaporation rate of the base in vacuum was 0.38 g/cm^{2}s.

The theoretical evaporation rate of the base in vacuum is higher than the actual evaporation rate of the base at 1.3 mbar like less than 0.3 g/cm^{2}s (Fig. 23). The evaporator surface area of the SPD is 4.8 dm^2. The evaporation time is defined as the time for the film material to be totally vaporized. Figure 23 presents the evaporation rates of SPD experiments with various residence times of 0.5, 1, 5 seconds. The feed rate set-point of experiment 9 and 10 were 0.37 L/h, and the evaporation rates were close to the theoretical evaporation rate.

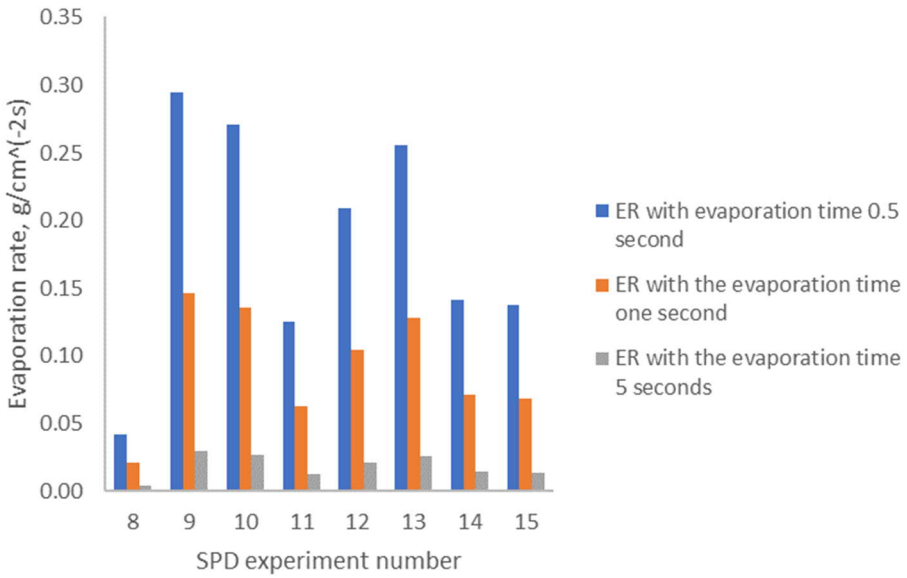

Figure 23. The evaporation rate of the base 2 based on SPD experimental results at various estimated evaporation times

7.1.5. The mean free path

SPD has a short distance between the evaporating and condensing surfaces to enable vaporized molecules to reach the cooling surface and condense without any collisions with foreign gas molecules (Lutišan & Cvengroš, 1995). The distillation space gap can be less than the mean free path (MFP) of the molecules evaporated (Krell, 1982). The theoretical mean free path was calculated by the equation (3.3.6).

The evaporation pressure was assumed to be 1.3 mbar or 130 Pa. The evaporation temperature of the base was approximately 350 K as mentioned above. If the base particles were assumed in a cubic shape, the diameter of the base 2 was $6.27\ 10^{-10}$ meter. Finally, the mean free path was obtained as 249 mm, and this is higher than the usual distance between the evaporating and condensing surfaces of SPD (i.e. 20-50 mm). It is possible to distil the base 2 via SPD with the maximum pressure controlled less than 32 mbar to ensure the mean free path higher than 50 mm of the distance between the evaporating and condensing surfaces.

7.1.6. By-product

Hydrolysis products as by-product can be formed from the base in the presence of water. The amounts of the hydrolysis products analyzed using NMR in each stream are shown in Figure 24. The first by-product was generally found in greater quantity than the second by-product, both in the distillate and the residue. The feed with excess acid can generate more by-product as in experiments 14 and 15. SPD experiments indicated that by-product cannot be separated from the distillate.

Chromophores are impurities that affect the color of S2. The use of SPD reduces the amounts of chromophores in the distillate, in comparison to the feed.

UV-Vis analysis was used to compare the discoloration of the feed, distillate and residue collected from SPD experiments of S2. UV-Vis results indicated that the absorbance of the distillate was lower than the absorbance of the feed and the residue within wavelength ranges from 240 to 360 nm (see Appendix 11). It was observed that the color of the distillate was whitish solid, while the feed and the residue were yellow or orange.

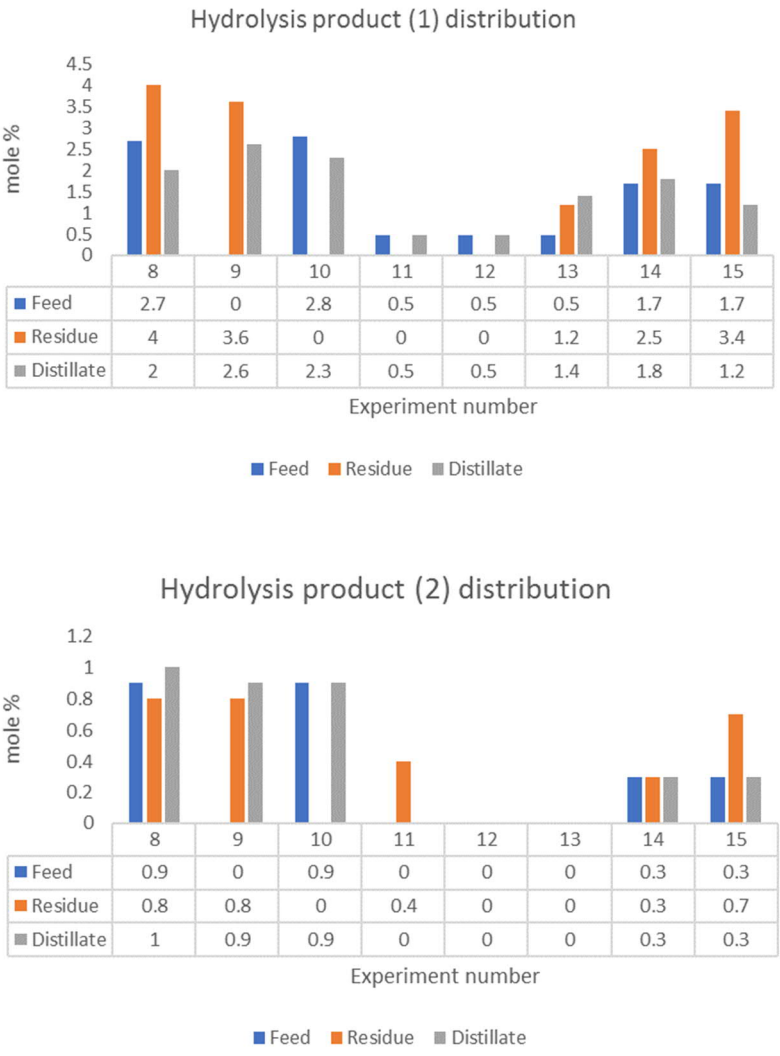

Figure 24. By-product distribution of SPD experiments with S2

7.2. Distillation results in comparison to the simulation results

An Aspen model was built with one RadFrac unit to simulate SPD experiments (Fig. 25). SPD model can be assumed as a single equilibrium-stage model (Ilmanen, 2017). However, the number of stages in Aspen is limited to two stages. Therefore, Murphree efficiencies were used for the first stage of 0.5 and the second stage of one. The condenser in Aspen was chosen as partial - vapor. The reflux ratio was set for no reflux (e.g. 0.001). The distillate to feed ratio was computed corresponding to the experimental results of short path distillation.

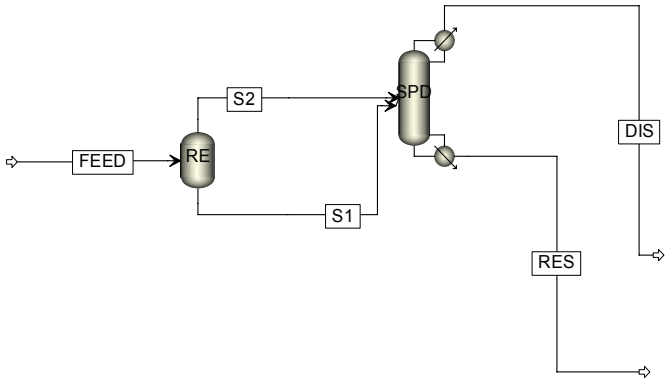

Figure 25. The flowsheet of Aspen model for SPD experiments

The model was used to simulate the experiment 10, 12, and 13 conducted at the same operating condition of 1.3 mbar and 160 ˚C. The distillate of the SPD experiments was assumed to include the total amount of distillate, cold trap, and loss. Therefore, the residue of the SPD experiments was used to evaluate the simulation results. These experiments were conducted at the fixed evaporator jacket temperature of 160 ˚C and the operating pressure of 1.3 -1.4 mbar. According to the simulation results, the distillate temperature was approximately 128 ˚C (Fig. 26).

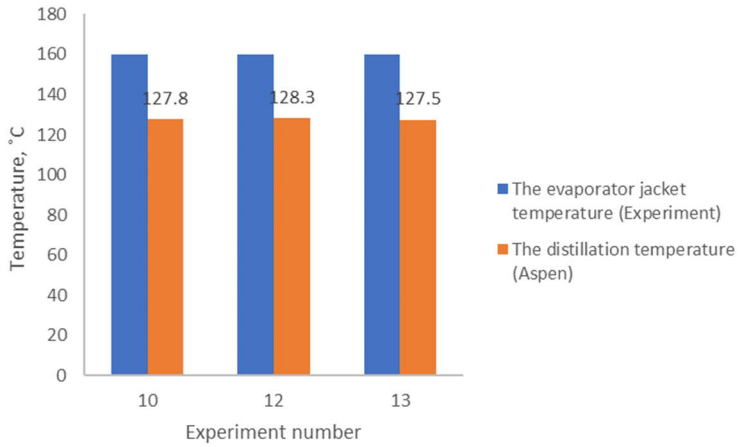

Figure 26. The evaporator jacket and the simulated distillate temperature

The mass percentage of the distillate fractions from the simulation results was as nearly as the experimental results (Fig. 27). The molar percentage of the base in the distillate from the simulation results was higher by approximately 10 % than from the experimental results.

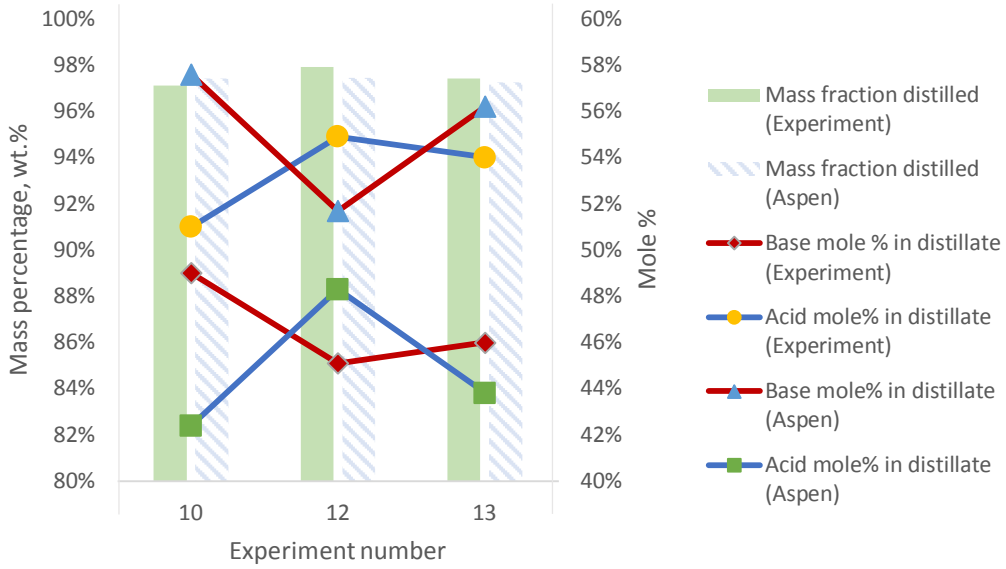

Figure 27. The mass fraction of the distillate and the molar fraction of the base and acid in the distillate, from the simulation and experimental results

The acid to base ratios of the distillate and the residue from the simulation results were lower compared to the experimental results (Fig. 28). The acid to base ratios of the distillate from the experiments (i.e. the blue line) were higher than one, while the simulation results were less than one (i.e. the orange line). The acid to base ratios of the residue from the experiments (i.e. the green line) were approximately 1.5, whereas the simulation results (i.e. the yellow line) were lower than 1.4.

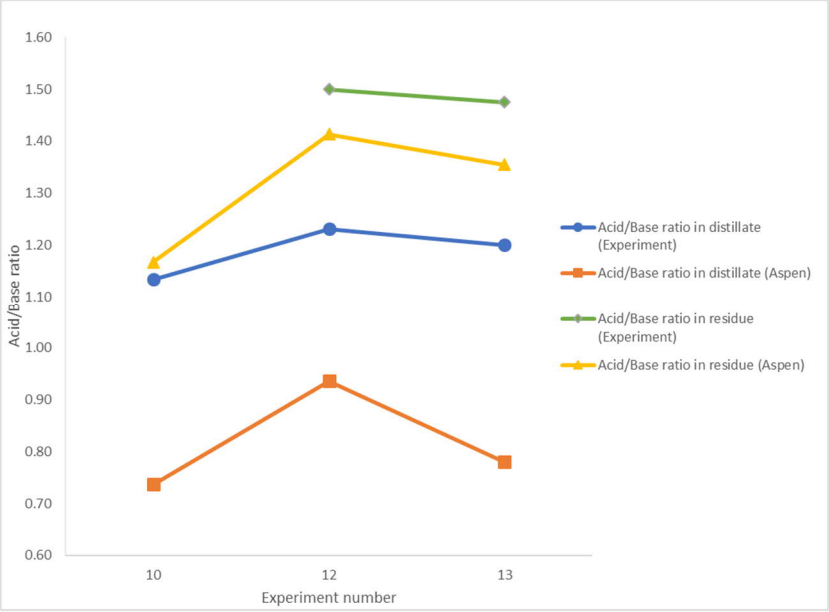

Figure 28. The acid to base ratios of the simulation and experimental results

The simulation results showed that the hydrolysis products were enriched in the residue and a small decrease was observed in the distillate (Fig. 29). However, the experimental results showed a contrasting by-product distribution.

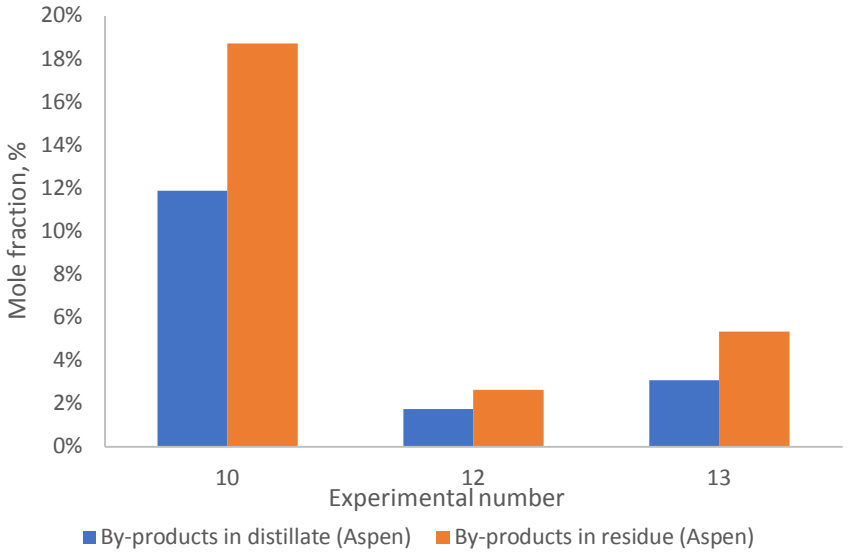

Figure 29. By-product distribution simulated results

7.3. Discussions and conclusions

S2 can exhibit thermal decomposition and oxidation during purification processes at high temperature. The evaporative behavior of S2 was studied through SPD parameters including distillation pressure, temperature and feed flow rate. The experimental results show the conditions to obtain the maximum amount of S2 in the distillate and the corresponding minimum amount of S2 and impurities in the residue.

The evaporation pressure was assumed similar to the operating pressure. The lower pressure can get the higher the separating efficiency. The evaporation temperature was studied via the evaporator jacket temperature. An increase of evaporator jacket temperature accelerated the evaporation of material and almost all of the base were obtained in the distillate. The residue stream contained the heaviest molecules which remained on the evaporator surface and can not reach the condenser surface. The acetic acid had lower volatility, and it was concentrated in the residue more than the base. However, the experimental results indicated not only

the volatile component but also the heavier components were vaporized and collected in the distillate. Therefore, the evaporator jacket temperature of 160 ˚C can be regarded as the best potential temperature for the operating pressure at 1.3 or 1.4 mbar. The recovery was approximately 97 wt.%. The mass loss of S2 was high because of the problems of the distillate and residue dosing pumps. However, the base loss can be minimized to 2 wt.% of the feed.

The feed flow rate can influence both heat transfer and production capacity. The slower the feed flow rate, the longer the residence time of S2 on the evaporator surface. This enhances heat transfer efficiency for higher recovery yield (Chen et al., 2012). The feed flow rate was set at 0.37 L/h to obtain higher separation efficiency than at 0.97 L/h.

The experiments showed that the base distilled together with the acid in the distillate. The distillate to residue ratio was from 11.2 to 73.3 to obtain the recovery rate over 90 wt.%. Nevertheless, the base was trapped in the cold trap together with the low molar mass impurities such as water and by-product. In addition, the experiments resulted in the removal of residual water in the distillate, because water was found only in the residue and in the cold trap.

The simulation results showed the acid to base ratio in the residue was higher compared to experiments. In addition, by-product was enriched in the residue. Moreover, the distillate temperature was approximately 128 ˚C.

It is possible to make several recommendations to improve the separation efficiency of the base 2. Even lower pressure than 1 mbar can be beneficial for S2 separation using SPD. In addition, the temperature probes can be installed inside the evaporator to study the evaporation temperature more accurately. The piping and dosing pumps of the residue and distillate parts were blocked by S2 crystallization during the experiments. The internal condenser and residue jacket temperatures

need to be set as high as 100 ˚C. Moreover, a modification of the cold trap can be devised to obtain the pure base 2 more efficiently.

8. RESULTS AND DISCUSSIONS FOR SHORT PATH DISTILLATION EXPERIMENTS FOR S1

This chapter reports the distillation experiment results for S1 using short path distillation. Section 8.1 presents the heat transfer coefficient study with the pure base 1. This section reports the distillation experimental conditions and results, included by-product distribution. Section 8.2 discusses the SPD experimental results.

8.1. Distillation results

8.1.1. The heat transfer coefficient of SPD

The pure base 1 was distilled at 3.5 mbar via SPD. The evaporator jacket temperature was set at 140 ˚C. The feed quantity was 124.18 g. The obtained distillate amount was 114.85 g. The loss was 9.33 g. The feed was heated to 80 ˚C. The distillate and residue jacket temperatures were set 100 ˚C to prevent the crystallization of S1. The wiper speed was fixed at 300 rpm. The feed, distillate and residue flow rate were controlled at 0.37 L/h.

The operating pressure of 3.5 mbar was assumed to be the same as the evaporation pressure. The evaporation temperature of the pure base 1 was computed through the Antoine equation with the Antoine parameters as shown in Table 12. The vapor pressure of 3.5 mbar corresponds to a temperature of 347 K, according to the vapor pressure correlation.

Table 12. Adjustable parameters of Antoine equation for vapor pressure of base 1 (Ostonen, 2017)

	S1
A	25.951
B	- 6973.88
C	$-4.1116 \cdot 10^{-4}$

According to the temperature profile inside the SPD (Fig. 30), the temperature of the heating fluid (T_{1w}) and the cooling fluid (T_{2w}) can be controlled through the jacket temperatures. The temperature difference of the distillation gap can be estimated by the results of the heat transfer coefficient study. The boiling point temperature (T_1) and the dew point temperature (T_2) can be estimated from the conductive heat transfer.

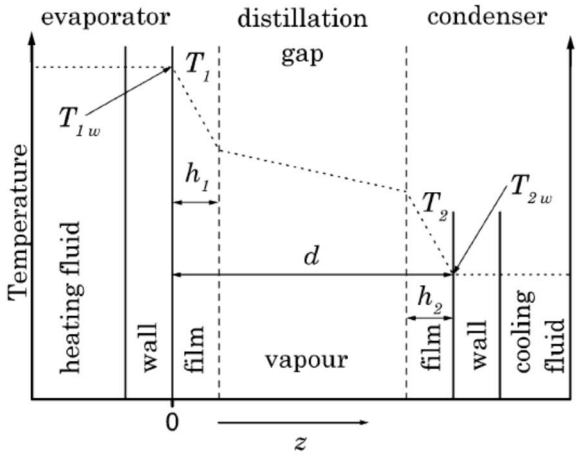

Figure 30. The schematic diagram of temperature profile inside SPD (Lutisan et al., 2002)

The heat transfer of the distilled liquid S1 was calculated:

$q_{liquid} = n\ c_p\ \Delta T = 0.0115 \cdot 216 \cdot 49 = 122\ (W)$ (9.1)

where: C_p: the specific heat capacity at 298.15 K = 216 (J/(mol.K)) (Ostonen, 2017)

ΔT: the temperature difference of the feed = 74 K -25 K = 49 (K)

n: the molar amount of the base 1 distilled = 114.85 (g) / 124.187 (g/mol)/ 80 (s) = 0.0115 mol/s

The thermal conductivity (k) was computed through Fourier's law of thermal conduction:

$$q_{oil} = \frac{k\ A\ \Delta T}{L} \quad (9.2)$$

where: L: the thickness of the evaporator = 3 mm or 0.003 m

A: the heat transfer surface as the evaporator surface = 0.048 m^2

ΔT: the temperature difference = 140 – 74 = 66 K

The conductive heat transfer was equal to the heat transfer of distilled liquid. Consequently, the thermal conductivity (k) of the heating oil was 0.115 (W/ (m.K)). While the supplier's heating oil data has the thermal conductivity at 140 ˚C = 0.115 (W/ (m.K)). The experimental result was close to the actual thermal conductivity of the heating fluid.

Due to lack of thermodynamic data of S2, the obtained thermal conductivity of 0.115 (W/ (m.K)) and the difference of temperature between the evaporator jacket and the evaporation film of 66 ˚C, were used to define the evaporative temperature

for S2 using SPD at 1.3 mbar and 160 ˚C of evaporator jacket temperature. Solver in Excel was used to find the optimal ΔT to make the difference between the evaporative heat transfer and conductive heat transfer to zero. The results are summarized in Table 13. Consequently, the evaporation temperature can be 108 °C, while the evaporator jacket temperature was 160 ˚C.

Table 13. The estimated evaporation temperature of base 2 using SPD

The evaporative heat transfer of the base	The conductive heat transfer of the heating fluid
$q_{base} = n_{base}\, c_{p,base}\, \Delta T$	$q_{oil} = \frac{k\, A\, \Delta T}{L}$, (for 80 seconds)
with	with k =0.115 (W/(m.K))
n_{base} =98.6 (g) /106.6385 (g/mol)/80 (s) = 0.0116 (mol/s)	A = 0.048 m^2, L = 0.003 m
$c_{p,base}$ = 295 (J/(mol.K)) at 80 °C	
Δ T = 28 (K)	Δ T = 52 (K)
Solver solution for q_{base} = 95.5 (W)	q_{oil} = 95.68 (W)
$T_{0,feed}$ = 80 ˚C, T_{evap} = 80 + 28 = 108 °C	T_{jacket} = 160 ˚C, T_{evap} = 160 - 52 = 108 °C

8.1.2. Distillation experimental conditions and results

Pure S1 was used to study the behavior of SPD during distillation experiments. Table 14 presents the experimental results with the mass fraction and the acid to base ratios. There are several SPD parameters that can influence the separation performance, such as the distillation pressure and temperature. The other parameters were constant during the experiments. The SPD was checked at the lowest operating pressure (e.g. 0.1 mbar). The higher the evaporator jacket temperature can obtain the higher mass fraction of distillate and the lower mass fraction of residue. The distillate amount was increased from 56 to 63 wt.% of the

feed, corresponding to the evaporator jacket temperature raised from 120 to 130 ˚C. Conversely, the residue amount decreased from 18 to 12 wt.% of the feed. Nevertheless, the residue was collected at 1 wt.% of the feed in experiment 18. The appropriate distillation conditions to get the maximum yield of PIL solvent 1 were at 0.34 mbar and 140 ˚C of evaporator jacket temperature.

1H-NMR analytical results were used to calculate the acid to base ratios. The acid to base ratio in the distillate was lower than in the residue. Consequently, the acid was vaporized in the distillate less than the acid in the residue. A part of the base was found in the cold trap. The base as a light component was trapped in the cold trap. In addition, water was captured in the cold trap. However, the amount of water was not quantified. Therefore, the total material after the experiments was higher than the total material at the beginning. The cold trap can trap moisture remaining in the apparatus from the cleaning procedure with water on the previous day. Nevertheless, the loss of the base was approximately 10 wt.% of the feed (Fig. 31).

Table 14. Distillation conditions of short path distillation experiments with S1

Experi-ment #	Type of feed	Pressure (mbar)	Evapora-tor jacket temp. (ºC)	Feed flow rate (L/h)	Feed jacket temp. (ºC)	Wiper speed (rpm)	Condensate jacket temp. (ºC)	Distillate rate (L/h)	Residue jacket temp. (ºC)	Residue rate (L/h)	Distillate (wt.%)	Residue (wt.%)	Cold trap (wt.%)	Feed acid:base	Distillate acid:base	Residue acid:base	Cold trap
16	Pure PIL	0.1	120	0.56	60	350	45	0.37	60	0.37	56	18	52	0.97: 1	1.17: 1	1.26: 1	only base
17	Pure PIL	0.12	130	0.37	75	350	51	0.37	60	0.37	63	12	14	0.97: 1	1.3: 1	1.28: 1	only base
18	Pure PIL	0.34	140	0.37	80	350	80	0.37	80	0.37	83	1	34	1.16: 1	1.19: 1	1.33:1	only base
19	Pure PIL	0.69	120	0.37	82	350	42	0.37	60	0.37	58	23	18	1: 1	0.85: 1	1.36: 1	only base

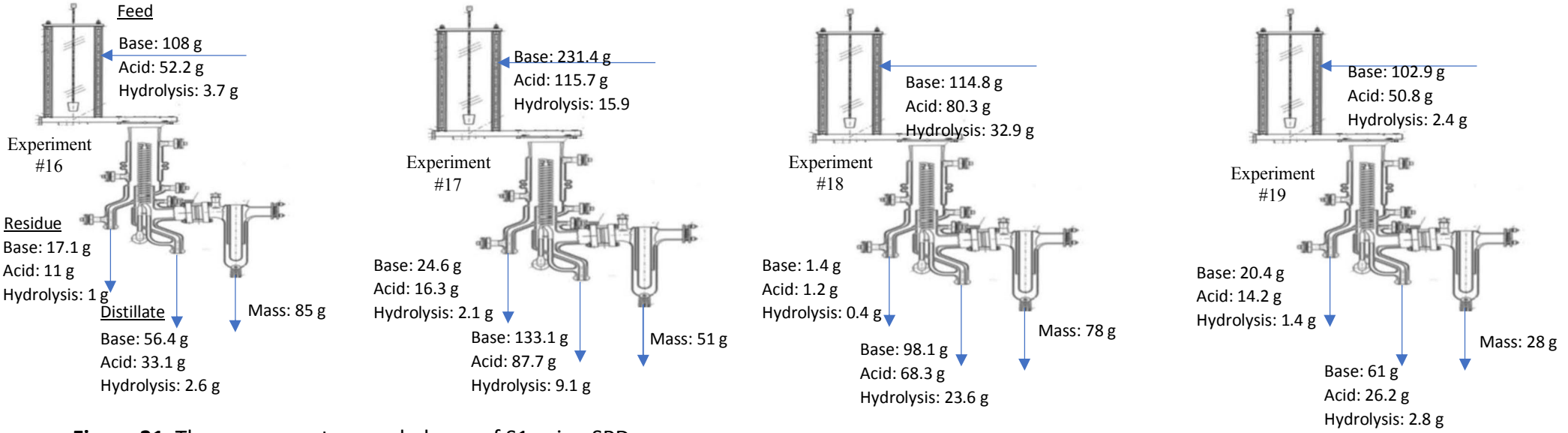

Figure 31. The components mass balance of S1 using SPD

8.1.3. By-product

From previous studies, the base 1 and S1 can form by-product at high temperature through a reversible hydrolysis reaction. Figure 32 shows the by-product distribution in the feed, distillate and residue for SPD experiments of S1. All the feeds contained by-product. The amounts of by-product were lower in the distillate than in the residue. Further studies could determine whether it is possible to remove by-product.

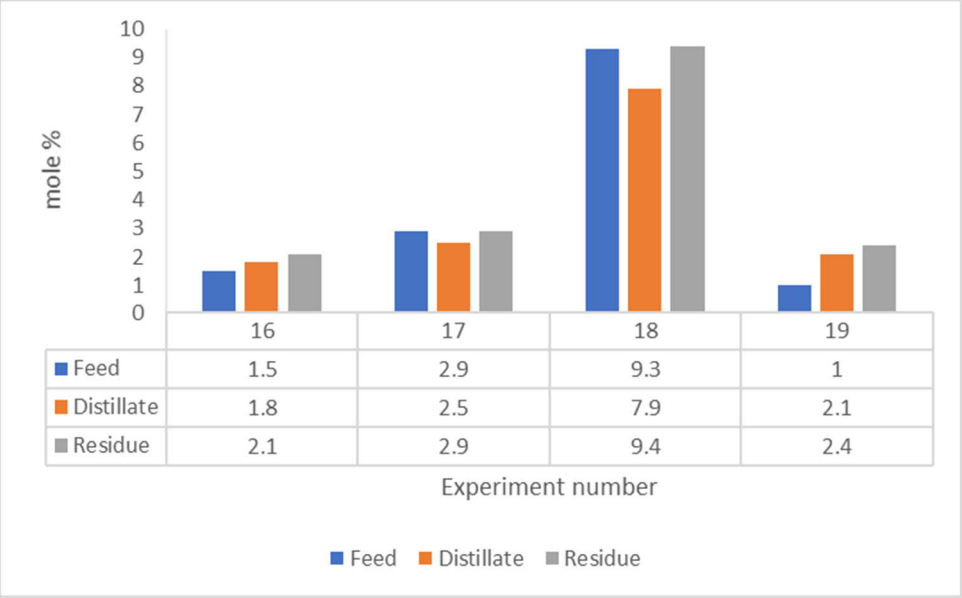

Figure 32. By-product distribution of SPD experiments with S1

8.2. Discussions and conclusions

The evaporation of S1 was studied using short path distillation. From a previous study, the acid to base ratio of the complex of S1 can be 1.67:1 (Ahmad et al., 2016). The results showed that S1 was collected in the distillate as PIL with excess acid. The acid to base ratio of the distillate was less than 1.2:1, while the residue had the acid to base ratio less than 1.3:1. The optimal temperature and pressure conditions for S1 purification can be 140 ˚C and 0.34 mbar. At these conditions, the

mass fraction of the residue was 1 wt.% of the feed. S1 can be synthesized by equimolar of the base 1 (purity of 98 wt.%) and acetic acid (purity over 99 wt.%), therefore, the impurities can be estimated approximately 3 wt.%. It is possible to use higher distillation temperature than 140 ˚C, or a lower distillation pressure than 0.34 mbar, to purify S1 efficiently, by leaving more impurities in the residue. Moreover, the base can be partly trapped in the cold trap. The cold trap can be modified to obtain a pure base from the distillation experiment. Study of the temperature profile of SPD can be beneficial for further increasing the separation efficiency.

9. CONCLUSIONS

The purpose of this study was to determine whether it is possible to purify PIL via distillation. The study involved the distillation experiments for PIL which comprised an equimolar mixture of the base solvent 2 and acetic acid. The use of PILs has been receiving more attention in the dissolution of pulp to produce manmade cellulose fibers. Impurities can be accumulated from various sources, such as inorganic materials, lignin, carbohydrates, other cellulose derivatives, chromophores and hydrolysis products in used PILs.

Short path distillation is suitable method for thermally sensitive and high boiling point materials. SPD is a potential method for separating a small quantity of impurities due to the differences of the mean free path of gas molecules. SPD is an apparatus constructed with a gap between the evaporator and the condenser of length equal to or less than the mean free path of evaporated molecules. This design can limit the collisions of vaporized molecules with foreign gas molecules in transit from the heating surface to the cooling surface. According to the kinetic theory of gases, the mean free path is directly proportional to the evaporation temperature while it is inversely proportional to the evaporation pressure. The theoretical mean

free path of the base 2 was computed at 249 mm, much higher than the distance ranges between the evaporator and condenser surfaces of SPD from 20 to 50 mm.

The batch distillation experimental results showed that pure base 2 can be partially vaporized and condensed from a mixture of S2, if the feed had an acid to base ratio of less than 1.5. The residue of batch distillation experiments contained excess acetic acid and had the same acid to base ratio as the last distillate fractions. The SPD experimental results showed that the acid to base ratio of the distillate was from 0.9:1 to 1.22:1, if the feed had an acid to base ratio of less than 1.5.

The results of the study increase knowledge of the evaporation behavior of S1 and S2 using SPD in vacuum conditions. In addition, the vapor pressure of the base 2 was studied via batch distillation experiments. The optimal conditions for obtaining maximum distillate and separation of impurities was accomplished through variation of the distillate pressure and temperature. The lower the pressure can obtain the higher the separation efficiency. The slower the feed flowrate can get the higher the separation efficiency. For short path distillation experiments, the recovery yield of base 2 was 97 wt.% and the base yield in the distillate was 94 wt.% at 1.3 mbar and an evaporator jacket temperature of 160 °C. For batch distillation experiments, the purity of base 2 was 99 wt.% as can be seen in the first fractions.

The thesis provides solutions to the problem of removing impurities from PILs. The by-product was only found in the bottom fractions in batch distillation experiment. Based on the short path distillation results, the distillate was found to contain fewer by-product than the residue. The distillate was changed to whitish solid while the color of the feed was dark brown or orange. In addition, residual water was separated from the distillate. Moreover, the base can be partly trapped in the cold trap.

Overall, this thesis has provided useful results for the purification of PILs using short path distillation. However, there are several limitations of the work. It was impossible to evaluate the simulation model for all the experimental results. Few samples could be analyzed by Karl-Fischer titration due to solidification problems at room temperature of samples.

Further research can be conducted at even lower pressures than 1 mbar. It is possible to implement several modifications of SPD to increase separation efficiency. For instance, it can be included by devising a cold trap modification to trap light molar mass molecule more efficiently, or by studying the temperature profile inside the SPD. It is suggested to repeat experiments via SPD with feed added water and excess acetic acid in the PIL. A multi-pass distillation using SPD, or at least two stages of SPD, can be seen as a new approach to improving the purity of ionic liquid and completely removing light molecular weight impurities.

BIBLIOGRAPHY

Abdulwahab, M., 2013. *Master's thesis: Modelling of ionic liquids' thermal separation and recycling in biomass fractionation.* Aalto University.

Ahmad, W., Ostonen, A., Jakobsson, K., Uusi-Kyyny, P., Alopaeus, V., Hyväkkö, U. and King, A. W. T., 2016. Feasibility of thermal separation in recycling of the distillable ionic liquid [DBNH][OAc] in cellulose fiber production. *Chemical engineering research and design*, Volume 114, pp. 287-298.

Alford, R., Burns, M. and Burns, N., 2011. Dixon rings - A revolutionary random column packing. *Filtration,* Volume 11, pp. 218-223.

Anugwom, I., Eta, V., Virtanen, P., Mäki-Arvela, P., Hedenström, M., Hummel, M., Sixta, H. and Mikkola, J. P., 2014. Switchable ionic iiquids as delignification solvents for lignocellulosic materials. *ChemSusChem*, Volume 7, pp. 1170-1176.

Arul, J., Boudreau, A., Makhlouf, J., Tardif, R. and Bellavia, T., 1988. Fractionation of anhydrous milk fat by short-path distillation. *JAOCS,* Volume 65, pp. 1642-1646.

Avram, A. M., Ahmadiannamini, P., Qian, X. and Wickramasinghe, S. R., 2017. Nanofiltration membranes for ionic liquid recovery. *Separation science and technology*, Volume 52, pp. 2098-2107.

Babeanu, N. E., Nita, S., Popa, O., Marin, D. I. and Batrinescu, G. , 2018. Optimisation of squalene recovery from amaranth oil by short path distillation. Revista de Chimie, Volume 69, pp. 291-296.

Baird, Z. S., Dahlberg, A., Uusi-Kyyny, P., Osmanbegovic, N., Witos, J., Helminen, J., Cederkrantz, D., Hyväri, P., Alopaeus, V., Kilpeläinen, I., Wiedmer, S. K. and Sixta, H., 2019. Physical properties of 7-methyl-1,5,6-triazabicyclo[4.4.0]dec-5-ene (mTBD). *International journal of thermophysics,* Volume 40, pp. 1-23.

BASF, 2010. *Ionic Liquids at BASF SE,* BASF.

Beyersdorff, T., Schubert, T. J. S., Welz-Biermann, U., Pitner, W., Abbott, A. P., McKenzie, K. J. and Ryder, K. S., 2008. Synthesis of Ionic Liquids. Wiley-VCH Verlag GmbH & Co..

Blahusiak, M., Schlosser, S. and Cvengros, J., 2012. Simulation of a new regeneration process of solvents with ionic liquid by short-path distillation. *Separation and purification technology,* Volume 97, pp. 186-194.

Blanchard, L. A. and Brennecke, J. F., 2001. Recovery of organic products from ionic liquids using supercritical carbon dioxide. *Ind. Eng. Chem. Res.*, Volume 40, pp. 287-292.

Chen, L., Zeng, A., Dong, H., Li, Q. and Niu, C., 2012. A novel process for recovery and refining of L-lactic acid from fermentation broth. *Bioresource technology,* Volume 112, pp. 280-284.

Clare, B., Sirwardana, A. and MacFarlane, D. R., 2009. Synthesis, Purification and Characterization of ionic liquids. Monash University.

Earle, M., Esperanca, J. M. S. S., Gilea, M. A., Lopes, J. N. C., Rebelo, L. P. N., Mageee, J. W., Seddon, K. R. and Widegren, J. A., 2006. The distillation and volatility of ionic liquids. *Nature*, Volume 439, pp. 831-834.

Ferraz, R., Prudencio, C., Vieira, M., Fernandes, R., Noronha, J. P. and Petrovski, Z., 2015. Ionic liquid synthesis-Methodologies. *Organic chemistry*, Volume 4.

Fulmer, G. R., Miller, A. J. M., Sherden, N. H. Gottlieb, H. E., Nudelman, A., Stoltz, B. M., Bercaw, J. E. and Goldberd, K. J., 2010. NMR chemical shifts of trace impurities: common laboratory solvents, organics, and gases in deuterated solvents relevant to the organometallic chemist. *Organometallics,* Volume 29, pp. 2176-2179.

Ghandi, K., 2014. A review of ionic liquids, their limits and applications. *Green and sustainable chemistry*, Volume 4, pp. 44-53.

Goodwin, A. R. H. , Sengers, J. V. and Peters, C. J. (2010). *Applied Thermodynamics of Fluids.* RSCPublishing.

Greaves, T. L. and Drummond, C. J., 2015. Protic ionic liquids: evolving structure - property relationships and expanding applications. *American chemical society,* Volume 115, pp. 11379-11448.

Han, L., Zhang S., Qi ,B-K-, Li H., Xie, F-Y. and Li, Y, 2019. Molecular distillation-induced deacidification of soybean oil isolated by enzyme assisted aqueous extraction:effect of distillation parameters. *Applied sciences*, Volume 9, pp. 1-13.

Hicknam, K., 1943. High-vacuum short-path distillation - A review . Chemical Reviews, Volume 34, pp. 51-106.

Huang, K., Wu, R., Cao, Y., Li, H. and Wang, J. , 2013. Recycling and reuse of ionic liquid in homogeneous cellulose acetylation. *Materials and product engineering,* Volume 21, pp. 577-584.

Hyde, A. M., Calabria, R., Arvary, R., Wang, X. and Klapars, A., 2019. Investigating the underappreciated hydrolytic instability of 1,8-Diazabicyclo[5.4.0]undec-7-ene and related unsaturated nitrogenous bases. *Organic process process & development*, Volume 23, pp. 1860-1871.

Ilmanen, P., 2017. Doctoral thesis: *Modeling of thin film evaporator for ionic liquid recycling.* Aalto University.

IOLITEC, 2019. *Applications of ionic lqiuids.* [Online]
Available at: https://iolitec.de/index.php/en/products/ionic_liquids/applications[Accessed 27 06 2019]

Kakko, T., King, A. W. T. and Kilpeläinen, I., 2017. Homogeneous esterification of cellulose pulp in [DBNH][OAc]. *Cellulose*, Volume 24, pp. 5341-5354.

Kazmi, B., Zahoor, A., Saud, H. and Ghouri, Z. K., 2018. Desulfurization of the dibenzothiophene (DBT) by using imidazolium-based ionic liquids (ILs). *Materials physics and chemistry*, Volume 1, pp. 1-11.

King, A. W. T., Asikkala, J., Mutikainen, I., Järvi, P. and Kilpeläinen, I., 2011. Distillable acid-base conjugate ionic liquids for cellulose dissolution and processing. *Angew. Chem. Int. Ed.*, Volume 50, pp. 6301-6305.

Koivisto, J., 2019. *Instructions to the NMR users.* Aalto University.

Krell, E., 1982. Chapter 5: Separating processes. In: *Handbook of laboratory distillation with an introduction to pilot plant distillation.* Elsevier .

Kroon, M. C. and Peters, C. J., 2010. Phase behaviour of ionic liquid systems. Royal Society of Chemistry.

Kubiczek, A. and Kaminski, W., 2017. Liquid-liquid extraction in systems containing butanol and ionic liquids - A review. *Chemical and process engineering,* Volume 38, pp. 97-110.

Kukla, N., 1996. Short path distillation gently separate heat sensitive substances. *CAV,* Volume 8, pp. 26-28.

Kukla, N., 1997. Gentle distillation in chemical industry. *Chemical engineering world,* Volume 32, pp. 33-36.

Kukla, N., 2000. Gentle separation distillation in vacuum protects thermally sensitive materials. *Process*, Volume 9, pp. 100-102.

Kuzmina, O. and Hallett, J. P., 2016. *Application, purification and recovery of ionic liquids.* Elsevier.

König, A., Stepanski, M., Kuszlik, A., Keil, P. and Weller, C., 2008. *Ultra purification of ionic liquids by melt crystallisation.* Elsevier.

Lauer, H. H. and Rozing, G. P., 2014. *High Performance Capillary Electrophoresis.* Agilent Technologies, Inc..

Lee, K. M., Ngoh, G. C. and Chua, A. S. M., 2015. Ionic liquid-mediated solid acid saccharification of sago waste: kinetic, ionic liquid recovery and solid acid catalyst reusability study. *Industrial crops and products,* Volume 77, pp. 415-423.

Liang, X., Fu, Y. and Chang, J., 2016. Recovery of ionic liquid via a hybrid methodology of electrodialysis with ultrafiltration after biomass pretreatment. *Bioresource technology*, Volume 220, pp. 289-296.

Lin, S. W. and Yoo, C. K., 2009. Short-path distillation of palm olein and characterization of products. *Eur. J. Lipid Sci. Technol.,* Volume 111, pp. 142-147.

Lipscomb, G., Varanasi, S., Pari-Pati, P. and Dadi, A. P., 2012. *Ionic liquid recovery and purification in biomass treatment processes.* Patent No. WO 2012/064868 A2.

Lopes, J. N. A. C. and Rebelo, L. P. N., 2010. Ionic liquids and reactive azeotropes: the continuity of the aprotic and protic classes. *Phys. Chem. Chem. Phys.*, Volume 12, pp. 1948-1952.

Losetty, V., Sivapragasam, M. and Wilfred, C. D. AP, 2016. Recent advances and thermophysical properties of acetate-based protic ionic liquids. *Chemical Sciences Journal*, Volume 7, pp. 1-7.

Lovelock, K. R. J. and Licence, P., 2013. Ionic liquid studied at ultra-high vacuum. In: *Ionic liquid UnCOILed: Critical expert overviews.* John Wiley & Sons, Inc..

Lutišan, J. and Cvengroš, J., 1995. Mean free path of molecules on molecular distillation. *The chemical engineering journal,* Volume 56, pp. 39-50.

Lutišan, J., Cvengroš, J. and Micov M., 2002. Heat and mass transfer in the evaporating film of a molecular evaporator. *Chemical Engineering Journal,* Volume 85, pp. 225–234.

Mai, N. L., Nguyen, N. T., Kim, J. I., Park, H. M., Lee, S. K. and Koo, Y. M., 2012. Recovery of ionic liquid and sugars from hydrolyzed biomass using ion exclusion simulated moving bed chromatography. *Journal of Chrmotography A,* Volume 1227, pp. 67–72.

Masri, A. N., Mi, A. M. and Leveque, J-M., 2016. A review on dicationic ionic liquids: classification and application. *Industrial engineering & management*, Volume 5, pp. 1–7.

Massonne, K., 2010. *Distillation of ionic liquids.* Patent No. US 2010/0300870 A1.

McCabe, W. L., Harriott, P. and Smith, J. C., 2005. *Unit operations of chemical engineering.* McGraw-Hill, 7 edition.

Mestrelab, 2019. *MestReNova manual*.

MettlerToledo, 2019. *Good Titration Practice in KF Titration*.

Meyer, F., Eggers, R., Oehlke, K., Harbaum-Piayda, B., Schwarz, K. and Siddiqi, M. A., 2011. Application of short path distillation for recovery of polyphenols from deodorizer distillate. *Eur. J. Lipid Sci. Technol,* Volume 113, pp. 1363–1374.

Michud, A., 2016. Doctoral thesis: *Development of a novel process for the production of man-made cellulosic fibers from ionic liquid solution.* Aalto University .

Nichols, L., 2019. *Fractionating columns.* [Online]
Available at:
https://chem.libretexts.org/Bookshelves/Organic_Chemistry/Book%3A_Organic_Chemistry_Lab_Techniques_(Nichols)/5%3A_Distillation/5.3%3A_Fractional_Distillation/5.3B%3A_Fractionating_Columns [Accessed 27 06 2019]

Nowicki, J., Muszynski, M. and Mikkola, J-P., 2016. Ionic liquid derived from organosuperbases: en route to superionic liquids. R*oyal society of chemistry*, Volume 6, pp. 9194–9208.

Oliveira, A. C. M. and Miller, M. R., 2014. Purification of Alaskan Walleye Pollock (Gadus chalcogrammus) and New Zealand Hoki (Macruronus novaezelandiae) liver oil using short path distillation. *Nutrients*, Volume 6, pp. 2059–2076.

Osch, D. J. G. P., Kollau, L. J. B. M., Bruinhorst, A., Asikainen, S., Rocha, M. A. A. and Kroon, M. C., 2017. Ionic liquid and deep eutectic solvents for lignicellulosic biomass fractionation. *Phys. Chem. Chem. Phys.*, Volume 19, pp. 2636–2665.

Ostonen, A., 2017. *Thermodynamic study of protic ionic liquids,* Aalto University.

Oterhals, A. and Berntssen, M. H. G., 2010. Effects of refining and removal of persistent organic pollutants by short-path distillation on nutritional quality and oxidative stability of fish oil. *J. Agric. Food Chem*, Volume 58, pp. 12250–12259.

Parviainen, A., King, A. W. T., Mutikainen, I., Hummel, M., Selg C., Hauru, L. K. J., Sixta, H. and Kilpeläinen, I., 2013. Predicting cellulose solvating capabilities of acid-base conjugate ionic liquids. *ChemSuschem*, Volume 6, pp. 2161–2169.

Parviainen, A., Wahlström, R., Liimatainen, U., Liitiä, T., Rovio, S., Helminen, J. K. J., Hyväkkö, U., King, A. W. T., Suurnäkki, A. and Kilpeläinen, I., 2015. Sustainability of cellulose dissolution and regeneration in 1,5-diazabicyclo[4.3.0]non-5-enium acetate: a batch simulation of the IONCELL-F process. *Royal society of chemistry*, Volume 5, pp. 69728–69737.

Parviainen, A. P., 2016. Doctoral thesis: *Acid-base conjugate ionic liquids in lignocellulose processing: synthesis, properties and applications*. Helsinki University.

Pietsch, A. and Jaeger, P., 2007. Concentration of squalene from shark liver oil by short-path distillation. *Eur. J. Lipid. Sci. Technol*, Volume 109, pp. 1077–1082.

Plechkova, N. V. and Seddon, K. R., 2007. Applications of ionic liquids in the chemical industry. *Chemical society reviews*, Volume 37, pp. 123–150.

Proionic, 2019. *Proionic.* [Online]
Available at: https://www.proionic.com/company/downloads.php
[Accessed 27 06 2019].

Ribeiro, F. M. S., Lima, C. F. R. A. C., Silva, A. M. S. and Santos, L. M. N. B. F., 2018. Experimental evidence for azeotrope formation from protic ionic liquids. *ChemPhysChem*, Volume 19, pp. 2364–2369.

Rooney, D., Jacquemin, J. and Gardas, R., 2010. Thermophysical properties of ionic liquids. Springer.

Runge, W., 2014. *Case study: Solvent Innovation GmbH ,* KIT.

Schäfer, T., Rodrigues, C. M., Afonso, C. A. M. and Crespo, J. G., 2001. Selective recovery of solutes from ionic liquids by pervaporation- a novel approach for purification and green processing. *Chem.Commun.,* pp. 1622–1623.

Seader, J. D., Henley ,E. J. and Roper, D. K., 2011. *Separation process principles.* John Wiley & Sons, Inc.

Sigma-Aldrich, 2019. *Introduction to ionic liquids.* [Online]
Available at: https://www.sigmaaldrich.com/technical-documents/articles/chemfiles/ionic-liquids0.html
[Accessed 27 06 2019].

Sigma-Alrich, 2019. *CBILS©.* [Online]
Available at: https://www.sigmaaldrich.com/technical-documents/articles/technology-spotlights/cbils.html
[Accessed 27 06 2019]

Sinnott, R. K., 2005. *Chemical engineering design.* Elsevier, 6 edition.

Siriwardana, A. I., 2015. Industrial applications of ionic liquids. Springer.

Sklavounos, E., Helminen, J. K. J., Kyllönen, L., Kilpeläinen, I. and King, A. W. T., 2016. Ionic liquids: Recycling. *Encyclopedia of inorganic and bioinorganic chemistry*, pp. 1–15.

Skoog, D. A., Holler, F. J. and Crouch, S. R., 2018. *Principles of instrumental analysis,* 7 edition.

Smith, C. L., 2012. *Distillation control: An engineering perspective.* John Wiley & Sons, Inc. .

Tagliaro, F., Manetto, G., Crivellente, F. and Smith, F. P., 1998. A brief introduction to capillary electrophoresis. *Forensic Science International,* Volume 92, pp. 75–88.

Tan, S. S. Y. and MacFarlane, D. R., 2009. Ionic liquids in biomass processing. Springer Verlag Berlin Heidelberg.

Taylor, A. W., Lovelock, K. R. J., Deyko, A., Licence, P. and Jones, R. G., 2010. High vacuum distilaltion of ionic liquids and separation of ionic liquid mixtures. *Physical chemistry chemical physics*, Volume 12, pp. 1772–1783.

TCI, 2019. *Ionic Liquids [Specialty Synthesis].* [Online]
Available at: https://www.tcichemicals.com/eshop/en/be/category_index/12582/ [Accessed 27 06 2019]

Walas, S., 1990. *Chemical process equipment.* Butterworth-Heinemann .

Wasserscheid, P. and Welton, T., 2003. *Ionic liquids in synthesis.* WILEY-VCH.

Vallinkoski, A. V. (2019). *Tutkijakolmikon perustama liuotinyritys voi mullistaa tekstiilituotannon.* Noudettu osoitteesta https://www.helsinki.fi/fi/uutiset/luonnontieteet/tutkijakolmikon-perustama-liuotinyritys-voi-mullistaa-tekstiilituotannon[Accessed 27 06 2019]

Vazquez, L. and Akoh, C. C., 2010. Fractionation of short and medium chain fatty acid ethyl esters from a blend of oils via ethanolysis and short-path distillaiton. *Chem Soc*, Volume 87, pp. 917–928.

Xu, X., Jacosen, C., Nielsen, N. S., Heinrich, M. T. and Zhou, D., 2002. Purification and deodorization of structured lipids by short path distillation. *Eur. J. Lipid Sci. Technol.*, Volume 104, pp. 745–755.

Xu, X., 2005. Short-path distillation for lipid processing.

Yesappa, L., Niranjana, M., Ashokkumar, S. P., Vijeth, H., Basappa, M., Dwivedi, J., Petwal, V. C., Ganesh, S. and Devendrappa, H., 2018. Optical properties and ionic conductivity studies of an 8 MeV electron beam irradiated poly(vinylidene fluoride-co-hexafluoropropylene)/LiClO4 electrolyte film for opto-electronic applications. *The Royal Society of Chemistry*, Volume 8, pp. 15297–15309.

Zhou, J., Sui, H., Jia, Z., Yang, Z., He, L. and Li, X., 2018. Recovery and purification of ionic liquids from solutions: a review. *The Royal Society of Chemistry*, Volume 8, pp. 32832–32864.

Zhou, Q., Lu, X., Zhang, S. and Guo, L., 2011. Physicochemical properties of ionic liquids. John Wiley & Sons, Inc..

Zhu, D., Huang, F-X., Xu, S-L. and Li, Y., 2016. Multi-scale simulation of falling film short-path distillation. *Canadian Society for Chemical Engineering*, Volume 94, pp. 1533–1538.

Zou, L. and Akoh, C. C., 2012. Identification of tocopherols, tocotrienols, and their fatty acid esters in residues and distillates of structured lipids purified by short-path distillation. *Journal of agricultural and food chemistry,* Volume 61, pp. 238–246.

Zuiderweg, F. J., 1957. *Laboratory manual of batch distillation.*

APPENDICES

Appendix 1. **The list of ionic liquid applications** (IOLITEC, 2019) (Siriwardana, 2015), (Sklavounos et al., 2016), (Plechkova & Seddon, 2007), (Greaves & Drummond, 2015), (Wasserscheid & Welton, 2003)

Application fields	**Specific application areas** *(Note: P: Pilot, C: Commercialized, R&D: Research & Development, *: no information)*
Electrochemistry	Batteries (R&D)
	Super-capacitors (C)
	Solar panels (*)
	Fuel cells (R&D)
	Sensors (C)
	Metal finishing (P)
	Electro-optics (P)
	Space propulsion (*)
Analytics	Matrices for mass spectrometry (P)
	Analyze extraction media (P)
	Stationary phase of CE, HPLC, GC (C)
	Protein crystallization (C)
	Karl-Fischer titration (C)
Synthesis & Catalysts	Organic reactions (C)
	Nano particles synthesis (C)
	Microwave chemistry (*)
	Multiphasic reactions & extractions
	Catalysts/Biocatalysis (C)
	Enzymatic reactions (R&D)
	Polymerization-Dimerization and oligomerization of olefins (P and C)
	Acid scavenging (P and C)

Process technology	Gas separation (R&D)
Extraction/Separation	Enhanced oil extraction (*)
	Upgrading minerals (e.g. ores, oil, sand, etc.) (*)
	Extraction or separation of heavy elements (P)
	Membranes (*)
	Extractive distillation (P and C)
	Liquid-liquid extraction (P and C)
Bio-refinery	Biomass processing (P)
	Extractives isolation & processing (*)
	Biofuels production (*)
Heat transport	Thermal fluids (R&D)
	Phase change material (R&D)
	Sorption cooling (P)
Functional fluids	Lubricants (P)
	Coatings (*)
	Surfactants (P)
	Hydraulic fluids (C)
	Plasticizes (*)
	Compatibilizers for pigment pastes (C)
	Antistatic additives for cleaning fluids (C)
Engineering	Liquid crystals (*)
	Carbon dioxide/Gas capture or purification (P)
	Ionic compressor (P and C)
	Nano particle stabilization (*)
	Chemical modification or regeneration of biopolymer (*)
	Protein crystallization and stabilization (*)
	Biocides (*)
Pharmaceutical industry	Drug delivery (*)
	Active pharmaceutical ingredients (*)

Appendix 2. Ionic liquids separation and purification methods

Methods	Specific methods	Descriptions	Advantages	Disadvantages	References
Phase separation	• Aqueous biphasic systems (ABS) or Ionic liquid –based three phase partitioning (ILTPP)	Using cosmotropic salt (e.g. K_3PO_4) into aqueous solution of ILs form an upper IL-rich phase and a lower salt-rich phase	Low energy use Easy and rapid removal Low cost and scalable	Disposal of additional salts ILs contamination	(Lee et al., 2015) (Sklavounos et al., 2016)
	• Induced phase separation using additives	Using organic co-solvents as carbohydrates or $ScCO_2$	Environmentally friendly process	Complex process and high energy consumption Low extraction efficiency with organic co-solvents	(Siriwardana, 2015) (Tan & MacFarlane, 2009) (Kuzmina & Hallett, 2016)
Crystallization	• Solution crystallization	ILs are crystallized out by cooling while impurities are remained in the solution	High purity	High energy consumption Solid handling issue in a large scale	(Sklavounos et al., 2016) (Kuzmina & Hallett, 2016)
	• Pressure-induced crystallization	Crystallization by using high pressure	High purity	Not all ILs crystallize under high pressure	(Sklavounos et al., 2016) (Kuzmina & Hallett, 2016)
	• Melt crystallization – Static and dynamic layer melting	A crystalized ILs layer is generated on a cooled surface as a heat exchanger	High purity ILs (≥99%)	High energy consumption	Sklavounos et al., 2016) (Kuzmina & Hallett, 2016)

	• Melt crystallization - Zone melting	A solid column of a melted ILs mixture is crystalized in a glass tube by cooling in a controlled way. A mobile energy source (e.g. IR laser) to melt a small region contained impurities with different molecular shape from ILs in a tube, then impurities move to the liquid zone in the end of the tube and travel slowly along the tube to leave purer materials behind	High purity ILs (≥99.9%)	Apply several melting/crystallization scans High energy consumption	(Sklavounos et al., 2016) (Kuzmina & Hallett, 2016)
Extraction	• Liquid-liquid extraction using solvents like water, organic solvents	Extraction hydrophobic ILs with water to remove metal or hydrophilic solutes from aqueous acid solution. Extraction of nonvolatile or thermally sensitive hydrophobic solutes from ILs by using organic solvents	Low energy use Low cost and scalable	Cross-contamination Toxic solvents	(Sklavounos et al., 2016) (Kuzmina & Hallett, 2016)
	• Liquid-liquid extraction using supercritical carbon dioxide	Load ILs to a high-pressure cartridge, then pressurized with CO_2 until reaching equilibrium. Depressurized the solute – saturated CO_2 phase in a flask of ethanol to weight the amount of organic solute or metal extracted	High selectivity Clean and energy-efficient technology	High pressure, CO_2 emission, safety issues High equipment cost Low recovery efficiency	(Blanchard & Brennecke, 2001) (Kuzmina & Hallett, 2016)

Distillation	• Vacuum distillation e.g. rotary evaporator, thin-film evaporator	Reduced pressure ILs remain as residue	Ultra-purification Prevent IL decomposition at ambient pressure	High energy usage Not yet practical in large scale Hydrolysis products problems	(Sklavounos et al., 2016)
	• Microwave-assisted distillation	Electromagnetic waves with radio frequencies used to heat ILs and remove water	No secondary waste products	High energy usage	(Tan & MacFarlane, 2009)
	• Molecular distillation	Short-path distillation under high-vacuum condition	Apply for heat-sensitive materials Short time exposure	High energy usage	(Kuzmina & Hallett, 2016)
	• Distillation by formation of carbene bases	Distillation of carbene base off acid anions and form the neutral carbene molecules, then reacted with fresh protic acids to re-form ILs	No secondary waste products	Operational difficulty to control an equimolar stoichiometry Higher cost	(Sklavounos et al., 2016) (Kuzmina & Hallett, 2016)
	• Distillation by decomposition reaction	ILs decompose into uncharged distillable compounds and re-form ILs under heating in vacuum condition	No secondary waste products	Operational difficulty to control decomposition process of ILs	(Sklavounos et al., 2016) (Kuzmina & Hallett, 2016)

	• Distillation as intact ion pairs	Distillation of aprotic ILs as intact ion pairs and condensation at lower temperatures without decomposition	No secondary waste products	Low distillation rate Operational difficulty	(Sklavounos et al., 2016) (Kuzmina & Hallett, 2016)
Membranes separation	• Pervaporation	ILs feed flow into a dense and non-porous membrane. The membrane downstream is kept under vacuum, while the membrane upstream is kept at atmospheric pressure	Mild operating conditions High selectivity Prevent ILs loss due to evaporation	Require development of high selectivity membranes Require larger membranes areas	(Schäfer et al., 2001)
	• Membrane distillation	A hydrophobic and porous membrane is used to remove water vapor from heated ILs and condensed on the distillate side	Concentration ILs from aqueous solution	Fouling	(Lipscomb, 2012) (Sklavounos et al., 2016)
	• Nanofiltration	Using modified ultra-filtration membranes to recover ILs in the permeate	Remove low molecular weight impurities (e.g. sugars) Low energy demand	Require appropriate membranes Control the performance of membranes (i.e. thickness and structure of solid layer)	(Avram et al., 2017)

	• Ultrafiltration	Using ultra filtration membranes (e.g. OAPMP-220)	Remove low molecular weight residual (e.g. lignin) Low energy demand	Fouling IL loss	(Liang et al., 2016)
	• Reverse osmosis	A membrane with the pore and chemical structure inhibit ILs ions	Permeating water or other solvents Low energy demand	IL retained Feed pressure control	(Sklavounos et al., 2016)
	• Electrodialysis	Pass through a series of ion exchange membranes under an applied electric current. ILs cations transport through the cation exchange membranes while ILs anions accumulate in the anion exchange membranes concentrate compartment.	Remove non-ionic solutes	Energy efficiency	(Kuzmina & Hallett, 2016)
Adsorption	• Adsorption by ion exchange resins	Prepare an ion exclusion liquid chromatography column, the proton ions in resin exchanged with cationic parts, charge species as ILs excluded from the charge resin, impurities as nonelectrolytes retained	Pre-concentration of ILs from aqueous solution for further processes	Pressure loss causes number of columns increasing and reduce ILs recovery efficiency Anions of ILs remain in the original solution	(Mai et al., 2012) (Sklavounos et al., 2016) (Kuzmina & Hallett, 2016)

	• Adsorption onto solid supports (e.g. activated carbon, silica, soils, sediments)	ILs are diluted with organic solvents to reduce viscosity before sorbents exposure Stirring ILs over activated carbon then passing down a short alumina column	Easy operation	Sorbents remain as nano-particulates contamination Physicochemical properties of ILs change after sorbents exposure	(Sklavounos et al., 2016) (Kuzmina & Hallett, 2016)
Force field	• Gravity separation	ILs mixtures form two immiscible liquids and separate by gravity	Low cost and scalable	Low separation efficiency	(Kuzmina & Hallett, 2016)
	• Centrifugation	Using a centrifugal contactor to separate aqueous dispersions of hydrophobic ILs	Rapid separation	Small throughput	(Kuzmina & Hallett, 2016)
	• Magnetic separation	Using a magnetic field to incorporate high-spin transition metal ions from ILs	Remove metal impurities	Low separation efficiency Require heating up prior separation Limited application	(Kuzmina & Hallett, 2016)

Appendix 3. Short path distillation applications

Objectives	SPD units	Controlling parameters	Results	References
Distillation of [Emin][OAc]	Patented molecular distillation	Pressure: 0.05 mbar Distillation temperature: 170 °C Feed: 200 g (4 hours)	Distillate: 170 g, purity >95% Residue: 30 g	(Massonne, 2010)
Distillation of [Eeim][OAc]	Patented molecular distillation	Pressure: 0.05 mbar Distillation temperature: 170 °C Feed: 200 g (2 hours)	Distillate: 190 g, purity >95% Residue: 10 g	(Massonne, 2010)
Distillation of [TMGH][CO_2Et]	A Büchi Kugelrohr short-path distillation	Pressure: 1.3 mbar Distillation temperature: 100-200 °C Feed: 3 g (acid: base = 1:1) (1 hour)	Distillate: 99.4%, purity >99% Residue: 0.6%	(King et al., 2011)
Distillation of [DBNH][CO_2Et]	A Kugelrohr apparatus	Pressure: 1 mbar Distillation temperature: 170 °C Feed: 1.5 g (acid: base = 1:1)		(Parviainen et al., 2013)
Distillation of [Bmin][OAc], [Eeim][OAc] Distillation of [Emin][OAc]	A short-path distillation A short-path distillation	Pressure: 0.05 mbar Distillation temperature: 170 °C Pressure: 0.3 mbar Distillation temperature: 180 °C	Distillate: 90% Residue: 10% Distillate: 100% Residue: 0%	(Sklavounos et al., 2016)
Recover [Amin]Cl in homogeneous cellulose acetylation	Pope 2” wiped-film still from Pope Scientific Inc., Saukville, WI, USA, and with a diffusion pump and a high-vacuum pump.	Pressure: 0.13 mbar Distillation temperature: 95 °C Feed rate: 1 mL/min Feed temperature: 80 °C Scrapper speed: 440 rpm	Purity 99.5%	(Huang et al., 2013)

Purification of fish oil	Pope 2" wiped-film still from Pope Scientific Inc., Saukville, WI, USA, and with a diffusion pump and a high-vacuum pump. Surface area: 0.033 m^2 The estimated residence time: 10.9-14.5 L/h.m^2	Pressure: 0.05-0.06 mbar (1^{st} pass) and 0.01-0.02 mbar (2^{nd} pass) Evaporator temperature: 150 °C (1^{st} pass) and 210 °C (2^{nd} pass) Condenser temperature: 55 °C Feed: 1500 mL (60 °C), rate 360-480 mL/h Roller speed: 450 – 500 rpm	Remove lipid peroxides and lipid hydrolysis products	(Oliveira & Miller, 2014)
Deacidification of soybean oil	A wiped-film molecular distillation KDL5 from UIC GmbH, Alzenau, Germany, included a diffusion pump and a mechanical pump Surface area of the evaporator: 0.048 m^2 Surface area of the internal condenser: 0.065 m^2	Pressure: 6-10 bar Distillation temperature: 180 °C Condenser temperature: 40 °C Feed temperature: 50 °C Feed flow: 4 mL/min Scrapper speed: 220 rpm	Remove FFAs and avoid color darkening	(Han et al., 2019)
Fractionation of anhydrous milk fat into liquid and solid fat (triglycerides) fractions	Pilot scale wiped-film evaporator from The Pfaudler Co., Rochester, New York) Surface area of the evaporator: 0.115 m^2 Surface area of the condenser: 0.15 m^2	Pressure: 0.13-0.22 mbar Distillation temperature: 245-265 °C Feed temperature: 90-100 °C Feed rate: 15-43 kg/h	1^{st} liquid distillate: yield 2% 2^{nd} liquid distillate: yield 10% 3^{rd} semi-solid distillate: yield 32% Solid residues: yield 56%	(Arul et al., 1988)
Purification of structured lipids from the reaction of rape seed oil and capric acid	A bench-scale short path distillation KD6 from UIC GmbH, Alzenau-Hörstein, Germany	Pressure: 0.001 mbar Distillation temperature: 185 °C (Heat exchanger temperature 80 °C) Condenser temperature: 30 °C Feed rate: 66.5 mL/min	Poor results	(Xu et al., 2002)

Purification of squalene from shark liver oil	Pilot plant short-path distillation KD6 from UIC GmbH, Alzenau, Germany	Pressure: 0.1 mbar Distillation temperature: 215-230 °C Feed rate: 4 kg/h Feed temperature: 130-140 °C	Squalene 95%	(Pietsch & Jaeger, 2007)
Purification of diacylglycerols palm oil	A laboratory short-path distillation VKL-70 from VTA GmbH, Germany Surface area of the evaporator: 0.04 m^2	Pressure: 0.001 mbar Distillation temperature: 220-250 °C Feed rate: 0.5 kg/h Feed temperature: 80 °C	Distillate: 68-75%	(Lin & Yoo, 2009)
Distillation fatty acid ethyl esters from a blend of coconut oil and diary fat, into short and medium chain	Short-path distillation KDL-4 from UIC Inc., Joliet, IL, USA	Pressure: 0.14-0.2 mbar Distillation temperature: 40-80 °C Scrapper speed: 250 rpm Feed rate: 0.5 kg/h Feed temperature: 55 °C	Yield >80%	(Vazquez & Akoh, 2010)
Remove persistent organic pollutants in fish oil	Pilot plant short-path distillation KD6 from UIC GmbH, Alzenau-Hörstein, Gemany Surface area of the evaporator: 0.06 m^2	Distillation temperature: 206 °C Condenser temperature: 60 °C Scrapper speed: 400 rpm Feed rate: 6 kg/h	90% reduction	(Oterhals & Berntssen, 2010)
Purification of structured lipids as triacylglycerols by remove free fatty acids	Short-path distillation KDL-4 from UIC Inc., Joliet, IL, USA	Pressure: <0.13 mbar Distillation temperature: 185 °C Condenser temperature: 20-25 °C Scrapper speed: 200 rpm Feed rate: 100 mL/h Feed temperature: 65 °C	Remove most of free fatty acid	(Zou % Akoh, 2012)

Distillation of squalene from amaranth oil	Short-path distillation VKL-70 from VTA GmbH, Germany Surface area of the evaporator: 0.043 $m^{2.}$ Surface area of the condenser: 0.022 m^2	Pressure: 0.002 mbar Distillation temperature: 243 °C Condenser temperature: 60 °C Scrapper speed: 260 rpm Feed rate: 0.208 kg/h Feed temperature: 80-82 °C	Distillate 85%	(Babeanu et al., 2018)
Removal of traces of pesticides from rapeseed deodorizer distillate	A laboratory short-path distillation KDL-5 from UIC GmbH, Alzenau, Germany	Pressure: 0.006-0.01 mbar Distillation temperature: 100 °C Condenser temperature: 45 °C Scrapper speed: 300 rpm Feed rate: 0.208 kg/h Feed temperature: 50 °C	Remove ketones, aldehydes	(Meyer et al., 2011)

Appendix 4. The operation guide and troubleshooting for short path distillation device

Appendix 4.1: Short path distillation device operation guide

The operating procedure of SPD system is described by the following steps:

- Checking SPD and turning the power on.
- Melting a sample and the volume of the feed (to check the loss). It might take more than 1 hour.
- Removing the water residual inside SPD (if SPD is dry, skip this step)
  - turning on the heating unit of the feed at 80 °C (maybe the maximum temperature)
  - turning on the heating unit of the evaporator at 100 °C
  - turning on the heating unit of the internal condenser or distillate at 100 °C
  - turning on the heating unit of the residue at 100 °C
  - turning on the distillate and residue dosing pumps
  - putting plastic collectors under these pumps and the cold trap
  - collecting the remain water inside SPD
- Closing all valves of the vacuum pump system. Using vacuum grease to close the venting valve on the cold trap.
- Putting a small round flask (250 mL or 500 mL) to close the cold trap. Using vacuum grease to seal all the rest covers of its neck. Closing the cold trap valve (red color).
- Opening the valve V1 of the vacuum pump system and switching on the rotary vacuum pump. Plugging the diffusion pump. Waiting until the pressure is stable at least 30 min.
- Pouring to the feed vessel with using the silicon plug to close the feed system. The gear pump will be vacuum tight if the feed vessel contains liquid. Determining the weight of the feed.
- The feed is heated if the product is viscosity. The experiments kept the feed heating temperature at 80^{o}C for PIL solvent 1 and 2.
- Determining the gross weight of the distillate and residue receivers. Putting them under the dosing pumps.

- Turning on all heating units to the experimental temperatures (if skip the moisture removing step).
- Filling liquid nitrogen into the cold trap after the plant evacuation. This step repeats during the experiment as liquid nitrogen vaporizes fast (using a cork to close the top of the cold trap).
- Closing the valve V1 and opening the valve V2 of the vacuum pump system and waiting the value as low as possible (e.g. less than 0.1 mbar). It maybe takes 1 hour.
- Closing the valve V2. Opening the valve V1 and V3. (checking liquid nitrogen to ensure liquid vapor not go to the vacuum pump).
- Switching on the pressure gauge at different vacuum pressure.
- Turning on the wiper when all temperatures and vacuum pressure are reached. The vacuum pressure might be obtained lower when running the wiper. The wiper speed might be chosen to maintain the evaporator surface wetted completely. Higher the speed higher the residue. The motor speed of the wiper can be chosen lower than 70 rpm and followed the relationship of the motor speed and feed rate:

Set value	rpm	Feed rate (L/h)
000	00	0.001
100	10	0.18
300	30	0.54
500	50	0.9
700	70	1.26
900	90	1.62

- Opening the valve of the cold trap (the pressure increases but come back fast).
- Turning on the distillate and residue pumps (the pressure decreases, need to adjust the pressure, wait to stabilize).
- Starting distillation by turning on the feed dosing pump, removing the silicon plug, recording the operating time if necessary.
- Finishing the distillation process:
  - stopping the feed pump but keeping a little liquid to maintain the pressure for samples collecting

- turning off the heating units of the feed and the evaporator
- stopping the wiper when the evaporator temperature is less than 180°C
- turning off the heating units of the distillate and the residue (when no samples get out)
- turning off the distillate and residue pumps
- shutting off the valve between vacuum pump and vacuum line (V3)
- venting the cold trap by remove the glass plug and closing the valve of the cold trap. Removing the flask under the cold trap
- determining the sample weight of the distillate, residue and the cold trap
- running the vacuum pump at least 30 min with closed valves at the suction inlet, opening the gas ballast valve
- removing liquid from the cold trap
- turning off the power
- cleaning the device with distilled water

Appendix 4.2: Short path distillation device troubleshooting

SPD system can conduct at constant vacuum pressure, constant wiper speed, constant feed rate and feed temperature, constant evaporator jacket temperature, or constant cooling temperature in the internal condenser. The cooling temperature of the internal condenser should be above the melting point of the distillate product. The temperature difference between the evaporator jacket and the internal condenser should be at least 50ºC. For a watery solution, the temperature difference between the feed and the evaporator jacket temperature should be less than 100 ºC and the distillate quantity should be lower than 0.2 L/h to prevent breaking of the evaporator. Products containing high volatile components and solved gasses have to be degassed prior to distillation. The temperature of the cooling media of the internal condenser should be adjusted above the melting point of the distillate.

Several troubleshooting observed during the distillation experiments:

- The pressure can be obtained at lower pressure by filling the feed vessel, turning on pumps, switching on the wiper, and filling liquid nitrogen in the cold trap.

- The distillation until materials are included: metal parts - stainless steel 1.4571, glass parts - borosilicate glass 3.3, sealing material - FPM, PTFE and graphite. Depending on the distilled material, leakage can be found from the wiper basket shaft sealing (damaged or not lubricated), or from the fitting packing of the gear pump shaft, or crystallization inside piping and pumps. This can be addressed by choosing suitable materials, increasing the jacket temperatures.

Appendix 5. NMR measurement instructions

Nuclear magnetic resonance spectroscopy is a powerful tool for the quantitative determination of absorbing species. NMR is based on the measurement of electromagnetic radiation absorption of a certain atomic nuclei in a strong magnetic field as radio-frequency region (4-900 MHz), which lead to splitting their energy levels. Fourier transform (FT-NMR) spectrometer currently is the dominant commercially instrument. Based on types of NMR spectra, two available types of NMR instrument are wide-line spectrometers and high-resolution spectrometers. High-resolution Fourier transform spectrometers are quite expensive and equipped with superconducting magnets to provide the magnetic field with the strength from 1.4 to 23.5 tesla and frequencies from 60 to 1000 MHz. (Skoog et al., 2018)

The components of Fourier transform spectrometers NMR is presented in a schematic diagram of NMR (Yesappa et al., 2018). The central component is a superconducting magnet to ensure the sensitivity and resolution of the spectrometer at the highest field strength. The solenoid is made from superconducting niobium-tin or niobium-titanium wire in the liquid helium flask held in the outer filled liquid nitrogen. The sample is placed in the middle of magnet poles and surrounded by a transmitter-receiver coil. Radio-frequency radiation signals pass into radio frequency transmitter to create an intensive and reproducible pulse in the transmitter coil. The strength and the quality of radio-frequency radiation are controlled by the computer. The free-induction decay signal is collected from the receiver coil and amplified to the phase-sensitive detector. The detector produces the low-frequency, time-domain signal, which is digitized and saved in the control console for Fourier transform analysis. The results are plotted as frequency-domain spectrum in a

computer. The areas of ^{1}H NMR signals are proportional to the number of protons responsible for the peak. (Skoog et al., 2018)

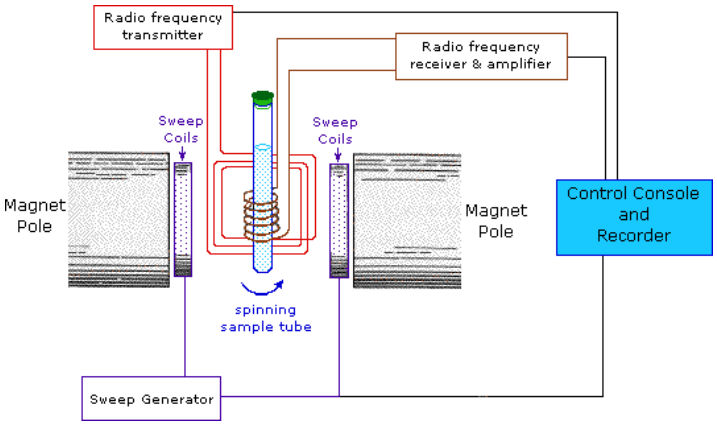

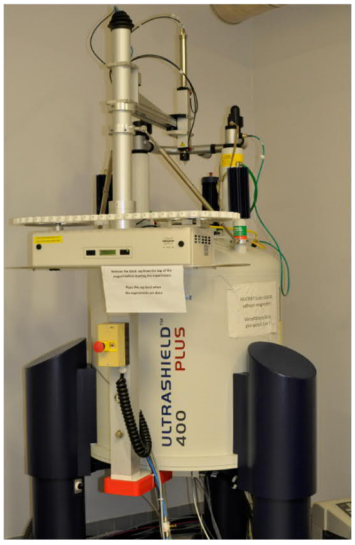

NMR instrumental characteristics can enhance the performance of NMR. A filed-frequency lock system is to offset the effect of magnet field fluctuations by using a reference nucleus as the deuterium in the solvent. The reference signal is monitored in a second transmitter coil at maximum resonance frequency and recorded the changes of the intensity to correct the magnet gap or drift into the coil. Shimming is to compensate for magnetic inhomogeneities. Shim coils are pairs of wire loops to control the current passed into the primary magnetic field. Spinning the sample along longitudinal axis reduces magnetic field inhomogeneities effects, but it causes sideband on the absorption bands. (Skoog et al., 2018)

NMR instrument was used AVIII400 (400 MHz spectrometer) from Bruker as can be seen above. The equipment has a 5 mm liquid-state broadband probe for ^{1}H, ^{13}C, ^{19}F, and ^{31}P. The sample preparation for ^{1}H NMR is required 1-5 mg sample diluted in deuterated solvents as dimethylsulfoxide D6 (99.8% D) (DMSO-d_6) to make homogeneous non-viscous samples (Koivisto, 2019). The sample is prepared in a clean glass sample tube and put to the sample tray of NMR instrument. The measurement is automatically controlled by NMR software in a computer. The spectra were integrated by MetsReNova software.

Appendix 6. Capillary Electrophoresis (CE) measurement instructions

Capillary electrophoresis is a separation method that occurs in a buffer-filled capillary under the influence of electric field. CE is a high-speed, high-resolution method for small sample volumes. A small band of the sample is injected into an aqueous buffer solution contained in a narrow capillary. Ions of the sample are migrated toward one of the electrodes located at each end of the buffer under a high voltage. The migration rate depends on charge, size, and molecular structure of a given species. At the same size of ions, the migration rate is faster with the greater charge, while at the same charge of ions, the migration rate id faster with the smaller size of ions. The electrophoresis separation is based on the difference from the rate of migration for analytes in the sample. (Skoog et al., 2018)

The electroosmotic flow (EOF) occurs as the bulk liquid migrating toward the cathode under a high voltage condition as the diagram below. The inside wall of the fused-silica capillary is negatively charged. The buffer cations create the electric double layer at the negative surface of the capillary. The cations in outer layer of the double layer are attracted to the negative electrodes as the cathode. (Skoog et al., 2018)

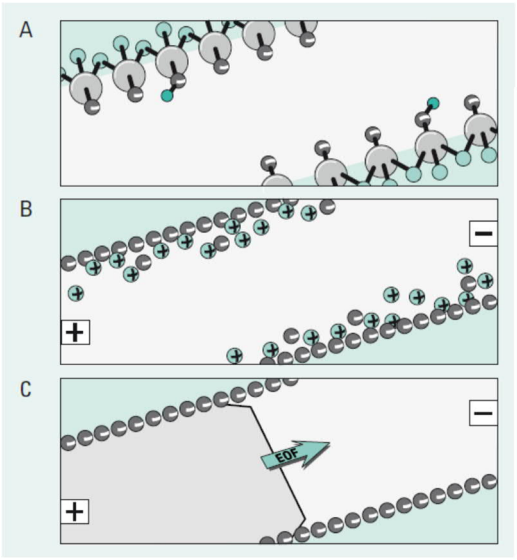

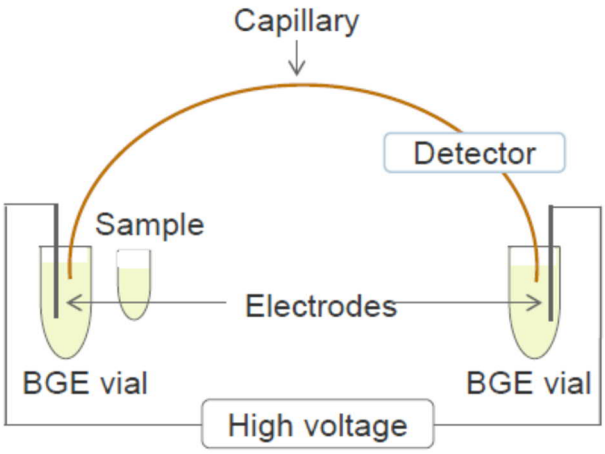

The schematic principles of the electroosmotic flow: A) negatively charged fused silica surface of the capillary B) hydrated cations of the buffer accumulating near the surface of the capillary, C) bulk flow in flat flow velocity profile towards the cathode upon under applied electric high voltage field (Lauer & Rozing, 2014)

UV absorption detection is adopted by detecting directly through 'a window' obtained by burning polyimide coating of fused silica capillaries (Tagliaro et al., 1998). Multiwavelength detection is applied by using diode array to obtain more information from a single measurement (Tagliaro et al., 1998). On the other hand, indirect absorbance detection is applied by using an ionic chromophore placed in the electrophoresis buffer (Skoog et al., 2018). The detector receives a constant signal with the presence of chromophore substance and then decreases when the analyte band passes through the detector (Skoog et al., 2018). The analyte is determined from the absorbance decreasing and plotted in a graph between migration time and absorbance (Skoog et al., 2018). Buffer additives can enhance the electrophoretic separation with various purposes, such as organic solvents, anionic/cationic/neutral surfactants, organic amines, metal ions, polymers, and so on (Tagliaro et al., 1998).

Generally, CE instrument requires only a capillary, two buffer containers, a high voltage power supply, and a detector (Tagliaro et al., 1998). All CE experiments were performed with an Agilent 7100 CE system from Agilent Technologies Inc. (USA) as shown in a schematic diagram below. The instrument is equipped with a UV-Vis diode-array detector and an air-cooling device for capillary cassette. Uncoated fused silica capillary was from Polymicro Technologies, USA) with dimensions 50 µm internal diameter and 375 µm outer diameter. The length of capillary to the detector was 30 cm and the total length was 38.5 cm. Before use, a bare fused silica capillary was pretreated by flushing with it with 1M sodium hydroxide for 20 min, 10 min with 0.1 M sodium hydroxide, 25 min with deionized water, and 5 min with background electrolyte solution (BGE). Pretreated capillary was coated with 1 wt. % polybrene coating. Thiourea at a concentration of 0.5 mM dissolved in BGE solution was used as a neutral EOF marker to evaluate the performance of capillary. The sample injection method is the hydrodynamic injection. The CE separation conditions were as follows: sample injection 10 s at 10 mbar, temperature of the cassette and the autosampler 25 °C, UV detection at 200 nm, voltage -20 kV (solvent 1) and -25 kV (solvent 2), and sodium acetate buffer pH 4 with an ionic strength of 10 mM (solvent 1) or 20 mM (solvent 2). Before each run, the capillary was rinsed for 2 min with BGE solution. The electrophoretic runs were repeated 5 times.

Appendix 7. Karl-Fischer titration instructions

The water content in a sample can be identified by Karl-Fischer titration (K-F titration) through the reaction with iodine and excess sulfur dioxide. Alcohol like methanol is used as a solvent to ensure the stoichiometric ratio of the reaction between iodine and water at 1:1. Pyridine acts as a buffer agent to shift the equilibrium by neutralizing formed acids (i.e. HI and H_2SO_4). The rate of K-F titration depends on pH of the sample, and the pH range for K-F titration is 5.5-8. The general chemical equation for K-F titration is indicated as following reaction (MettlerToledo, 2019):

$$ROH + SO_2 + 3RN + I_2 + H_2O \rightarrow (RNH)SO_4R + 2(RNH)I$$

There are two different K-F titration techniques, including volumetric K-F titration and coulometric K-F titration. The colourmetric K-F titration is a method where iodine is generated by electrochemical oxidation in the reaction cell, to test trace water 1 ppm or 5%. On the other hand, the volumetric K-F titration is a method where iodine is added by a motorized piston burette, to test water content 100 ppm or 100%.

K-F titration instrument was used by Mettler Toledo DL53 with titrator DV705 as the picture above. Chemical reagents were used Hydranal composite 5, Hydranal methanol, and standard water 1% solution. The program was run KF117, KF119, KF127 and KF131. The sample size depends on the water content of the sample. According to the graph below, the

amount of water is fixed at 10 mg, the water content of the sample can be guessed from 1 ppm to 100%, then a line can be drawn to connect the estimated water content with the point of 10 mg and cross the amount of sample line at one point. This point is the sample weight for the titration.

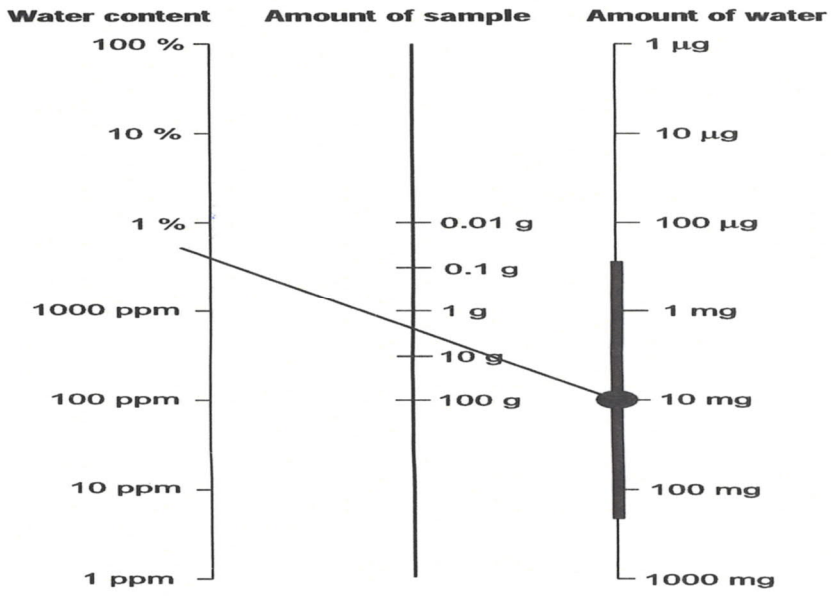

The testing procedure is explained as below:

- Rinse a syringe with sample
- After that fill the syringe with the suitable amount of sample. Wipe needle with a paper towel
- Place the syringe with sample on a balance. Tare to zero
- Press RUN on the titration
- Inject sample into the titration cell, pull back the syringe so that the last drop from the needle flows back to the needle
- Place again the syringe with sample on the balance and record the weight of measured sample
- Enter the weight number on the titrator and start the titration measurement

Appendix 8. Batch distillation experiments

Appendix 8.1: Experiment #1

Samples	Weight, g	Mass percentage, wt.%
Feed	134	100
Fraction 1	24	18
Fraction 2	18	31
Fraction 3	24	49
Fraction 4	14	60
Fraction 4	25	78
Residue	5	4
Cold trap	5	4
OUT	115	86
Loss	19	14

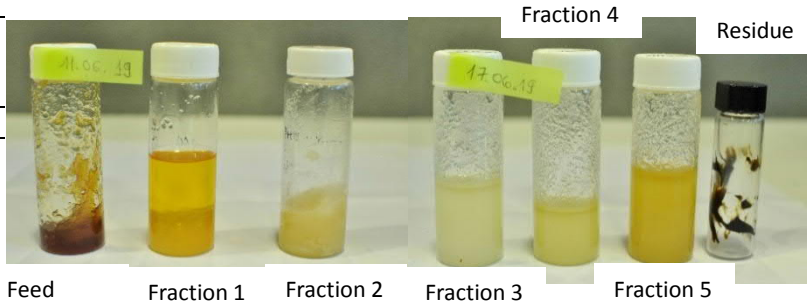

Samples	NMR results, base molar %	NMR results, hydrolysis (1), molar %	NMR results, hydrolysis (2), molar %	NMR results, acid, molar %	NMR results, water signal
Feed	38.3	1.1	0.4	60.2	no
Fraction 1	88.5	0	0	11.5	no
Fraction 2	44.4	0	0	55.6	no
Fraction 3	40	0	0	60	no
Fraction 4	40	0	0	60	no
Fraction 5	40	0	0	60	no
Residue	9.5	13.2	17.2	60.2	no
Cold trap	0	0	0	0	only water

Samples	CE results, base molar %	CE results, hydrolysis, molar %	CE results, by-product, molar %	CE results, acid, molar % (calculated)	Karl-Fischer results, water, mass%
Feed	45.7 ± 1.2	0	0	54.3 ± 1.2	N/A
Fraction 1	65.3 ± 1.2	0	0	34.7 ± 1.2	0.11
Fraction 2	47.3 ± 1.3	0	0	52.7 ± 1.3	N/A
Fraction 3	45.7 ± 0.8	0	0	54.3 ± 0.8	0.68
Fraction 4	47.3 ± 2.2	0	0	52.7 ± 2.2	0.13
Fraction 5	48.9 ± 1.1	0	0	51.1 ± 1.1	0.13
Residue	3.5 ± 0.1	6.6 ± 0.1	0	89.9 ± 0.1	N/A

Time, hour	Bottom temp., °C	Condensate temp., °C	Pressure, mbar	Notes
00:00	124	68	0,24	Fraction 1 collected
00:26	136	115	0,22	
00:36	138	121	0,22	Fraction 2 collected
00:45	139	124	0,3	
00:51	141	122	0,21	Fraction 3 collected
01:03	145	124	0,21	
01:10	149	122	0,23	Fraction 4 collected
01:22	171	115	0,25	
01:29	176	113	0,27	Fraction 5 collected
01:35	186	113	0,29	
01:40	200	111	0,31	

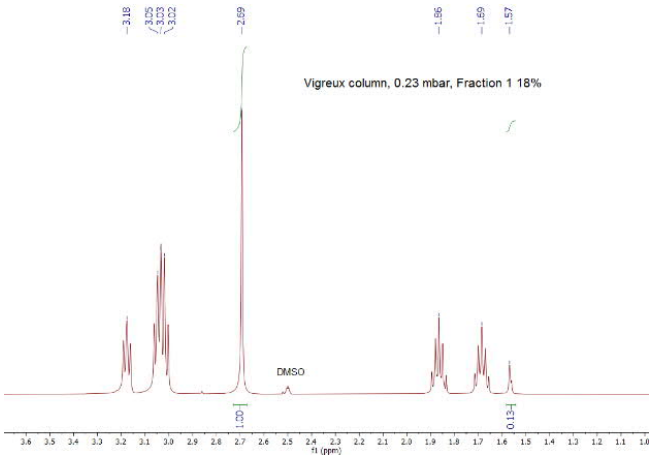

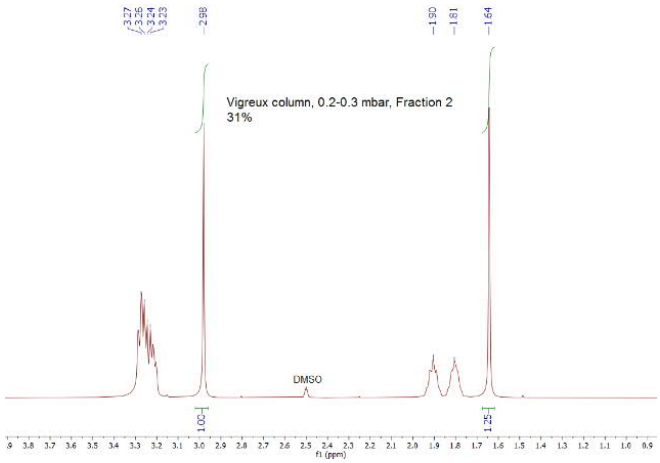

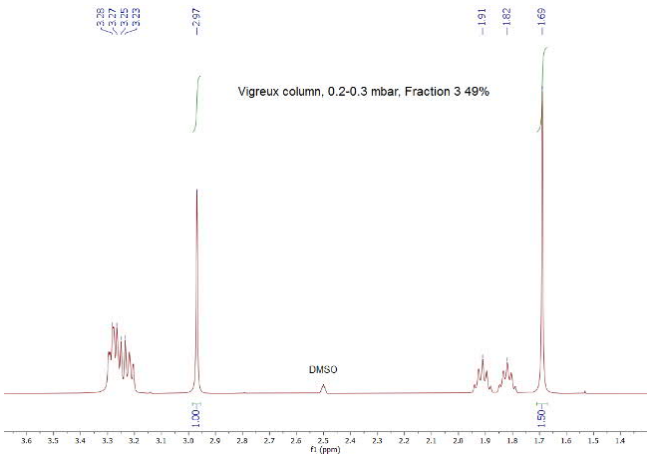

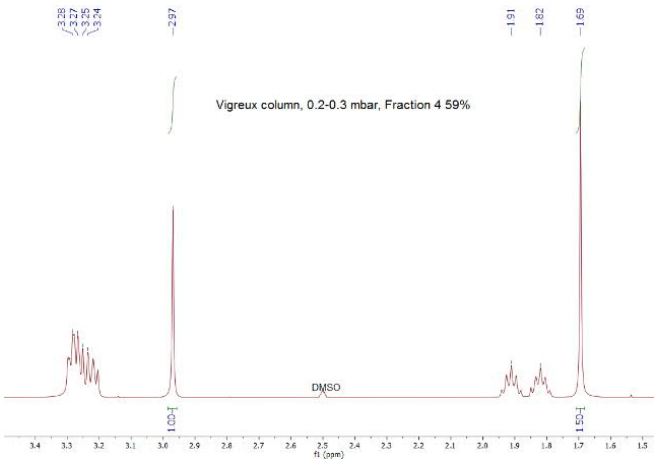

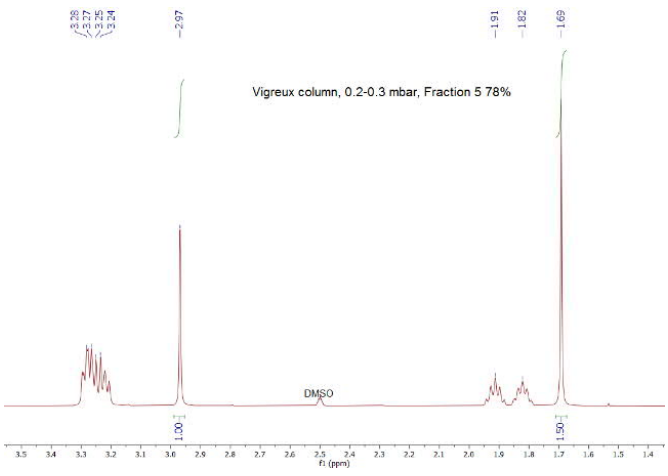

Appendix 8.2: Experiment #2

Samples	Weight, g	Mass percentage, wt.%
Feed	81	100
Fraction 1	15	19
Fraction 2	24	48
Fraction 3	6	56
Residue	34	42
Cold trap	2	2
OUT	81	100
Loss	0	0

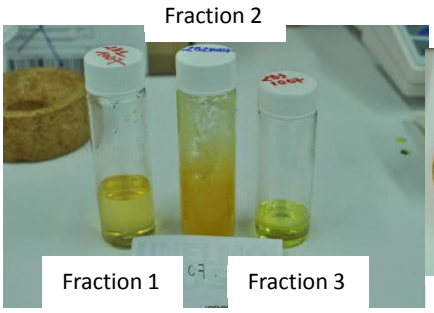

Fractions from the distillate collector

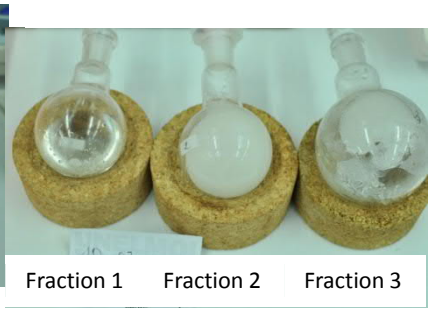

Samples	NMR results, base molar %	NMR results, hydrolysis (1), molar %	NMR results, hydrolysis (2), molar %	NMR results, acid, molar %	NMR results, water signal
Feed	49.8	0	0	50.2	no
Fraction 1	90.9	0	0	9.1	no
Fraction 2	50	0	0	50	no
Fraction 3	40.2	0	0	59.8	no
Residue	39.7	0	0	60.3	no
Cold trap	0	0	0	0	only water

Samples	CE results, base molar %	CE results, hydrolysis, molar %	CE results, by-product, molar %	CE results, acid, molar % (calculated)	Karl-Fischer results, water, mass%
Feed	35 ± 0.4	0	0	65 ± 0.4	N/A
Fraction 1	61.3 ± 1.5	0	0	38.7 ± 1.5	N/A
Fraction 2	44.4 ± 1.2	0	0	55.6 ± 1.2	N/A
Fraction 3	41.8 ± 1.5	0	0	58.2 ± 1.5	N/A
Residue	37 ± 1.7	0	0	63 ± 1.7	N/A

Time, hour	Bottom temp., °C	Condensate temp., °C	Pressure, mbar	Notes
00:00	134	88	0,7	Fraction 1 collected
00:01	134	90	0,7	
00:05	134	79	0,7	
00:07	134	73	0,7	
00:10	135	71	0,7	Fraction 2 collected
00:12	136	93	0,7	
00:15	138	106	0,7	
00:20	142	113	0,7	
00:25	146	116	0,7	
00:38	161	113	0,7	
00:42	164	112	0,7	Fraction 3 collected
00:55	172	123	0,7	

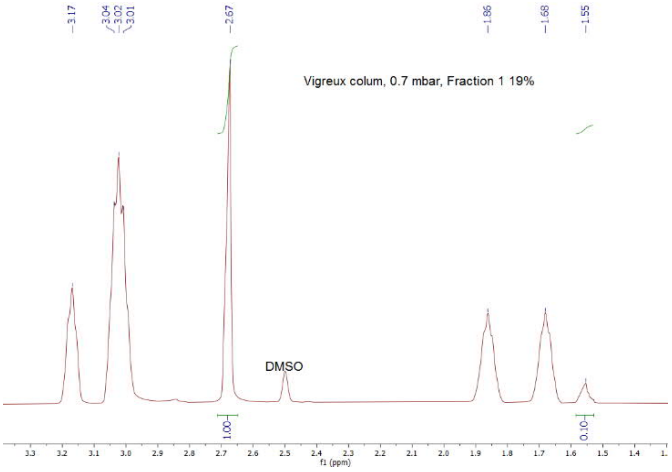

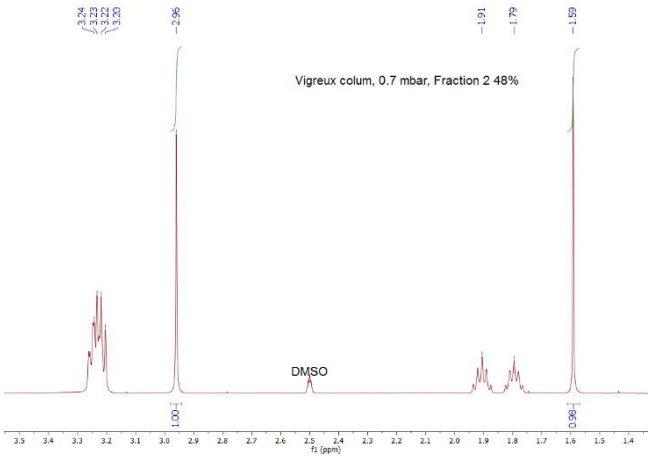

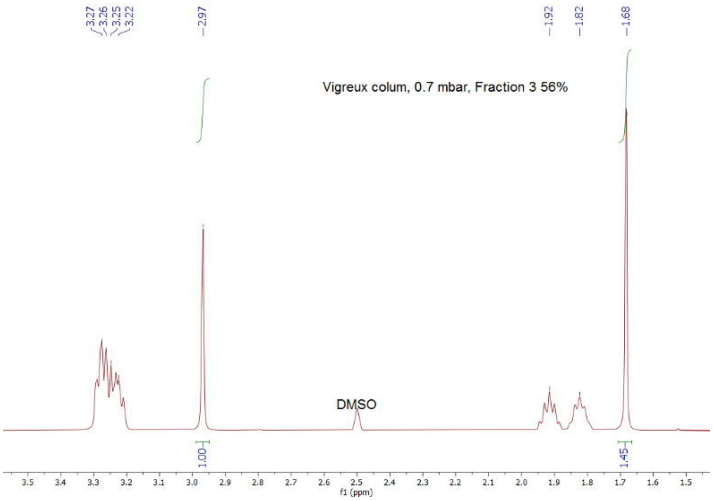

Appendix 8.3: Experiment #3

Samples	Weight, g	Mass percentage, wt.%
Feed	110	100
Fraction 1	18	16
Fraction 2	29	43
Fraction 3	16	57
Residue	42	38
Cold trap	1	1
OUT	106	96
Loss	4	4

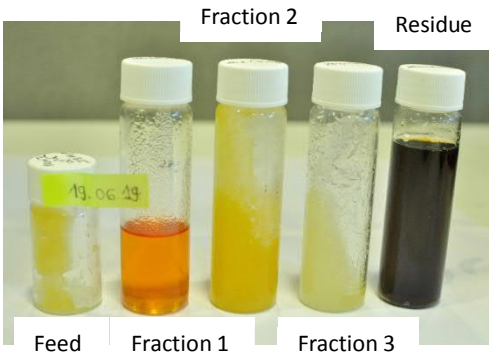

Samples	NMR results, base molar %	NMR results, hydrolysis (1), molar %	NMR results, hydrolysis (2), molar %	NMR results, acid, molar %	NMR results, water signal
Feed	50	0	0	50	no
Fraction 1	97.1	0	0	2.9	no
Fraction 2	49	0	0	51	no
Fraction 3	40	0	0	60	no
Residue	38.5	0.8	0	60.7	no

Samples	CE results, base molar %	CE results, hydrolysis, molar %	CE results, by-product, molar %	CE results, acid, molar % (calculated)	Karl-Fischer results, water, mass%
Feed	50.6 ± 2.1	0	0	49.4 ± 2.1	N/A
Fraction 1	63.1 ± 0.6	0	0	36.9 ± 0.6	0.18
Fraction 2	55.5 ± 2.1	0	0	44.5 ± 2.1	N/A
Fraction 3	42.4 ± 0.4	0	0	57.6 ± 0.4	0.07
Residue	47.3 ± 1.2	0	0	52.7 ± 1.2	0.1

Time, hour	Bottom temp., °C	Condensate temp., °C	Pressure, mbar	Notes
00:00	136	84	1,1	Fraction 1 collected
00:01	137	79	1,1	
00:04	137	74	1,1	
00:06	134	68	1,1	
00:14	136	72	1,1	
00:24	139	86	1,1	
00:33	140	91	1,1	
00:48	140	94	1,1	Fraction 2 collected
00:57	140	107	1,1	
01:13	145	108	1,1	
01:21	145	118	1,1	
01:33	146	121	1,1	
01:39	146	122	1,1	Fraction 3 collected
01:51	149	124	1,1	
01:53	152	124	1,1	
02:05	159	122	1,1	
02:10	161	122	1,1	

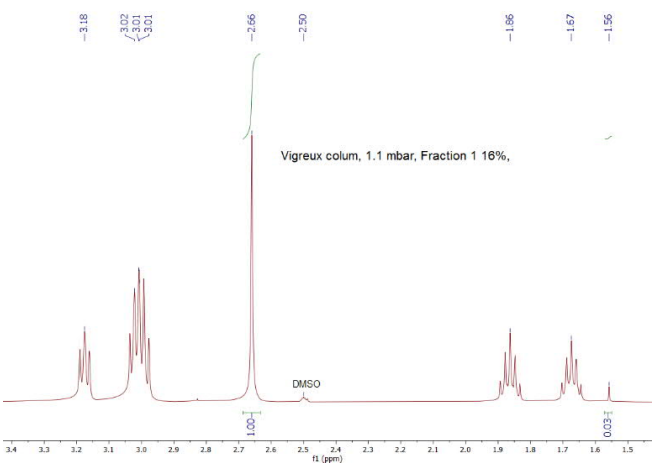

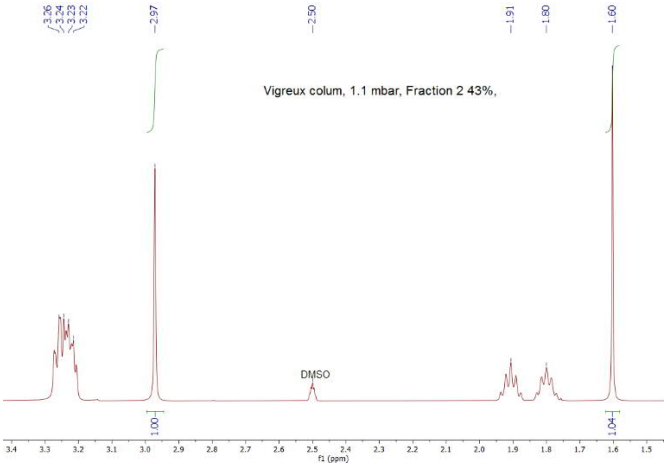

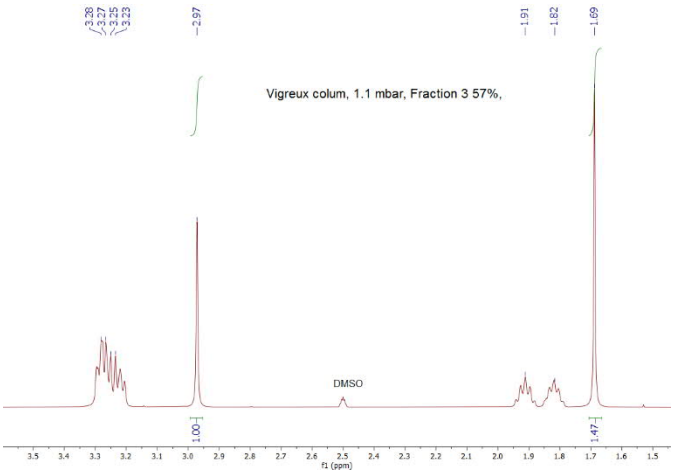

Appendix 8.4: Experiment #4

Samples	Weight, g	Mass percentage, wt.%
Feed	129	100
Fraction 1	26	20
Fraction 2	8	26
Fraction 3	33	52
Residue	61	47
Cold trap	4	3
OUT	132	102
Loss	-3	-2

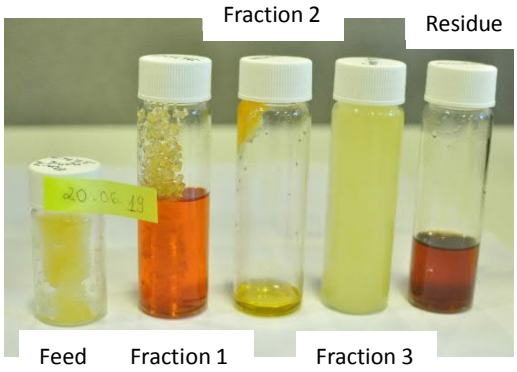

Samples	NMR results, base molar %	NMR results, hydrolysis (1), molar %	NMR results, hydrolysis (2), molar %	NMR results, acid, molar %	NMR results, water signal
Feed	50	0	0	50	no
Fraction 1	98	0	0	2	no
Fraction 2	78.1	0	0	21.9	no
Fraction 3	40.7	0	0	59.3	no
Residue	38.9	0	0	61.1	no
Cold trap					

Samples	CE results, base molar %	CE results, hydrolysis, molar %	CE results, by-product, molar %	CE results, acid, molar % (calculated)	Karl-Fischer results, water, mass%
Feed	50.6 ± 2.1	0	0	49.4 ± 2.1	N/A
Fraction 1	56.6 ± 0.5	0	0	43.4 ± 0.5	0.18
Fraction 2	65.3 ± 2.5	0	0	34.7 ± 2.5	N/A
Fraction 3	47.3 ± 0.8	0	0	52.7 ± 0.8	0.07
Residue	47.3 ± 0.5	0	0	52.7 ± 0.5	0.1

Time, hour	Bottom temp., °C	Condensate temp., °C	Pressure, mbar	Notes
00:00	141	102	5	Fraction 1 collected
00:08	147	100	5	
00:10	147	99	5	
00:17	147	98	5	
00:31	148	101	5	Fraction 2 collected
00:47	148	137	5	
00:53	147	136	4.9	Fraction 3 collected
01:13	148	140	4.9	
01:26	148	140	4.9	
01:40	149	139	4.9	

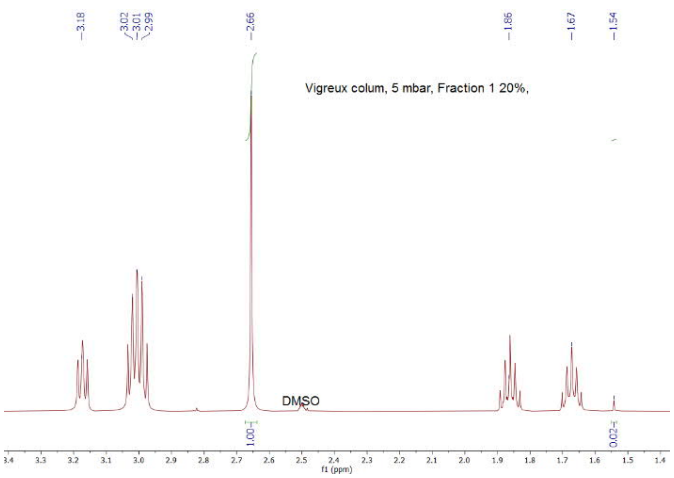

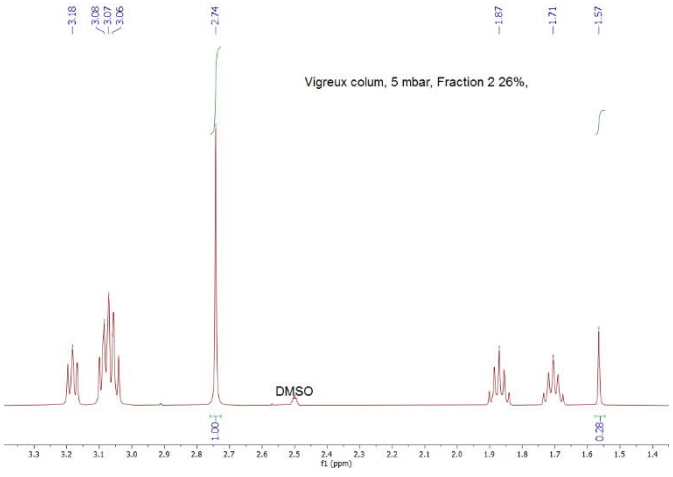

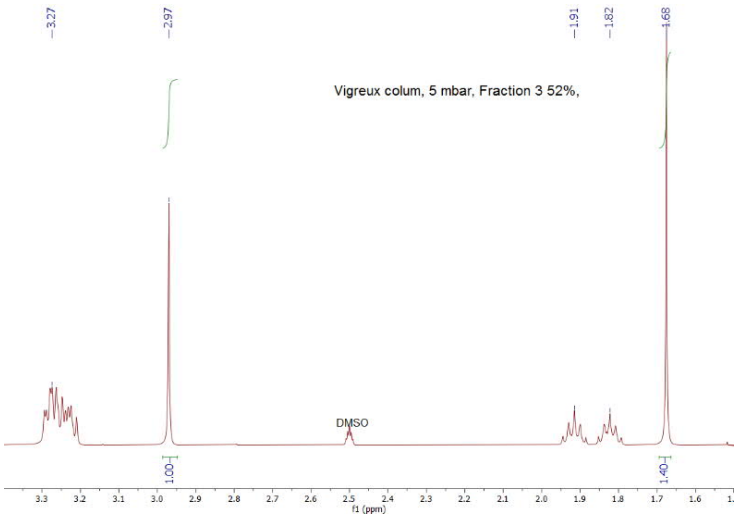

Appendix 8.5: Experiment #5

Samples	Weight, g	Mass percentage, wt.%
Feed	146	100
Fraction 1	17	12
Fraction 2	10	18
Fraction 3	29	38
Fraction 4	19	51
Fraction 5	23	67
Fraction 6	13	76
Residue	20	14
Cold trap	2	1
OUT	133	91
Loss	13	9

Fractions from the distillate collector

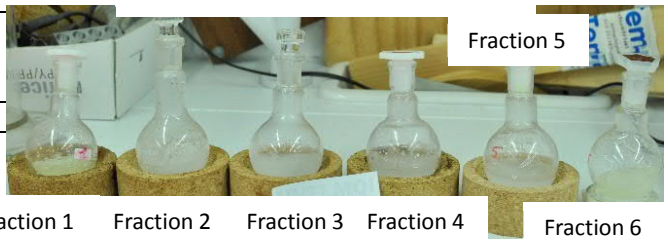

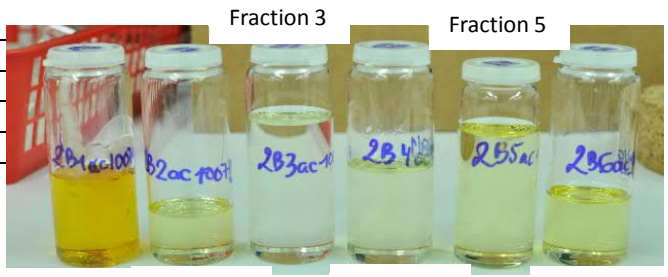

Samples	NMR results, base molar %	NMR results, hydrolysis (1), molar %	NMR results, hydrolysis (2), molar %	NMR results, acid, molar %	NMR results, water signal
Feed	40.8	0	0	59.2	no
Fraction 1	61	0	0	39	no
Fraction 2	41.5	0	0	58.5	no
Fraction 3	40	0	0	60	no
Fraction 4	40	0	0	60	no
Fraction 5	40	0	0	60	no
Fraction 6	40	0	0	60	no
Residue	36.5	1.1	0.4	62	no
Cold trap					

Samples	CE results, base molar %	CE results, hydrolysis, molar %	CE results, by-product, molar %	CE results, acid, molar % (calculated)	Karl-Fischer results, water, mass%
Feed	40.5 ± 1.7	0	0	59.5 ± 1.7	N/A
Fraction 1	47.3 ± 0.6	0	0	52.7 ± 0.6	
Fraction 2	53.1 ± 0.7	0	0	46.9 ± 0.7	N/A
Fraction 3	36.3 ± 1.2	0	0	63.7 ± 1.2	
Fraction 4	40.5 ± 1.4	0	0	59.5 ± 1.4	
Fraction 5	40 ± 0.7	0	0	60 ± 0.7	
Fraction 6	37.9 ± 0.9	0	0	62.1 ± 0.9	
Residue	37.9 ± 1.7	0	0	62.1 ± 1.7	

Time, hour	Bottom temp., °C	Condensate temp., °C	Pressure, mbar	Notes
00:00	139	74	0.7	Fraction 1 collected
00:06	136	116	0.7	
00:11	136	121	0.7	
00:13	136	122	0.7	
00:18	137	125	0.7	Fraction 2 collected
00:24	138	129	0.7	
00:27	139	131	0.7	
00:34	140	131	0.7	Fraction 3 collected
00:41	142	136	0.7	
00:46	141	129	0.7	
00:51	139	127	0.7	
01:00	138	125	0.7	
01:02	133	96	0.7	Fraction 4 collected
01:05	134	108	0.7	
01:12	136	116	0.7	
01:27	139	116	0.7	
01:28	140	116	0.7	
01:31	140	115	0.7	Fraction 5 collected
01:44	148	114	0.7	
01:49	154	113	0.7	
02:02	177	107	0.7	
02:03	180	106	0.7	Fraction 6 collected
02:08	210	106	0.7	

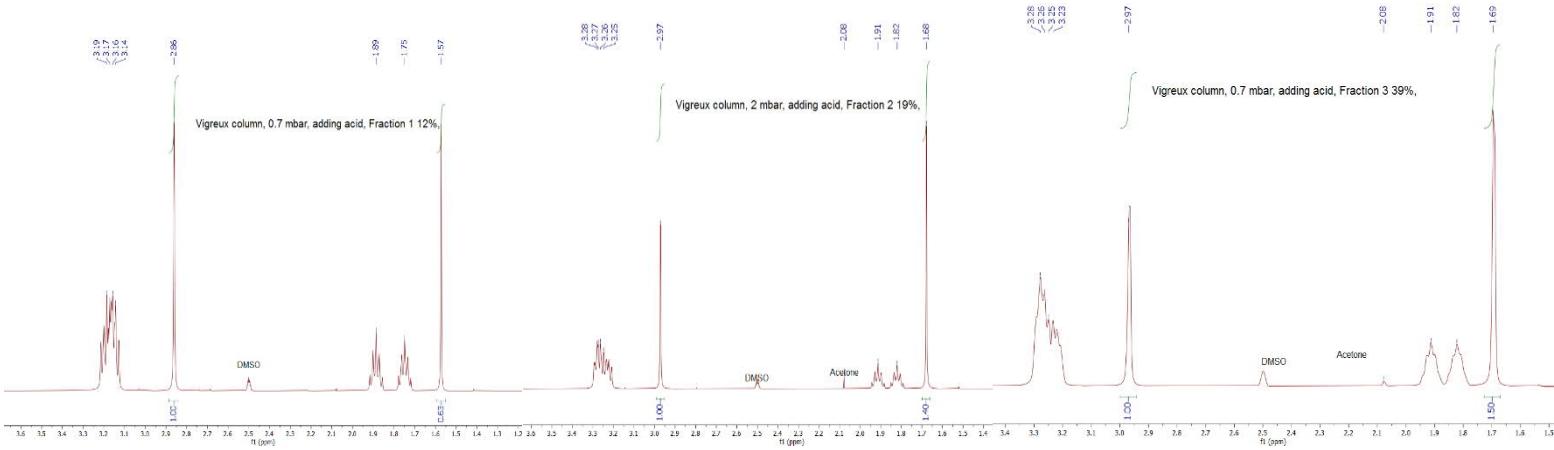

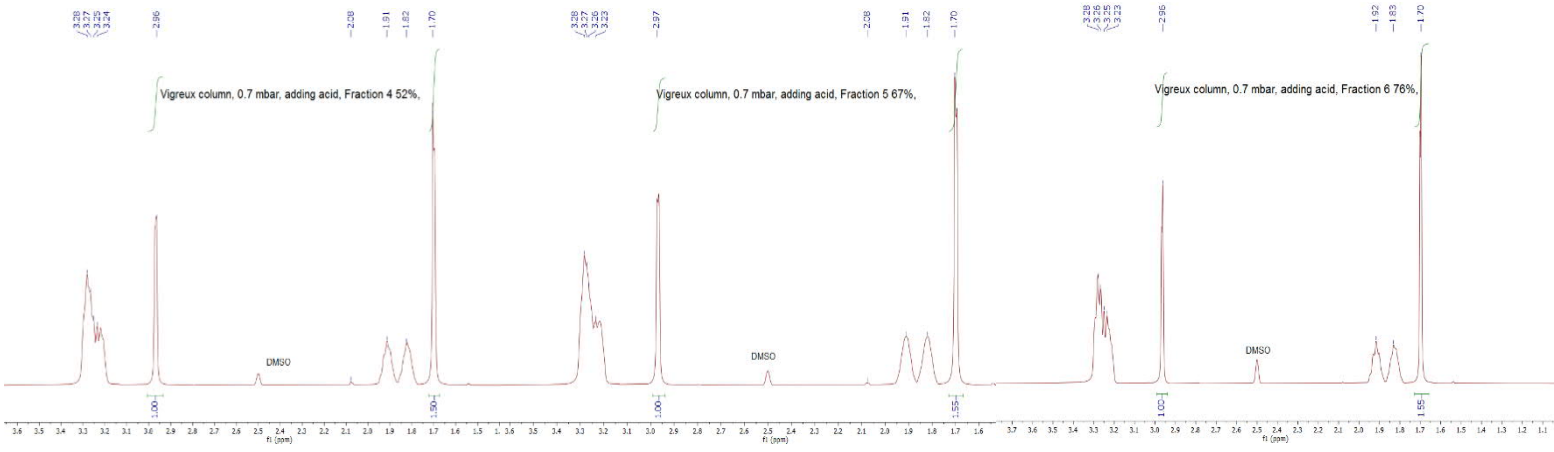

Appendix 8.6: Experiment #6

Samples	Weight, g	Mass percentage, wt.%
Feed	111	100
Fraction 1	36	32
Fraction 2	32	61
Fraction 3	21	80
Residue	13	11
Cold trap	5	5
OUT	106	95
Loss	6	5

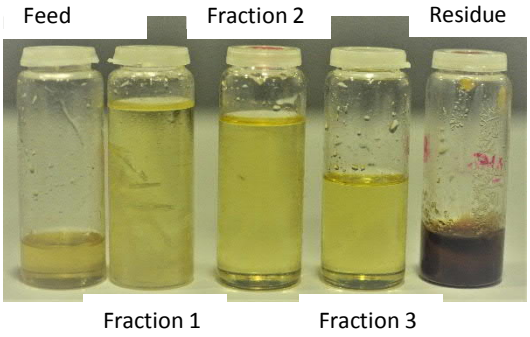

Samples	NMR results, base molar %	NMR results, hydrolysis (1), molar %	NMR results, hydrolysis (2), molar %	NMR results, acid, molar %	NMR results, water signal
Feed	37.6	0	0	62.4	no
Fraction 1	37.9	0	0	62.1	no
Fraction 2	39.8	0	0	60.2	no
Fraction 3	40.3	0	0	59.7	no
Residue	35	0.7	0.3	64	no
Cold trap					

Samples	CE results, base molar %	CE results, hydrolysis, molar %	CE results, by-product, molar %	CE results, acid, molar % (calculated)	Karl-Fischer results, water, mass%
Feed	35.2 ± 0.7	0	0	64.8 ± 0.7	N/A
Fraction 1	25 ± 0.7	0	0	75 ± 0.7	
Fraction 2	40.2 ± 0.6	0	0	59.8 ± 0.6	N/A
Fraction 3	39.2 ± 0.9	0	0	60.8 ± 0.9	
Residue	36.5 ± 0.5	0	0	63.5 ± 0.5	

Time, hour	Bottom temp., °C	Condensate temp., °C	Pressure, mbar	Notes
00:00	140	101	0.7	Fraction 1 collected
00:02	139	121	0.7	
00:07	138	124	0.7	
00:13	138	124	0.7	
00:26	138	124	0.7	
00:41	140	122	0.7	Fraction 2 collected
00:56	148	122	0.7	
01:02	157	120	0.7	
01:09	152	121	0.7	
01:10	153	122	0.7	
01:17	169	115	0.7	Fraction 3 collected
01:25	162	121	0.7	
01:27	178	122	0.7	

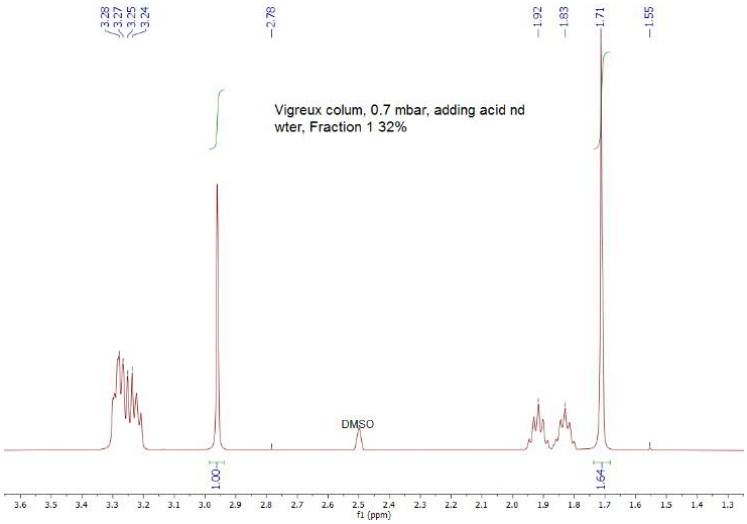

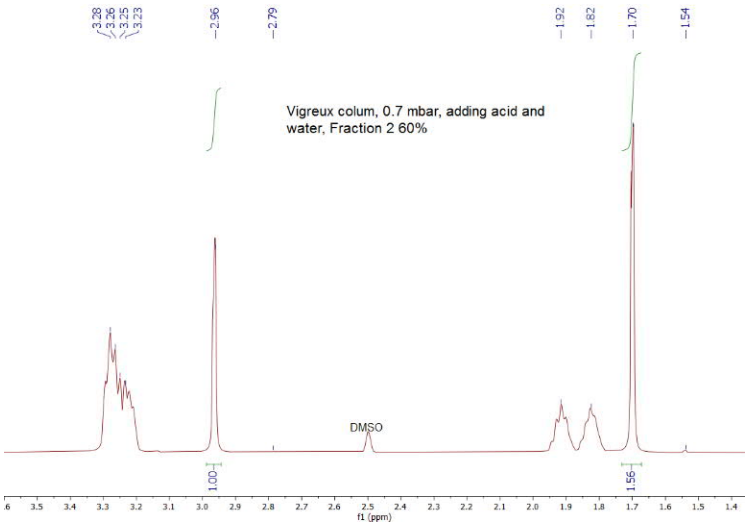

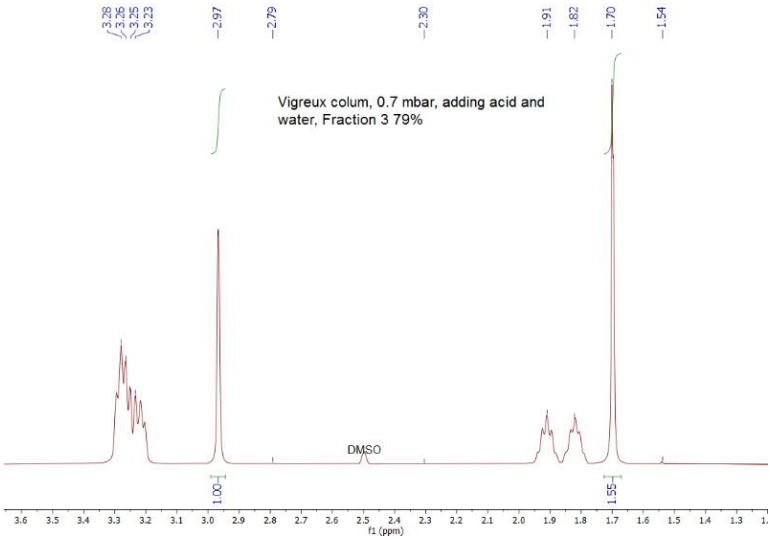

Appendix 8.7: Experiment #7

Samples	Weight, g	Mass percentage, wt.%
Feed	185	100
Fraction 1	19	10
Fraction 2	16	19
Fraction 3	6	22
Residue	87	47
Cold trap	NA	NA
OUT	128	69
Loss	57	31

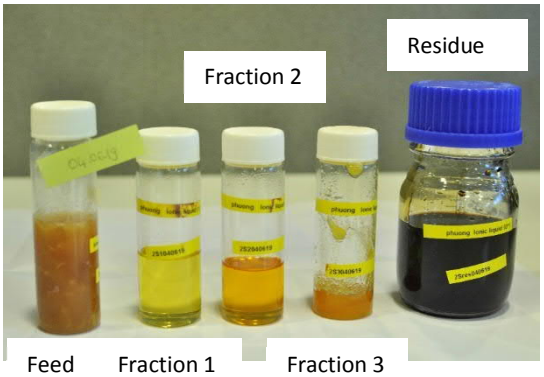

Samples	NMR results, base molar %	NMR results, hydrolysis (1), molar %	NMR results, hydrolysis (2), molar %	NMR results, acid, molar %	NMR results, water signal
Feed	49.5	1	0	49.5	no
Fraction 1	100	0	0	62.1	no
Fraction 2	100	0	0	60.2	no
Fraction 3	62.5	0	0.6	36.9	no
Residue	39.5	0	1.2	59.3	no
Cold trap					

Samples	CE results, base molar %	CE results, hydrolysis, molar %	CE results, by-product, molar %	CE results, acid, molar % (calculated)	Karl-Fischer results, water, mass%
Feed	42.4 ± 1.7	0	0	57.6 ± 1.7	N/A
Fraction 1	59.6 ± 3.3	0	0	40.4 ± 3.3	
Fraction 2	61.8 ± 2.4	0	0	38.2 ± 2.4	N/A
Fraction 3	58.7 ± 2.4	0	0	41.3 ± 2.4	
Residue	44.1 ± 1.3	0	1 ± 0.08	55.9 ± 1.3	

Time, hour	Bottom temp., °C	Condensate temp., °C	Pressure, mbar	Notes
00:00	176	94	2.2	Fraction 1 collected
00:08	175	96	2.5	
00:16	175	96	2.6	
00:23	177	96	2.6	
00:38	177	96	2.7	
00:45	174	97	2.7	
01:01	177	97	2.7	Fraction 2 collected
01:22	177	101	2.8	
01:37	178	97	2.7	
01:40	178	96	2.8	
01:44	177	97	2.9	
02:07	178	98	3	Fraction 3 collected
02:27	179	112	3	

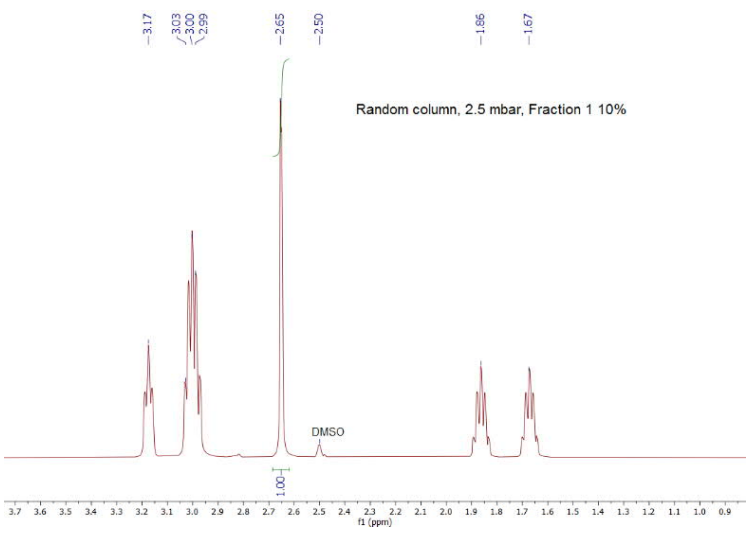

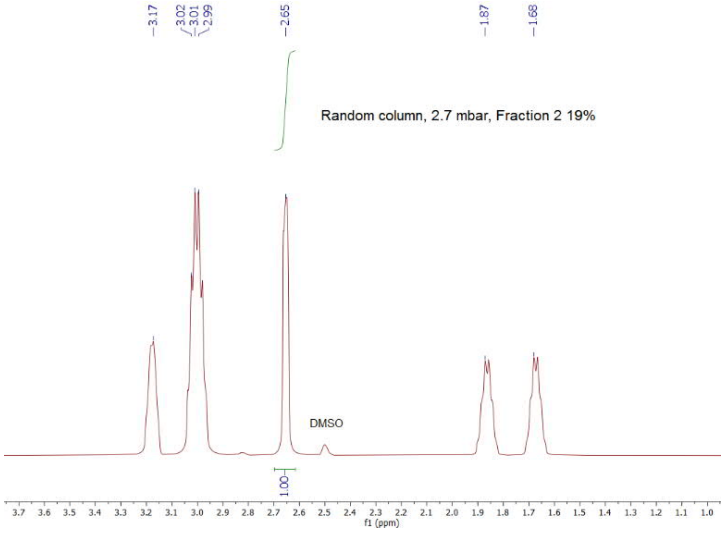

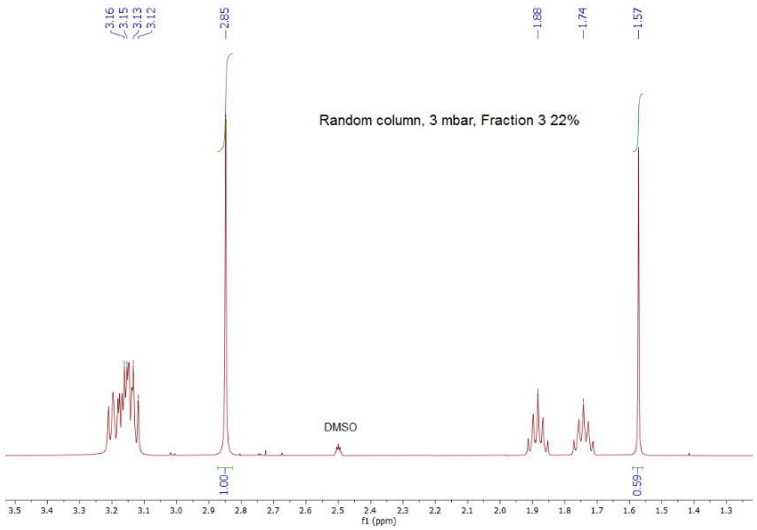

Appendix 9. The minimum equilibrium stages of Vigreux column

A distillation column was operated at total reflux to get an infinite reflux ratio. The steady state operating condition was achieved as the distillate and bottom flow rates were zero, and the feed condition was maintained without any influences. The mixture of n-heptane and toluene was used to define the minimum number of equilibrium stages of Vigreux column by McCabe-Thiele method. The vapor-liquid equilibrium curve was drawn based on the previous study and indicated as Table X below.

The mixture of n-heptane and toluene was filled to the round bottom flask and boiled up by the electrical heater (111 W). After reaching steady state in one hour, the bottom temperature was around 108 ºC and the top temperature was around 98 ºC. Both small bottom and top samples were collected and measured by Gas Chromatography (Agilent). The minimum number of equilibrium stages of Vigreux column is 9.5 or 10 stages as a graph below.

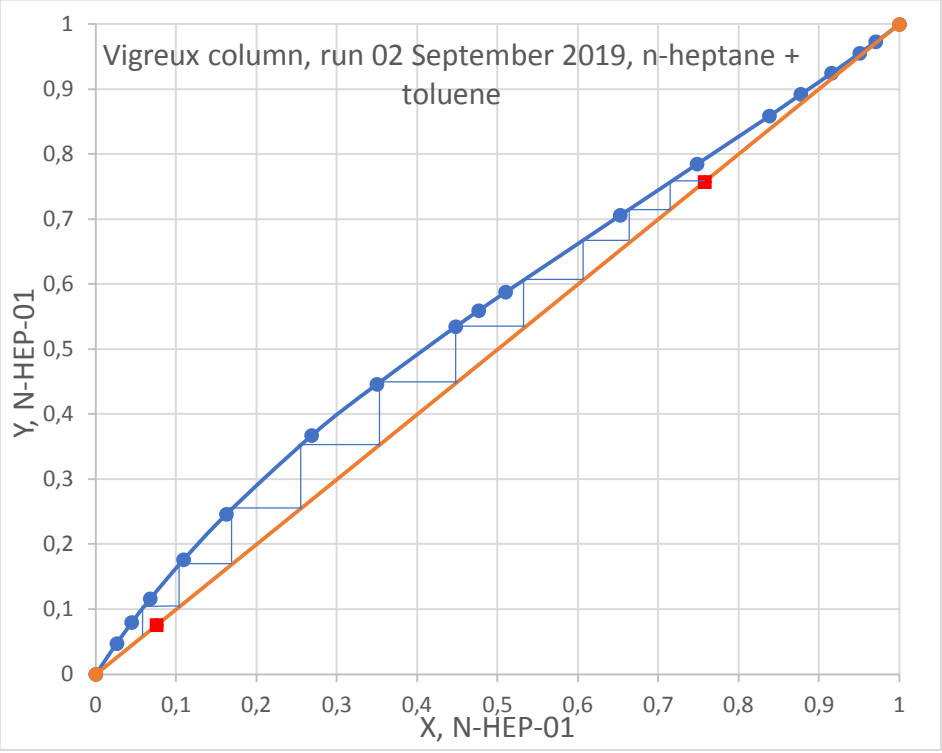

Appendix 10. Aspen simulation results

Appendix 10.1: Experiment #1

	DIS1	DIS2	DIS3	DIS4	DIS5	DIS6	DIS7	DIS8	DIS9	DIS10	FEED
	FRA1	FRA2	FRA3	FRA4	FRA5	FRA6	FRA7	FRA8	FRA9	FRA10	
	LIQUID	LIQUID	LIQUID	LIQUID	LIQUID	LIQUID	LIQUID	LIQUID	LIQUID	LIQUID	LIQUID
Substream: MIXED											
Mole Flow kmol/hr											
Base	3.2E-04	3.2E-04	1.7E-04	4.4E-05	1.5E-05	3.6E-06	6.9E-07	2.8E-07	1.1E-07	4.1E-08	8.8E-04
IL3:2	3.5E-06	1.5E-05	9.2E-05	1.0E-04	1.5E-04	1.4E-04	6.3E-05	6.0E-05	5.7E-05	4.4E-05	1.8E-03
Mole Frac											
Base	9.9E-01	9.6E-01	6.5E-01	3.0E-01	8.9E-02	2.5E-02	1.1E-02	4.6E-03	2.0E-03	9.5E-04	3.3E-01
IL3:2	1.1E-02	4.5E-02	3.5E-01	7.0E-01	9.1E-01	9.8E-01	9.9E-01	1.0E+00	1.0E+00	1.0E+00	6.7E-01
Total Flow kmol/hr	3.2E-04	3.4E-04	2.7E-04	1.5E-04	1.7E-04	1.4E-04	6.4E-05	6.1E-05	5.7E-05	4.4E-05	2.7E-03
Total Flow kg/hr	5.0E-02	5.7E-02	7.1E-02	5.8E-02	7.6E-02	6.9E-02	3.1E-02	2.9E-02	2.8E-02	2.1E-02	1.0E+00
Total Flow l/min	7.9E-04	8.6E-04	8.0E-04	5.4E-04	6.9E-04	6.0E-04	2.7E-04	2.5E-04	2.4E-04	1.8E-04	9.1E-03
Temperature C	6.5E+01	6.6E+01	7.1E+01	8.2E+01	9.7E+01	1.0E+02	1.1E+02	1.1E+02	1.1E+02	1.1E+02	2.5E+01
Pressure bar	2.3E-04	2.3E-04	2.3E-04	2.3E-04	2.3E-04	2.3E-04	2.3E-04	2.3E-04	2.3E-04	2.3E-04	1.0E+00
Enthalpy cal/mol	-1.4E+04	-1.4E+04	-1.5E+04	-1.6E+04	-1.6E+04	-1.6E+04	-1.6E+04	-1.6E+04	-1.6E+04	-1.6E+04	-1.8E+04
Enthalpy cal/gm	-8.7E+01	-8.1E+01	-5.4E+01	-4.0E+01	-3.5E+01	-3.3E+01	-3.2E+01	-3.2E+01	-3.2E+01	-3.2E+01	-4.9E+01
Enthalpy cal/sec	-1.2E+00	-1.3E+00	-1.1E+00	-6.4E-01	-7.3E-01	-6.3E-01	-2.8E-01	-2.6E-01	-2.5E-01	-1.9E-01	-1.3E+01
Entropy cal/mol-K	-2.4E+01	-2.4E+01	-2.4E+01	-2.4E+01	-2.5E+01	-2.4E+01	-2.4E+01	-2.4E+01	-2.4E+01	-2.4E+01	-3.3E+01
Entropy cal/gm-K	-1.6E-01	-1.4E-01	-8.9E-02	-6.3E-02	-5.4E-02	-5.1E-02	-5.1E-02	-5.0E-02	-5.0E-02	-5.0E-02	-8.8E-02

fraction distilled	0.05	0.11	0.18	0.24	0.31	0.38	0.41	0.44	0.47	0.49
acid, mole %	0.02	0.06	0.34	0.51	0.58	0.59	0.60	0.60	0.60	0.60
base, mole%	0.98	0.94	0.66	0.49	0.42	0.41	0.40	0.40	0.40	0.40
a/b ratio	0.02	0.07	0.52	1.06	1.37	1.46	1.48	1.49	1.50	1.50

Appendix 10.2: Experiment #2

	DIS1	DIS2	DIS3	DIS4	DIS5	DIS6	DIS7	DIS8	DIS9	DIS10	FEED
	FRA1	FRA2	FRA3	FRA4	FRA5	FRA6	FRA7	FRA8	FRA9	FRA10	
	LIQUID	LIQUID	LIQUID	LIQUID	LIQUID	LIQUID	LIQUID	LIQUID	LIQUID	LIQUID	LIQUID
Substream: MIXED											
Mole Flow kmol/hr											
Base	3.1E-04	3.3E-04	1.6E-04	5.7E-05	1.7E-05	5.1E-06	1.2E-06	6.9E-07	2.5E-07	9.0E-08	8.8E-04
IL3:2	6.6E-06	3.2E-05	9.5E-05	1.5E-04	1.5E-04	1.3E-04	6.1E-05	9.2E-05	8.5E-05	7.8E-05	1.8E-03
Mole Frac											
Base	9.8E-01	9.1E-01	6.2E-01	2.8E-01	1.0E-01	3.6E-02	1.9E-02	7.4E-03	2.9E-03	1.1E-03	3.3E-01
IL3:2	2.1E-02	8.9E-02	3.8E-01	7.2E-01	9.0E-01	9.6E-01	9.8E-01	9.9E-01	1.0E+00	1.0E+00	6.7E-01
Total Flow kmol/hr	3.1E-04	3.6E-04	2.5E-04	2.1E-04	1.6E-04	1.4E-04	6.2E-05	9.3E-05	8.5E-05	7.8E-05	2.7E-03
Total Flow kg/hr	5.0E-02	6.7E-02	7.1E-02	8.1E-02	7.3E-02	6.6E-02	3.0E-02	4.5E-02	4.1E-02	3.8E-02	1.0E+00
Total Flow l/min	7.9E-04	9.6E-04	7.9E-04	7.7E-04	6.7E-04	5.9E-04	2.6E-04	3.9E-04	3.6E-04	3.3E-04	9.1E-03
Temperature C	8.3E+01	8.4E+01	9.0E+01	1.0E+02	1.1E+02	1.2E+02	1.2E+02	1.2E+02	1.2E+02	1.3E+02	2.5E+01
Pressure bar	7.0E-04	7.0E-04	7.0E-04	7.0E-04	7.0E-04	7.0E-04	7.0E-04	7.0E-04	7.0E-04	7.0E-04	1.0E+00
Enthalpy cal/mol	-1.2E+04	-1.3E+04	-1.4E+04	-1.5E+04	-1.5E+04	-1.5E+04	-1.5E+04	-1.5E+04	-1.5E+04	-1.5E+04	-1.8E+04
Enthalpy cal/gm	-7.7E+01	-6.9E+01	-4.9E+01	-3.7E+01	-3.3E+01	-3.1E+01	-3.1E+01	-3.1E+01	-3.0E+01	-3.0E+01	-4.9E+01
Enthalpy cal/sec	-1.1E+00	-1.3E+00	-9.5E-01	-8.3E-01	-6.7E-01	-5.7E-01	-2.5E-01	-3.8E-01	-3.5E-01	-3.2E-01	-1.3E+01
Entropy cal/mol-K	-2.1E+01	-2.0E+01	-2.1E+01	-2.2E+01	-2.2E+01	-2.2E+01	-2.2E+01	-2.2E+01	-2.2E+01	-2.2E+01	-3.3E+01
Entropy cal/gm-K	-1.3E-01	-1.1E-01	-7.4E-02	-5.5E-02	-4.9E-02	-4.7E-02	-4.6E-02	-4.6E-02	-4.6E-02	-4.6E-02	-8.8E-02

fraction distilled	0.05	0.12	0.19	0.27	0.34	0.41	0.44	0.48	0.52	0.56
acid, mole %	0.03	0.12	0.36	0.52	0.57	0.59	0.60	0.60	0.60	0.60
base, mole%	0.97	0.88	0.64	0.48	0.43	0.41	0.40	0.40	0.40	0.40
a/b ratio	0.03	0.13	0.56	1.08	1.34	1.45	1.47	1.49	1.50	1.50

Appendix 10.3: Experiment #3

	DIS1	DIS2	DIS3	DIS4	DIS5	DIS6	DIS7	DIS8	DIS9	DIS10	FEED
	FRA1	FRA2	FRA3	FRA4	FRA5	FRA6	FRA7	FRA8	FRA9	FRA10	
	LIQUID	LIQUID	LIQUID	LIQUID	LIQUID	LIQUID	LIQUID	LIQUID	LIQUID	LIQUID	LIQUID
Substream: MIXED											
Mole Flow kmol/hr											
Base	4.5E-04	2.8E-04	1.1E-04	2.9E-05	7.2E-06	2.2E-06	1.6E-06	3.9E-07	2.0E-07	1.3E-07	8.8E-04
IL3:2	2.2E-05	8.3E-05	1.7E-04	1.7E-04	1.0E-04	6.1E-05	1.2E-04	5.2E-05	5.0E-05	7.6E-05	1.8E-03
Mole Frac											
Base	9.5E-01	7.7E-01	3.8E-01	1.5E-01	6.5E-02	3.6E-02	1.3E-02	7.3E-03	4.0E-03	1.7E-03	3.3E-01
IL3:2	4.6E-02	2.3E-01	6.2E-01	8.5E-01	9.4E-01	9.6E-01	9.9E-01	9.9E-01	1.0E+00	1.0E+00	6.7E-01
Total Flow kmol/hr	4.7E-04	3.6E-04	2.8E-04	2.0E-04	1.1E-04	6.3E-05	1.2E-04	5.3E-05	5.0E-05	7.6E-05	2.7E-03
Total Flow kg/hr	8.0E-02	8.3E-02	1.0E-01	8.8E-02	5.2E-02	3.0E-02	5.7E-02	2.5E-02	2.4E-02	3.7E-02	1.0E+00
Total Flow l/min	1.2E-03	1.0E-03	9.9E-04	8.2E-04	4.7E-04	2.7E-04	5.0E-04	2.2E-04	2.1E-04	3.2E-04	9.1E-03
Temperature C	9.1E+01	9.5E+01	1.1E+02	1.2E+02	1.3E+02	1.3E+02	1.3E+02	1.3E+02	1.3E+02	1.3E+02	2.5E+01
Pressure bar	1.1E-03	1.1E-03	1.1E-03	1.1E-03	1.1E-03	1.1E-03	1.1E-03	1.1E-03	1.1E-03	1.1E-03	1.0E+00
Enthalpy cal/mol	-1.2E+04	-1.3E+04	-1.4E+04	-1.4E+04	-1.4E+04	-1.4E+04	-1.4E+04	-1.4E+04	-1.4E+04	-1.4E+04	-1.8E+04
Enthalpy cal/gm	-7.0E+01	-5.4E+01	-3.8E+01	-3.3E+01	-3.1E+01	-3.0E+01	-3.0E+01	-3.0E+01	-3.0E+01	-3.0E+01	-4.9E+01
Enthalpy cal/sec	-1.6E+00	-1.2E+00	-1.1E+00	-8.0E-01	-4.5E-01	-2.5E-01	-4.7E-01	-2.1E-01	-2.0E-01	-3.0E-01	-1.3E+01
Entropy cal/mol-K	-1.9E+01	-1.9E+01	-2.0E+01	-2.1E+01	-2.1E+01	-2.1E+01	-2.1E+01	-2.1E+01	-2.1E+01	-2.1E+01	-3.3E+01
Entropy cal/gm-K	-1.1E-01	-8.3E-02	-5.6E-02	-4.8E-02	-4.5E-02	-4.4E-02	-4.4E-02	-4.4E-02	-4.4E-02	-4.4E-02	-8.8E-02

fraction distilled	0.08	0.16	0.26	0.35	0.40	0.43	0.49	0.52	0.54	0.58
acid, mole %	0.06	0.26	0.48	0.56	0.58	0.59	0.60	0.60	0.60	0.60
base, mole%	0.94	0.74	0.52	0.44	0.42	0.41	0.40	0.40	0.40	0.40
a/b ratio	0.07	0.35	0.93	1.28	1.40	1.45	1.48	1.49	1.49	1.50

Appendix 10.4: Experiment #4

	DIS1	DIS2	DIS3	DIS4	DIS5	DIS6	DIS7	DIS8	DIS9	DIS10	FEED
	FRA1	FRA2	FRA3	FRA4	FRA5	FRA6	FRA7	FRA8	FRA9	FRA10	
	LIQUID	LIQUID	LIQUID	LIQUID	LIQUID	LIQUID	LIQUID	LIQUID	LIQUID	LIQUID	LIQUID
Substream: MIXED											
Mole Flow kmol/hr											
Base	2.6E-04	2.1E-04	1.7E-04	1.0E-04	7.2E-05	4.2E-05	1.3E-05	3.8E-06	1.4E-06	3.1E-07	8.8E-04
IL3:2	2.0E-05	3.1E-05	5.8E-05	7.3E-05	1.2E-04	2.1E-04	1.5E-04	7.7E-05	4.1E-05	9.9E-06	1.8E-03
Mole Frac											
Base	9.3E-01	8.7E-01	7.4E-01	5.8E-01	3.6E-01	1.6E-01	7.8E-02	4.7E-02	3.4E-02	3.1E-02	3.3E-01
IL3:2	7.1E-02	1.3E-01	2.6E-01	4.2E-01	6.4E-01	8.4E-01	9.2E-01	9.5E-01	9.7E-01	9.7E-01	6.7E-01
Total Flow kmol/hr	2.8E-04	2.4E-04	2.3E-04	1.7E-04	2.0E-04	2.5E-04	1.6E-04	8.1E-05	4.2E-05	1.0E-05	2.7E-03
Total Flow kg/hr	5.0E-02	4.8E-02	5.4E-02	5.1E-02	7.2E-02	1.1E-01	7.4E-02	3.8E-02	2.0E-02	4.8E-03	1.0E+00
Total Flow l/min	7.5E-04	6.6E-04	6.7E-04	5.6E-04	7.2E-04	1.0E-03	6.9E-04	3.5E-04	1.8E-04	4.4E-05	9.1E-03
Temperature C	1.1E+02	1.1E+02	1.1E+02	1.2E+02	1.2E+02	1.3E+02	1.4E+02	1.4E+02	1.4E+02	1.4E+02	2.5E+01
Pressure bar	5.0E-03	5.0E-03	5.0E-03	5.0E-03	5.0E-03	5.0E-03	5.0E-03	5.0E-03	5.0E-03	5.0E-03	1.0E+00
Enthalpy cal/mol	-1.1E+04	-1.1E+04	-1.2E+04	-1.2E+04	-1.3E+04	-1.3E+04	-1.4E+04	-1.4E+04	-1.4E+04	-1.4E+04	-1.8E+04
Enthalpy cal/gm	-6.1E+01	-5.6E+01	-4.9E+01	-4.1E+01	-3.5E+01	-3.1E+01	-2.9E+01	-2.9E+01	-2.9E+01	-2.9E+01	-4.9E+01
Enthalpy cal/sec	-8.5E-01	-7.4E-01	-7.3E-01	-5.9E-01	-7.0E-01	-9.4E-01	-6.0E-01	-3.0E-01	-1.6E-01	-3.8E-02	-1.3E+01
Entropy cal/mol-K	-1.6E+01	-1.6E+01	-1.6E+01	-1.7E+01	-1.8E+01	-1.9E+01	-1.9E+01	-1.9E+01	-1.9E+01	-1.9E+01	-3.3E+01
Entropy cal/gm-K	-9.1E-02	-8.2E-02	-6.8E-02	-5.7E-02	-4.8E-02	-4.3E-02	-4.1E-02	-4.0E-02	-4.0E-02	-4.0E-02	-8.8E-02

fraction distilled	0.05	0.10	0.15	0.20	0.27	0,38	0.46	0.50	0.52	0.52
acid, mole %	0.10	0.16	0.28	0.39	0.49	0,56	0.58	0.59	0.59	0.59
base, mole%	0.90	0.84	0.72	0.61	0.51	0.44	0.42	0.41	0.41	0.41
a/b ratio	0.11	0.19	0.38	0.63	0.95	1.25	1.38	1.43	1.45	1.45

Appendix 11. Short path distillation experiments

Appendix 11.1: Experiment # 8

Samples	Weight, g	Mass percentage, wt.%
Feed	63	100
Distillate	15	24
Residue	25	40
Cold trap	NA	NA
OUT	40	64
Loss	23	36

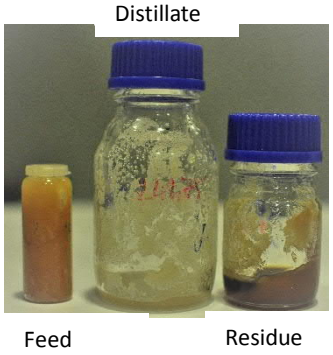

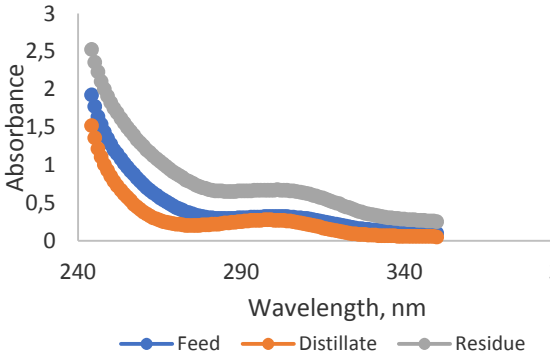

Samples	NMR results, base molar %	NMR results, hydrolysis (1), molar %	NMR results, hydrolysis (2), molar %	NMR results, acid, molar %	NMR results, water signal (Yes/No)
Feed	45.3	2.7	0.9	51.1	no
Distillate	49.8	2	1	47.2	no
Residue	39	4	0.8	56.2	no
Cold trap	NA	NA	NA	NA	NA

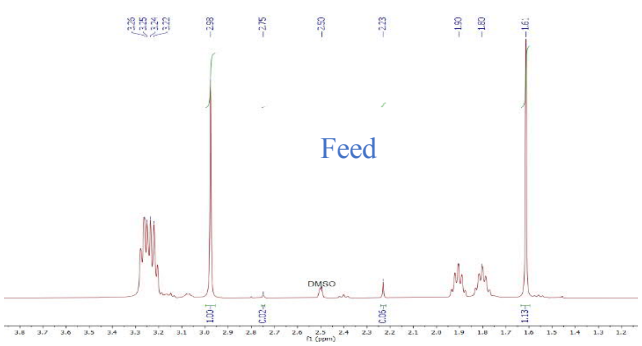

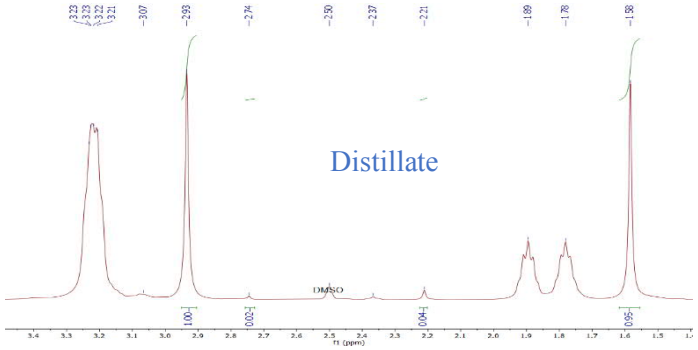

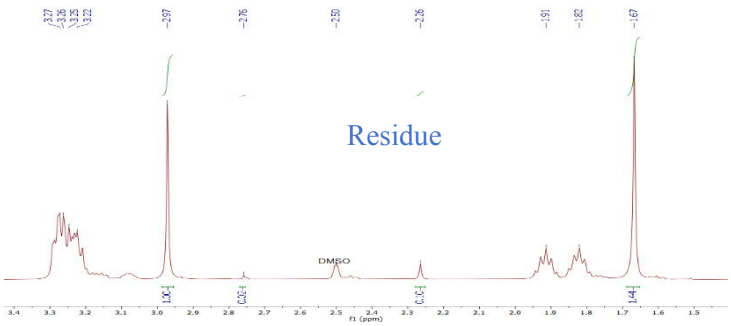

Samples	CE results, base molar %	CE results, hydrolysis, molar %	CE results, by-product, molar %	CE results, acid, molar % (calculated)	Karl-Fischer results, water, mass%
Feed	40.8 ± 0.7	0	0	59.2 ± 0.7	
Distillate	46.8 ± 1.1	0	0	53.2 ± 1.1	
Residue	40.2 ± 0.4	0	0	59.8 ± 0.4	
Cold trap	NA	NA	NA	NA	

Appendix 11.2: Experiment # 9

Samples	Weight, g	Mass percentage, wt.%
Feed	126	100
Distillate	110	87
Residue	1.5	1.2
Cold trap	1	0.8
OUT	112.5	89
Loss	13.5	11

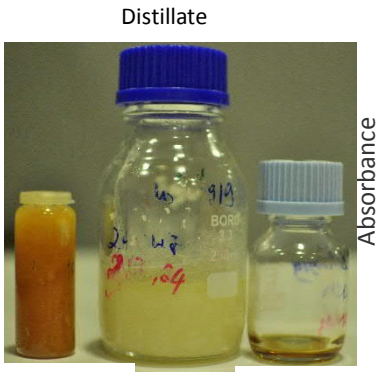

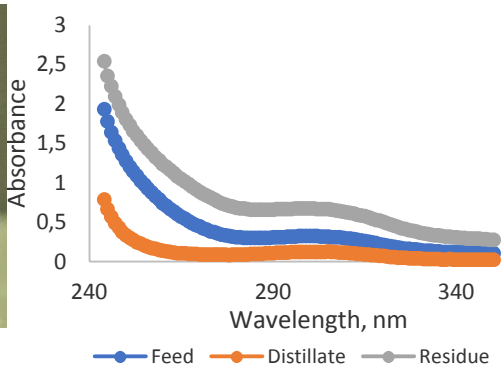

Samples	NMR results, base molar %	NMR results, hydrolysis (1), molar %	NMR results, hydrolysis (2), molar %	NMR results, acid, molar %	NMR results, water signal (Yes/No)
Feed	47	0	0	53	no
Distillate	44	2.6	0.9	52.5	no
Residue	40	3.6	0.8	55.6	no
Cold trap	99	1	0	0	yes

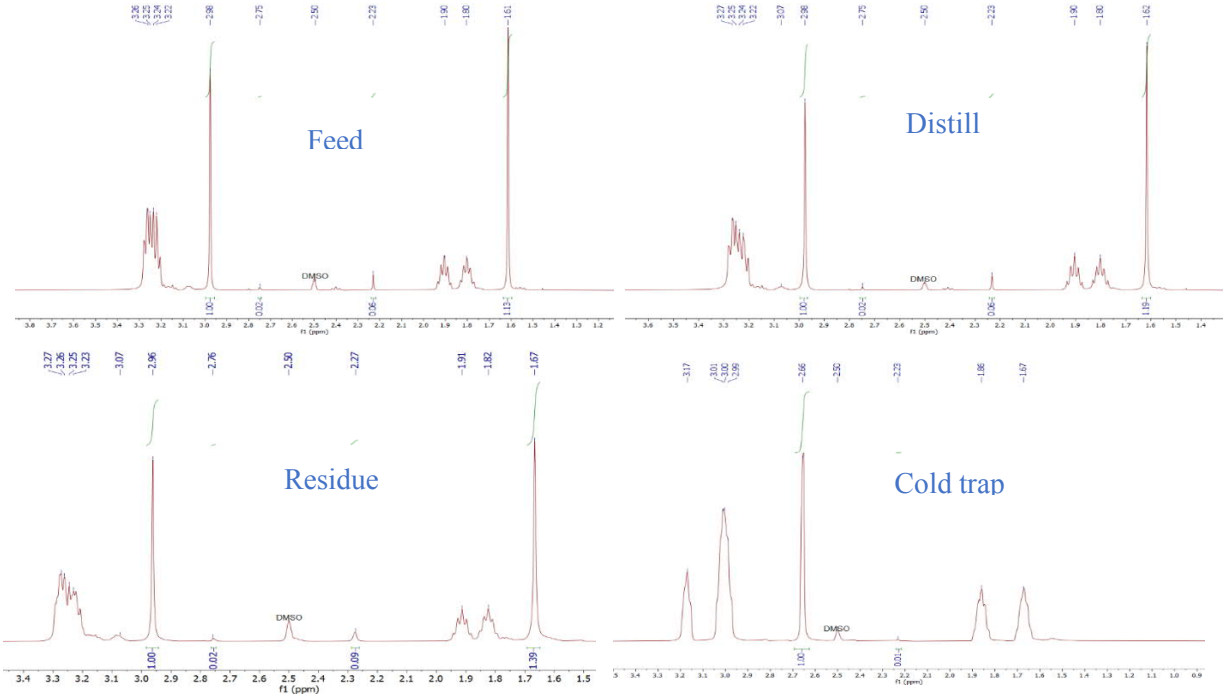

Samples	CE results, base molar %	CE results, hydrolysis, molar %	CE results, by-product, molar %	CE results, acid, molar % (calculated)	Karl-Fischer results, water, mass%
Feed	NA	NA	NA	NA	
Distillate	43.5 ± 0.8	0	0	56.5 ± 0.8	
Residue	43.7 ± 0.6	0	0	56.3 ± 0.6	
Cold trap	36.5 ± 0.5	0	0	63.5 ± 0.5	

Appendix 11.3: Experiment # 10

Samples	Weight, g	Mass percentage, wt.%
Feed	105	100
Distillate	99	94
Residue	3	3
Cold trap	8	8
OUT	109	105
Loss	- 4	- 5

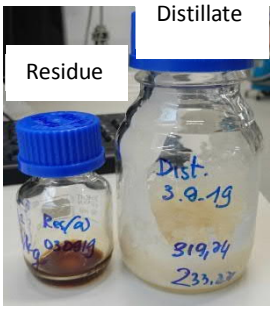

Samples	NMR results, base molar %	NMR results, hydrolysis (1), molar %	NMR results, hydrolysis (2), molar %	NMR results, acid, molar %	NMR results, water signal (Yes/No)
Feed	45.9	2.8	0.9	50.4	no
Distillate	45.5	2.3	0.9	51.3	no
Residue	NA				
Cold trap	31	41.3	3.7	24	

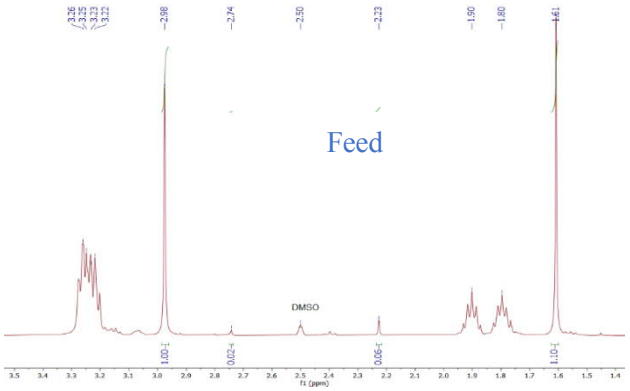

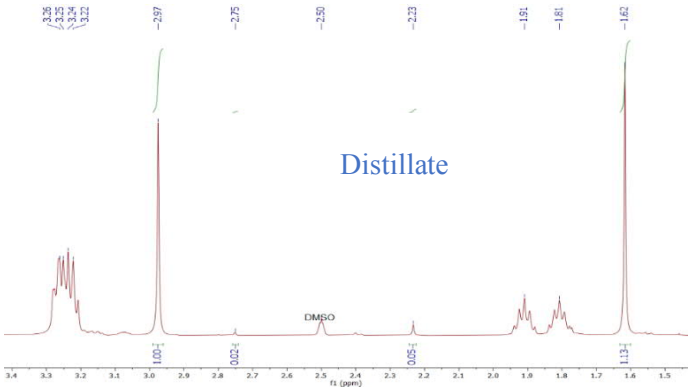

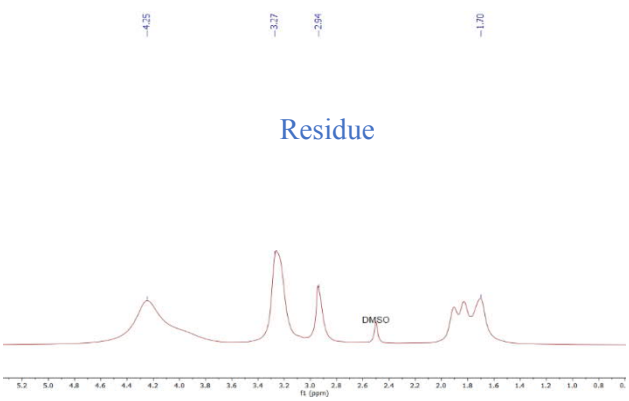

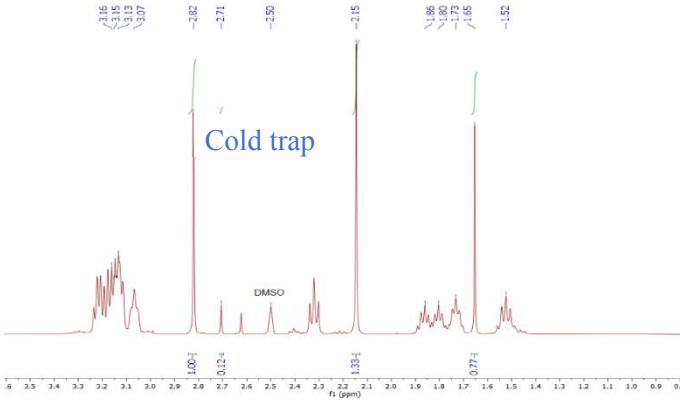

Samples	CE results, base molar %	CE results, hydrolysis, molar %	CE results, by-product, molar %	CE results, acid, molar % (calculated)	Karl-Fischer results, water, mass%
Feed	31.4 ± 1.6	0	0	68.6 ± 1.6	
Distillate	42.7 ± 0.4	0	0	57.3 ± 0.4	
Residue	43.5 ± 3.3	0	0	56.5 ± 3.3	
Cold trap	13 ± 1.5	0	0	87 ± 1.5	

Appendix 11.4: Experiment # 11

Samples	Weight, g	Mass percentage, wt.%
Feed	70	100
Distillate	44	63
Residue	2	3
Cold trap	2	3
OUT	48	69
Loss	22	31

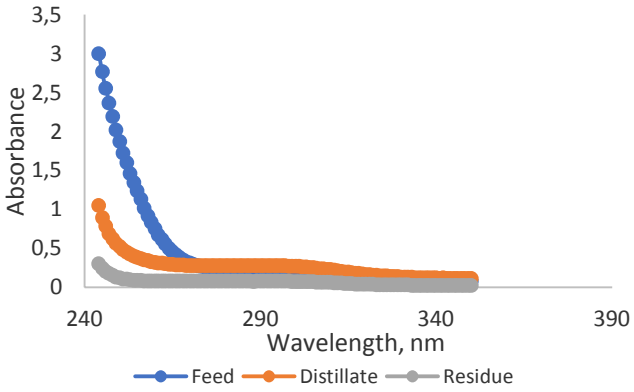

Samples	NMR results, base molar %	NMR results, hydrolysis (1), molar %	NMR results, hydrolysis (2), molar %	NMR results, acid, molar %	NMR results, water signal (Yes/No)
Feed	48.3	0.5	0	51.2	no
Distillate	45.5	0.5	0	54	no
Residue	43.3	0	0.4	56.3	no
Cold trap	only base	0	0	no acid	yes

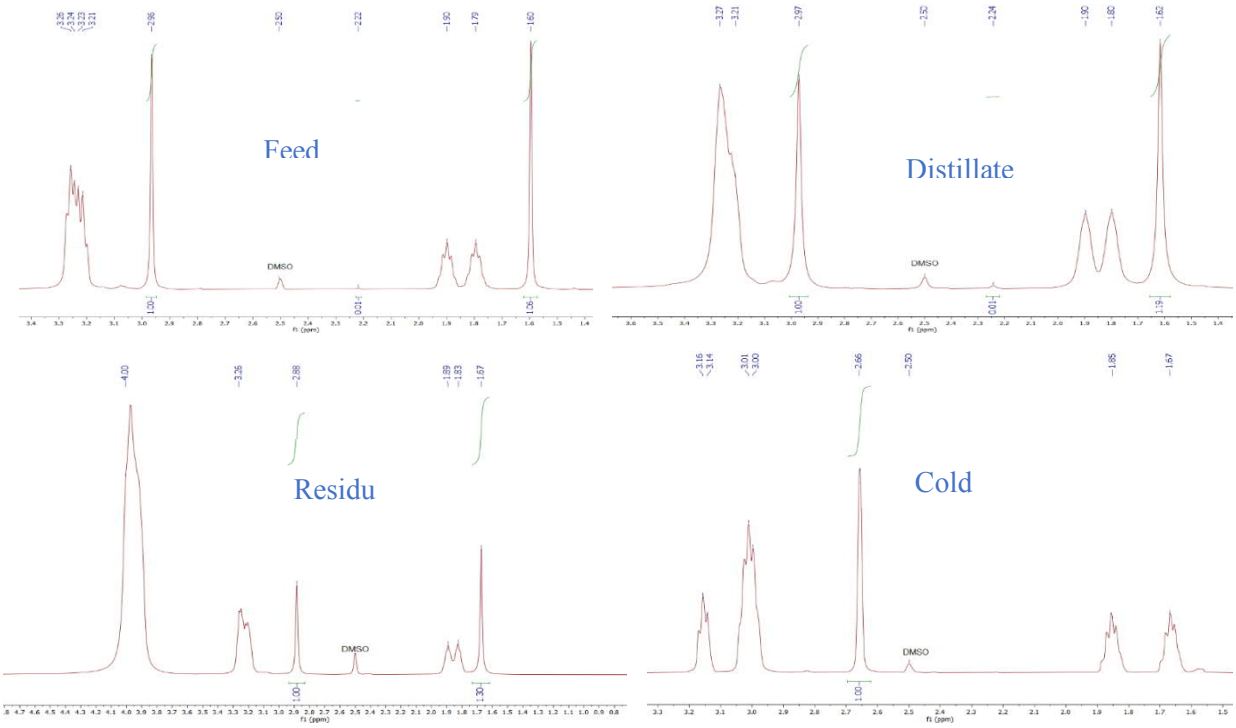

Samples	CE results, base molar %	CE results, hydrolysis, molar %	CE results, by-product, molar %	CE results, acid, molar % (calculated)	Karl-Fischer results, water, mass%
Feed	48.9 ± 2.3	0	0	51.1 ± 2.3	
Distillate	43 ± 1.7	0	0	57 ± 1.7	
Residue	26 ± 1	0	0	74 ± 1	
Cold trap	39 ± 0.7	0	0	61 ± 0.7	

Appendix 11.5: Experiment # 12

Samples	Weight, g	Mass percentage, wt.%
Feed	144	100
Distillate	75	52
Residue	3	2
Cold trap	3	2
OUT	81	56
Loss	63	44

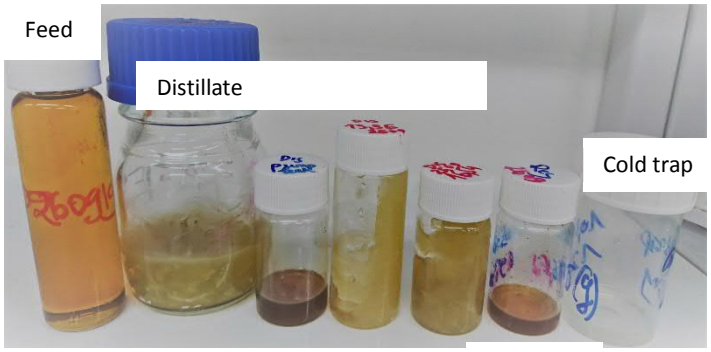

Samples	NMR results, base molar %	NMR results, hydrolysis (1), molar %	NMR results, hydrolysis (2), molar %	NMR results, acid, molar %	NMR results, water signal (Yes/No)
Feed	45.9	0.5	0	53.6	no
Distillate	44.6	0.5	0	54.9	no
Residue	40.2	0	0	59.8	no
Cold trap	99	1	0	0	yes

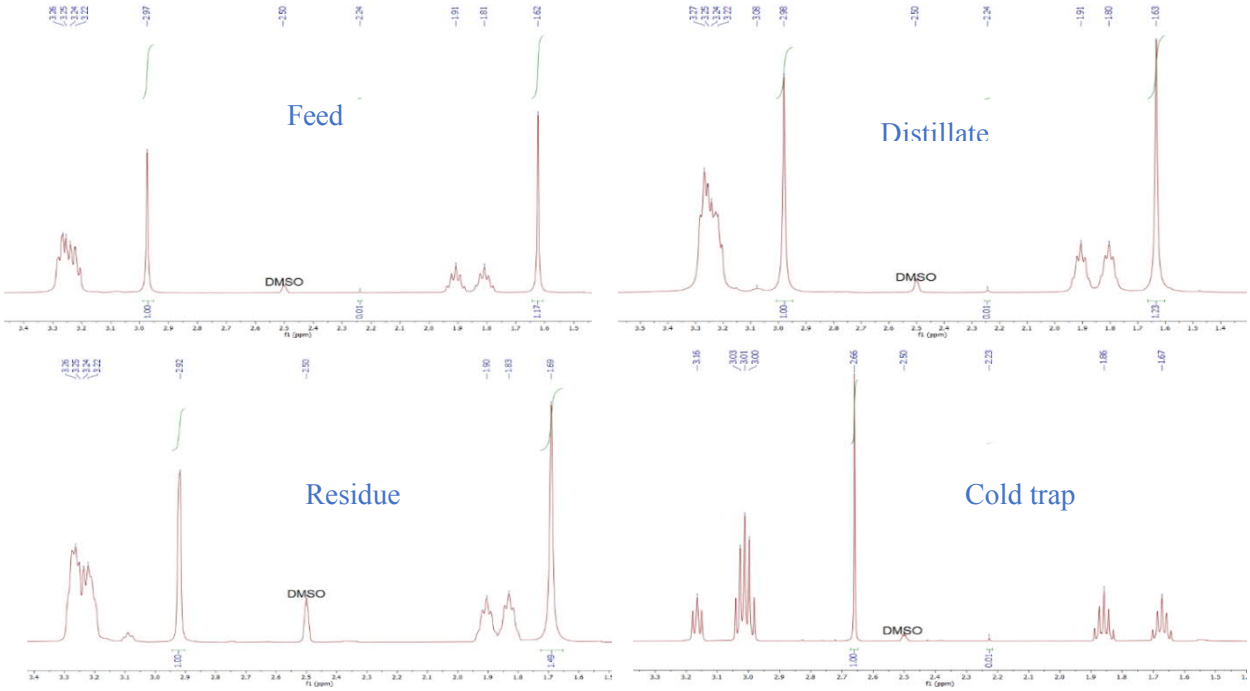

Samples	CE results, base molar %	CE results, hydrolysis, molar %	CE results, by-product, molar %	CE results, acid, molar % (calculated)	Karl-Fischer results, water, mass%
Feed	47.6 ± 0.6	0	0.5 ± 0.09	51.9 ± 0.6	
Distillate	46.7 ± 0.4	0	0.15 ± 0.06	53.15 ± 0.4	
Residue	25.5 ± 0.3	0	0.9 ± 0.1	73.6 ± 0.3	
Cold trap	60.7 ± 0.7	2.2 ± 0.3	0	37,1 ± 0.7	

Appendix 11.6: Experiment # 13

Samples	Weight, g	Mass percentage, wt.%
Feed	114	100
Distillate	92	81
Residue	3	3
Cold trap	4	3
OUT	99	87
Loss	15	13

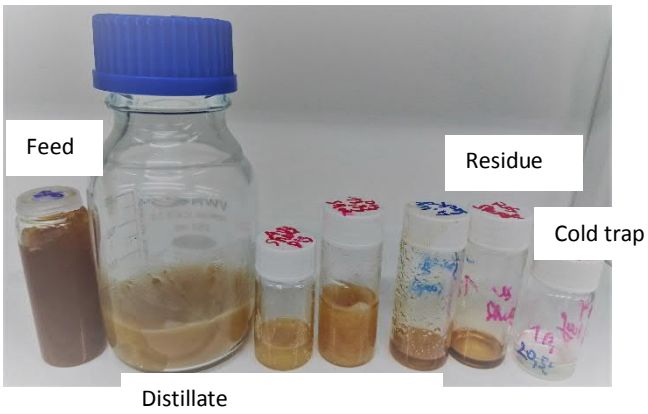

Samples	NMR results, base molar %	NMR results, hydrolysis (1), molar %	NMR results, hydrolysis (2), molar %	NMR results, acid, molar %	NMR results, water signal (Yes/No)
Feed	48.3	0.5	0	51.2	no
Distillate	45	1.4	0	53.6	no
Residue	39.5	1.2	0	59.3	no
Cold trap	only base	0	0	no acid	yes

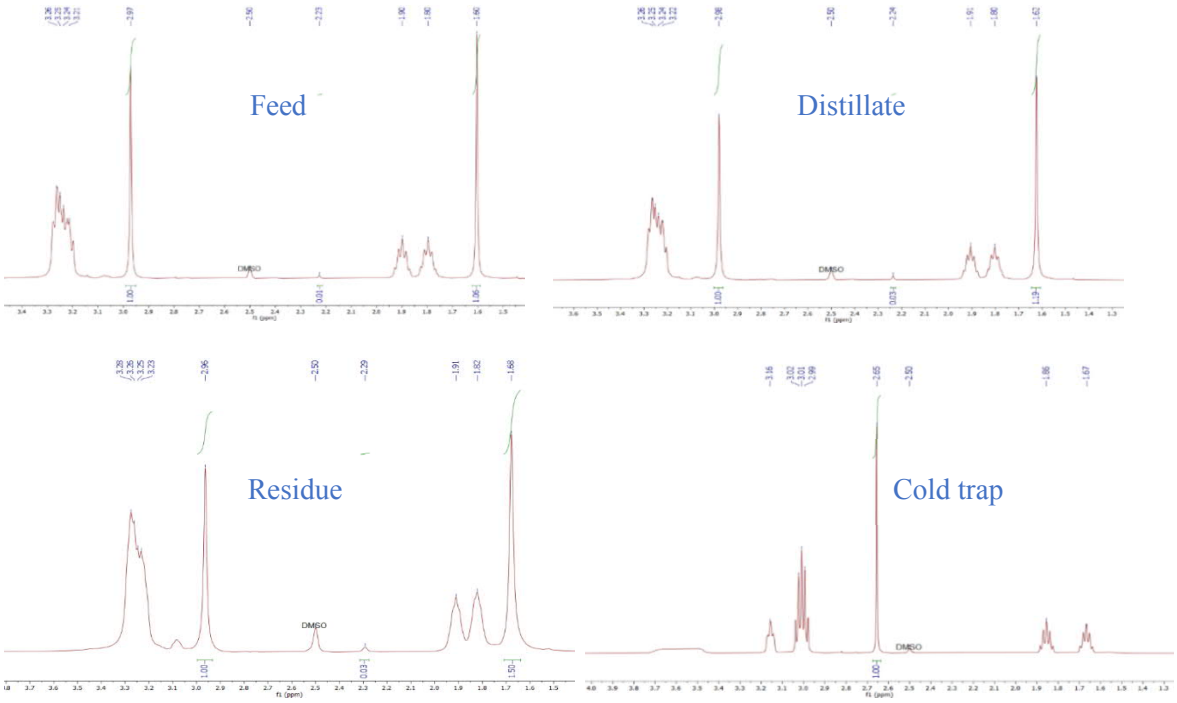

Samples	CE results, base molar %	CE results, hydrolysis, molar %	CE results, by-product, molar %	CE results, acid, molar % (calculated)	Karl-Fischer results, water, mass%
Feed	45.1 ± 0.6	0.1	0.06 ± 0.02	54.74 ± 0.6	
Distillate	45 ± 0.7	0.8 ± 0.4	0.09 ± 0.01	54.11 ± 0.7	
Residue	44.5 ± 0.6	1.3 ± 0.3	2.53 ± 0.08	51.67 ± 0.6	
Cold trap					

Appendix 11.7: Experiment # 14

Samples	Weight, g	Mass percentage, wt.%
Feed	99	100
Distillate	67	68
Residue	6	6
Cold trap	NA	NA
OUT	73	74
Loss	26	26

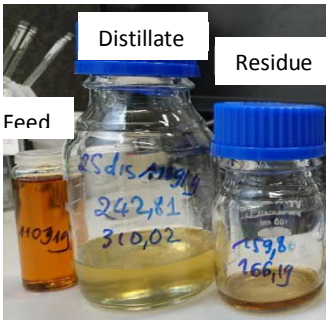

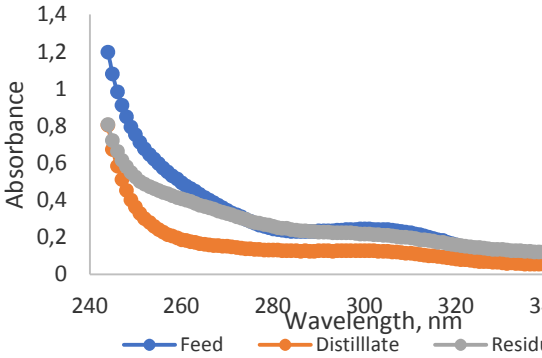

Samples	NMR results, base molar %	NMR results, hydrolysis (1), molar %	NMR results, hydrolysis (2), molar %	NMR results, acid, molar %	NMR results, water signal (Yes/No)
Feed	28.2	1.7	0.3	69.8	no
Distillate	30.1	1.8	0.3	67.8	no
Residue	31.3	2.5	0.3	65.9	no
Cold trap	NA	NA	NA	NA	NA

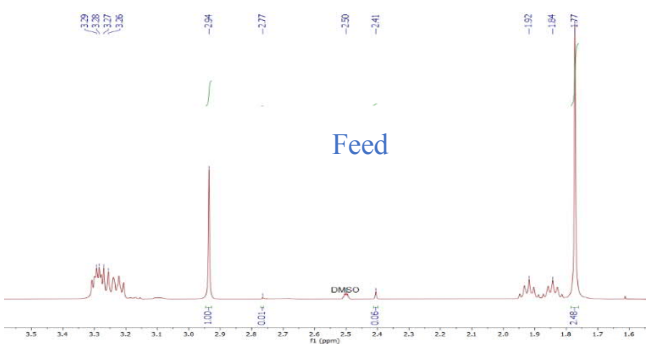

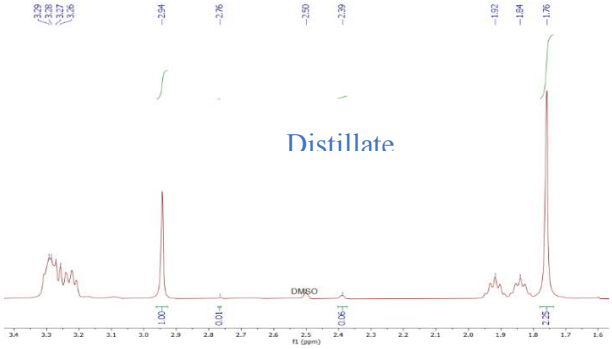

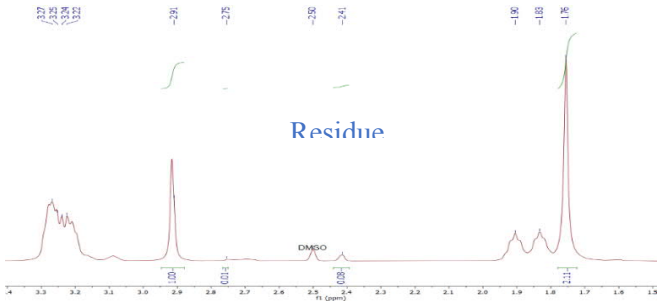

Samples	CE results, base molar %	CE results, hydrolysis, molar %	CE results, by-product, molar %	CE results, acid, molar % (calculated)	Karl-Fischer results, water, mass%
Feed	42 ± 0.8	0	0	58 ± 0.8	
Distillate	45.6 ± 0.6	0	0	54.4 ± 0.6	
Residue	28.2 ± 0.6	0	0	71.8 ± 0.6	
Cold trap	NA	NA	NA	NA	

Appendix 11.8: Experiment # 15

Samples	Weight, g	Mass percentage, wt.%
Feed	110	100
Distillate	64	58
Residue	41	37
Cold trap	13	12
OUT	118	107
Loss	- 8	- 7

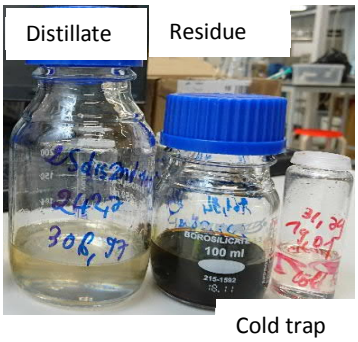

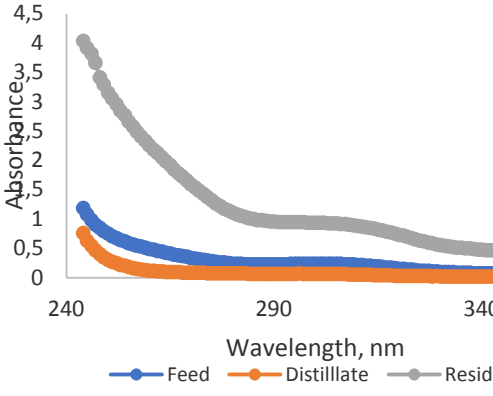

Samples	NMR results, base molar %	NMR results, hydrolysis (1), molar %	NMR results, hydrolysis (2), molar %	NMR results, acid, molar %	NMR results, water signal (Yes/No)
Feed	28.2	1.7	0.3	69.8	no
Distillate	30.4	1.2	0.3	58.1	no
Residue	34.3	3.4	0.7	61.6	no
Cold trap	no base	0	0		yes

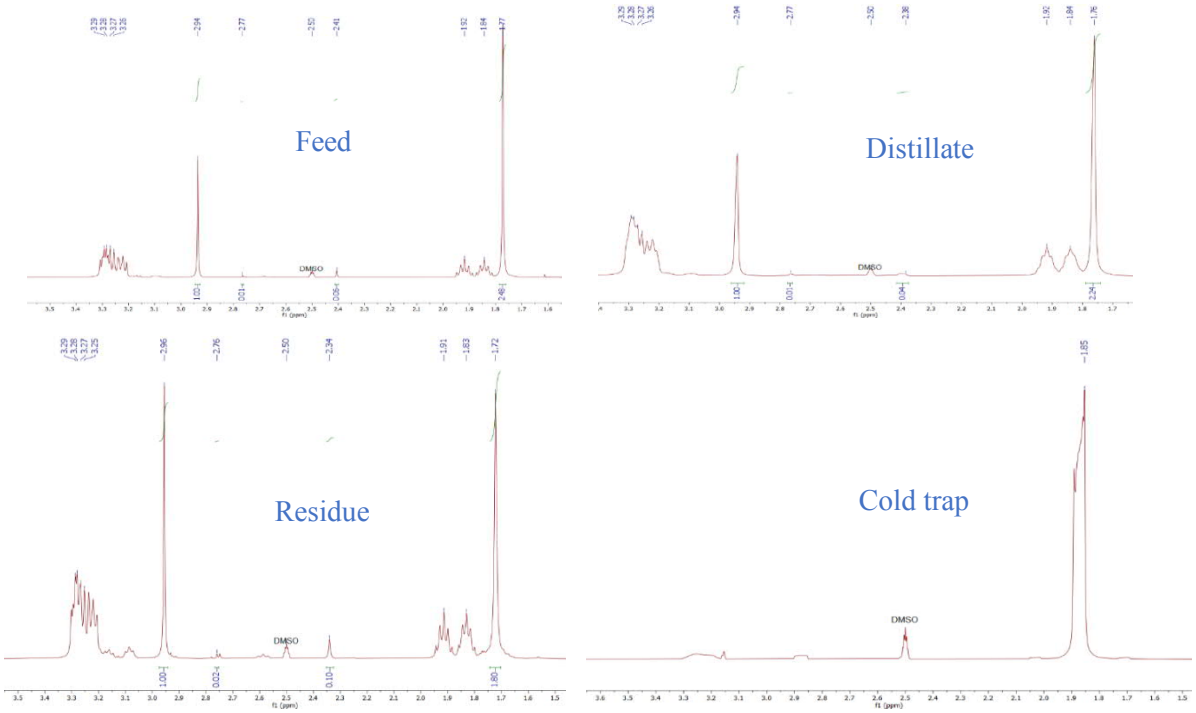

Samples	CE results, base molar %	CE results, hydrolysis, molar %	CE results, by-product, molar %	CE results, acid, molar % (calculated)	Karl-Fischer results, water, mass%
Feed	NA	NA	NA	NA	
Distillate	40.6 ± 0.7	0	0	59.4 ± 0.7	
Residue	41.5 ± 0.9	0	0	58.5 ± 0.9	
Cold trap	13.2 ± 0.6	0	0	86.8 ± 0.6	

Appendix 11.9: Experiment # 16

Samples	Weight, g	Mass percentage, wt.%
Feed	164	100
Distillate	92	56
Residue	29	18
Cold trap	85	52
OUT	206	126
Loss	-42	-26

Distillate Residue

Samples	NMR results, base molar %	NMR results, hydrolysis, molar %	NMR results, acid, molar %	NMR results, water signal (Yes/No)
Feed	49.2	1.5	49.3	no
Distillate	44	2	54	no
Residue	42	2	56	no
Cold trap	only base	significant	no acid	yes

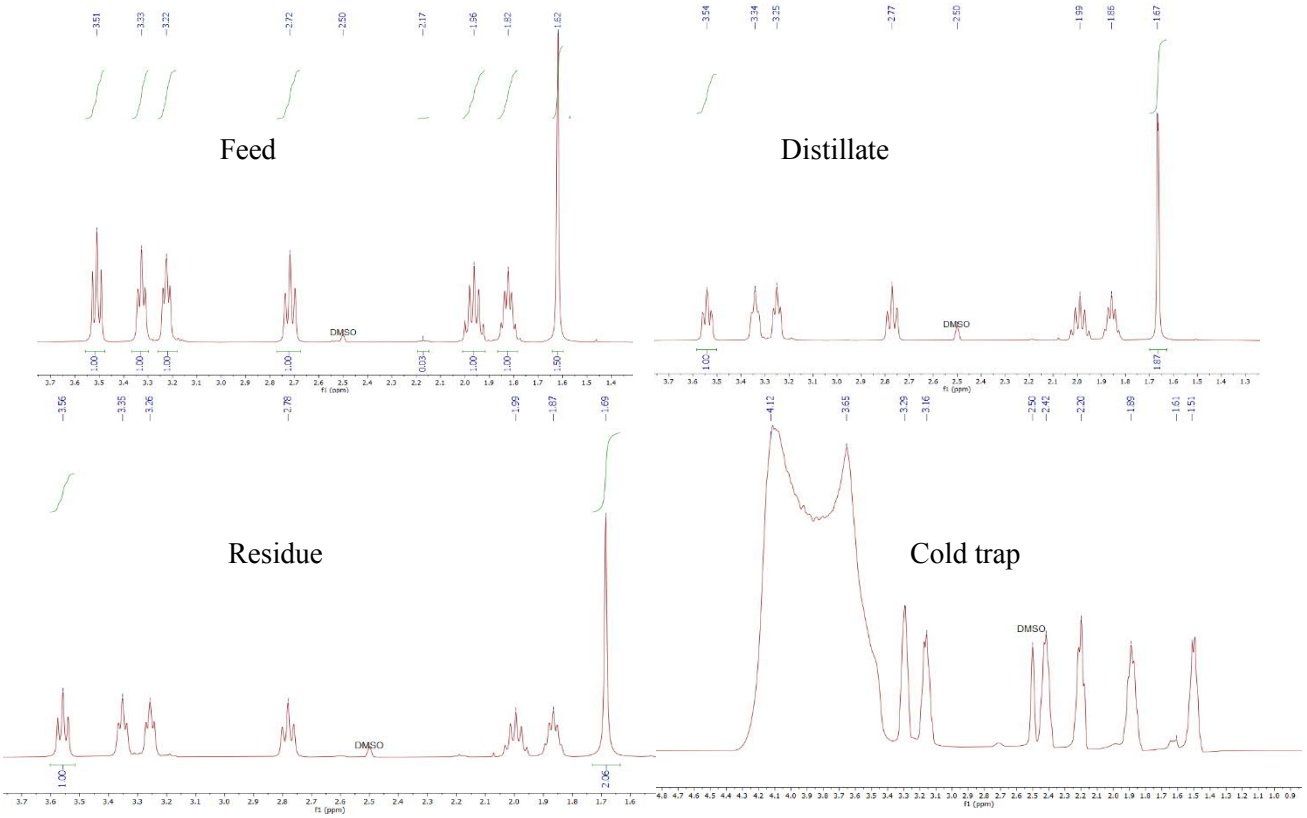

Samples	CE results, base molar %	CE results, by-product, molar %	CE results, acid, molar % (calculated)
Feed	57.7 ± 1.6	1.6 ± 0.03	40.6 ± 1.6
Distillate	45.1 ± 2	3.3 ± 0.16	51.7 ± 2
Residue	57.3 ± 1.7	2.5 ± 0.03	40.3 ± 1.7

Appendix 11.10: Experiment # 17

Samples	Weight, g	Mass percentage, wt.%
Feed	363	100
Distillate	230	63
Residue	43	12
Cold trap	51	14
OUT	324	89
Loss	39	11

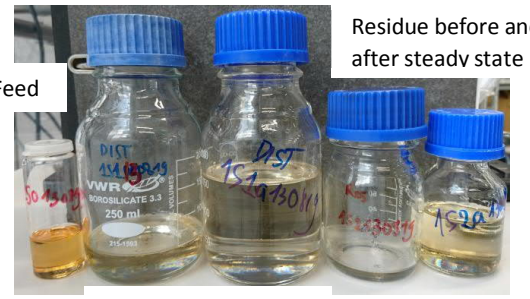

Samples	NMR results, base molar %	NMR results, hydrolysis, molar %	NMR results, acid, molar %	NMR results, water signal (Yes/No)
Feed	48	3	49	no
Distillate	41.1	2.5	56.4	no
Residue	40.9	2.9	56.2	no
Cold trap				yes

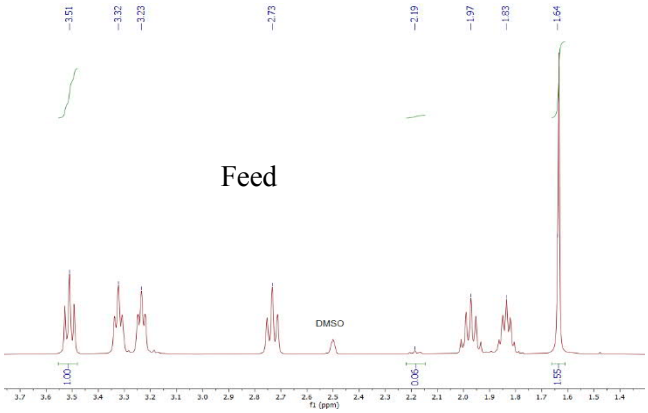

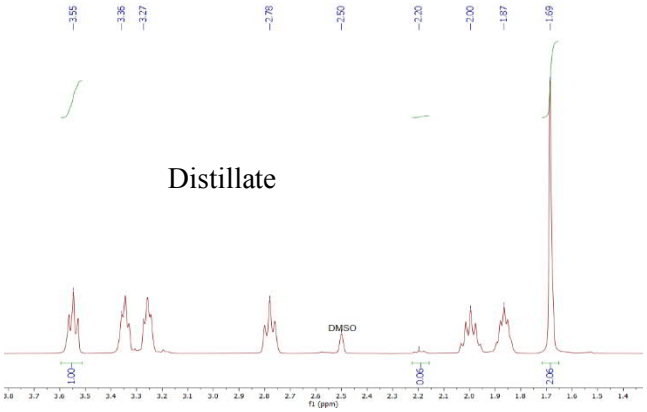

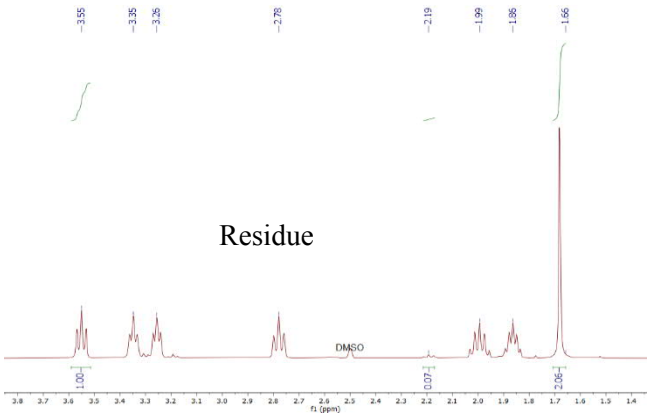

Samples	CE results, base molar %	CE results, by-product, molar %	CE results, acid, molar % (calculated)
Feed	58 ± 1.6	3.4 ± 0.12	38.6 ± 1.6
Distillate	48.8 ± 1.6	3 ± 0.12	48.2 ± 1.6
Residue	38.4 ± 1.3	3.5 ± 0.2	58.2 ± 1.3

Appendix 11.11: Experiment # 18

Samples	Weight, g	Mass percentage, wt.%
Feed	228	100
Distillate	190	83
Residue	3	1
Cold trap	78	34
OUT	271	119
Loss	-43	-19

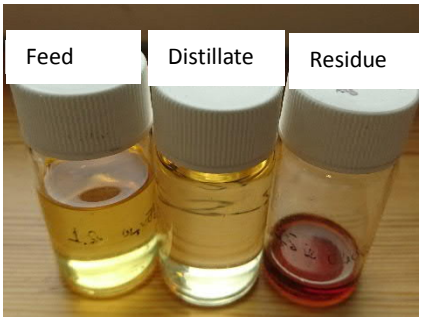

Samples	NMR results, base molar %	NMR results, hydrolysis, molar %	NMR results, acid, molar %	NMR results, water signal (Yes/No)
Feed	37	9	54	no
Distillate	38	8	54	no
Residue	34	9	57	no
Cold trap	only base	significant	no acid	yes

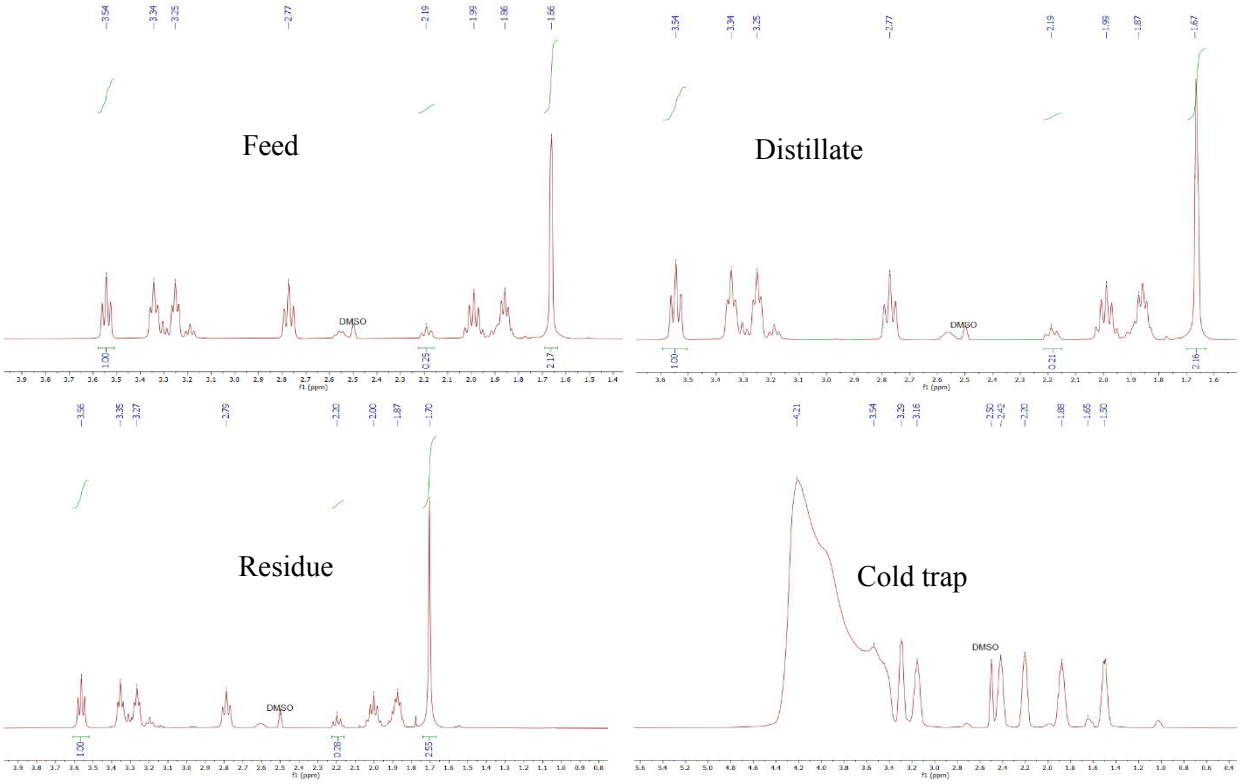

Samples	CE results, base molar %	CE results, by-product, molar %	CE results, acid, molar % (calculated)
Feed	42.6 ± 2.1	9.3 ± 0.76	48.2 ± 2.1
Distillate	45.1 ± 1.7	3.9 ± 0.42	50.9 ± 1.7
Residue	38.4 ± 1.1	6.2 ± 0.37	55.4 ± 1.1

Appendix 11.12: Experiment # 19

Samples	Weight, g	Mass percentage, wt.%
Feed	156	100
Distillate	90	58
Residue	36	23
Cold trap	20	18
OUT	154	99
Loss	2	1

Distillate Residue

Samples	NMR results, base molar %	NMR results, hydrolysis, molar %	NMR results, acid, molar %	NMR results, water signal (Yes/No)
Feed	49	1	50	no
Distillate	52	2	46	no
Residue	40	2	58	no
Cold trap	only base		no acid	

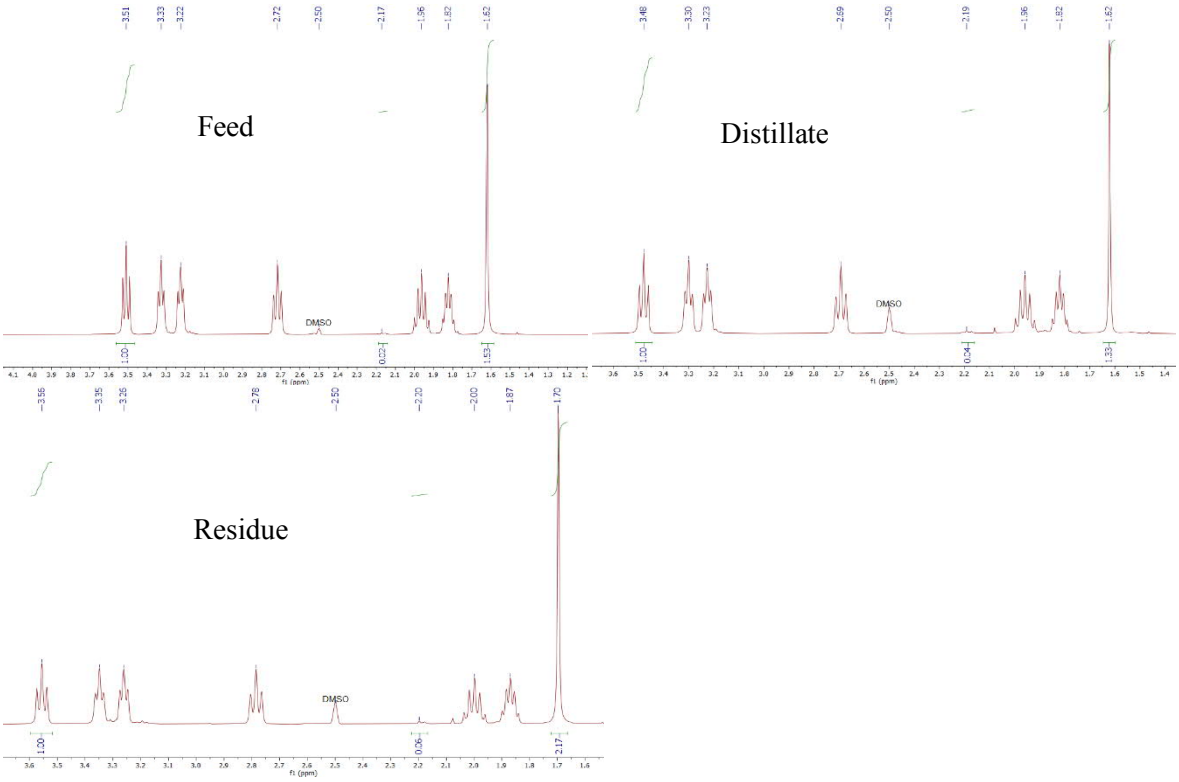

Samples	CE results, base molar %	CE results, by-product, molar %	CE results, acid, molar % (calculated)
Feed	54.3 ± 1.5	2.5 ± 0.12	43.2 ± 1.5
Distillate	48.1 ± 1.7	2.2 ± 0.08	49.7 ± 1.7
Residue	44 ± 1.6	2.9 ± 0.24	53.1 ± 1.6